DESIGN AND CHARACTERIZATION OF NOVEL PATCH-BASED REFLECTARRAYS

LEE SHIN ROU

MASTER OF ENGINEERING SCIENCE

LEE KONG CHIAN FACULTY OF ENGINEERING AND SCIENCE
UNIVERSITI TUNKU ABDUL RAHMAN
MAY 2017

DESIGN AND CHARACTERIZATION OF NOVEL PATCH-BASED REFLECTARRAYS

By

LEE SHIN ROU

A dissertation submitted to the Department of Electrical and Electronic Engineering,
Lee Kong Chian Faculty of Engineering and Science,
Universiti Tunku Abdul Rahman,
in partial fulfillment of the requirements for the degree of
Master of Engineering Science
May 2017

ABSTRACT

DESIGN AND CHARACTERIZATION OF NOVEL PATCH-BASED REFLECTARRAYS

Lee Shin Rou

Reflectarray is composed of an array of uniformly spaced radiating elements which are spatially illuminated with a feed source. An offset feed is usually preferred as it reduces the blockage of the broadside radiation beam. Reflectarray was found to be able to offer high antenna gain for long-distance communications, and it has combined the features of parabolic reflector and phased array. Unlike a parabolic reflector, reflectarray is light in weight, and it is easy to manufacture its planar radiating surface. Most importantly, unlike phased array, it does not require the use of any complex and high-loss feeding networks. Since then, reflectarray has become popular in wireless and radar applications. Reflectarray can steer radiation beam easily to any directions by manipulating the phase shifts of the radiating elements.

In my first project, the E-shaped patch resonator is proposed for designing a novel linearly polarized broadband reflectarray. The element is made up of a shorted E-shaped patch with a polystyrene foam placed beneath it, and no dielectric substrate is needed by the reflectarray. A full 11 × 11 reflectarray has been demonstrated at 7.9 GHz. It is found that the proposed

reflectarray is able to achieve an antenna gain of ~23.7dBi and a -1dB gain bandwidth of 8.1%.

In my second project, a reflectarray with circular polarization is designed using elliptical patches. The proposed element consists of two elliptical patches covering up the top surfaces of two substrates, respectively. The proposed element is found to be able to generate a broad reflection phase range of 550° by varying the major axis of the elliptical patches. A full 11 × 11 circularly polarized reflectarray has been designed at 10.5 GHz and its prototype has been fabricated. Measurement results show an antenna gain of 20.38dBi and a -1dB gain bandwidth of 11.6% are achievable. The measured 3-dB axial ratio bandwidth is found to be able to reach 12.47%.

In both of the projects, the Floquet method has been employed and the CST Microwave Design Studio was used for simulating the reflectarray configurations. Good agreement is observed between simulation and measurement. A complete parametric analysis has also been performed to study the effects of all important design parameters.

ACKNOWLEDGEMENTS

First of all, I would like to hand in millions of thanks to my supervisor, Dr. Lim Eng Hock and co-supervisor, Dr. Lo Fook Loong for guiding and assisting me throughout my research projects. I am extremely grateful that they are willing to spend their precious time for having discussions with me. The valuable advice and ideas given have contributed to the successful completion of my research.

Also, I truly appreciated the guidance given by Mr. Ho during the fabrication process. His guidance has created a better outcome to my research projects. Besides that, I would like to thank Mr. Phua and Wai Hau for assisting me in the prototype fabrications and measurements.

Lastly, I would like to express my gratitude to UTAR for providing the equipment, research materials and facilities during my research. In addition, the freely accessible online database has made the research easier as all the important literatures are easily obtainable.

APPROVAL SHEET

This dissertation entitled "**DESIGN AND CHARACTERIZATION OF NOVEL PATCH-BASED REFLECTARRAYS**" was prepared by LEE SHIN ROU and submitted as partial fulfillment of the requirements for the degree of Master of Engineering Science at Universiti Tunku Abdul Rahman.

Approved by:

_____
(Assoc. Prof. Dr. Lim Eng Hock)
Date:……..
Supervisor
Department of Electrical and Electronic Engineering
Lee Kong Chian Faculty of Engineering and Science
Universiti Tunku Abdul Rahman

_____
(Assoc. Prof. Dr. Lo Fook Loong)
Date:……..
Co-supervisor
Department of Electrical and Electronic Engineering
Lee Kong Chian Faculty of Engineering and Science
Universiti Tunku Abdul Rahman

LEE KONG CHIAN FACULTY OF ENGINEERING AND SCIENCE

UNIVERSITI TUNKU ABDUL RAHMAN

Date: 19 May 2017

SUBMISSION OF DISSERTATION

It is hereby certified that **LEE SHIN ROU** (ID No: **14UEM07940**) has completed this dissertation entitled "**DESIGN AND CHARACTERIZATION OF NOVEL PATCH-BASED REFLECTARRAYS**" under the supervision of Dr. Lim Eng Hock (Supervisor) from the Department of Electrical and Electronic Engineering, Lee Kong Chian Faculty of Engineering and Science (FES), and Dr. Lo Fook Loong (Co-Supervisor) from the Department of Electrical and Electronic Engineering, Lee Kong Chian Faculty of Engineering and Science (FES).

I understand that University will upload softcopy of my dissertation in pdf format into UTAR Institutional Repository, which may be made accessible to UTAR community and public.

Yours truly,

_____

(LEE SHIN ROU)

DECLARATION

I hereby declare that the dissertation is based on my original work except for citations and quotations which have been duly acknowledged. I also declare that it has not been previously or concurrently submitted for any other degree at UTAR or other institutions.

_____

(LEE SHIN ROU)

Date _____

TABLE OF CONTENTS

LIST OF TABLES

LIST OF FIGURES

CHAPTER 1

INTRODUCTION

1.1 Background and Issues

Antenna is a fundamental component of wireless communication systems. It is mainly used for transmitting or receiving electromagnetic waves. It can be physically designed into any shapes and sizes to fulfill different kinds of applications. For long distance communications, a high-gain antenna is usually preferable as the radiated power has to be focused into a certain direction, making it able to travel farther.

Parabolic reflector antenna is one of the conventional high-gain antennas and is mainly used to focus EM energy into a particular direction, as illustrated in Figure 1.1. However, it is very huge and heavy as its curvature is typically manufactured using metallic materials. It is also very troublesome to fabricate the curvature of the parabolic reflector antenna. This makes the parabolic reflector antenna inappropriate for space-borne applications. To enable beam scanning, a mechanical rotator is incorporated into the parabolic reflector antenna so that the direction of the radiation aperture can be changed easily. But it is inefficient in capturing the fast-changing signals due to the slow speed of beam scanning.

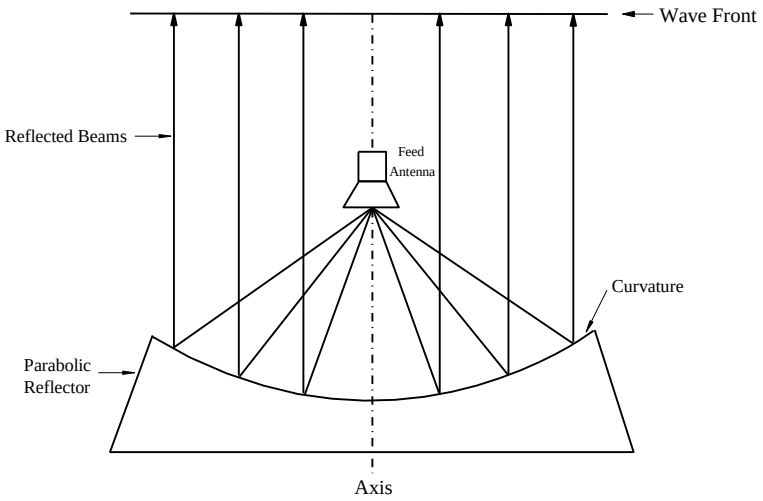

Figure 1.1: A typical parabolic reflector antenna.

Phased array is another type of the conventional high-gain antenna. It is mainly composed of power dividers, phase shifters and antenna arrays, as depicted in Figure 1.2. Unlike the parabolic reflector antenna, the phased array enables beam scanning by giving different phases to each of the antenna arrays, making it very useful for wireless communication applications. To provide an equal phase of input signals to the controllable phase shifters, power divider networks are usually required for splitting the incoming RF signals. For large-sized phased arrays, multiple power divider networks can cause high insertion loss in the antenna arrays.

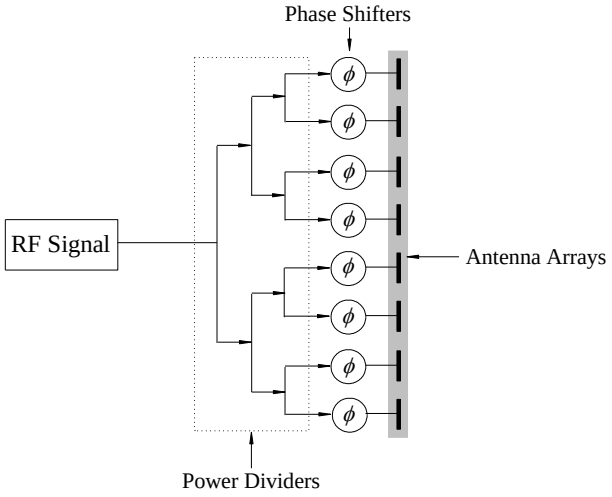

Figure 1.2: A typical configuration of phased array.

To overcome the weaknesses of the parabolic reflector antenna and the phased array, a new type of antenna named reflectarray has been introduced (Berry et al., 1963). It combines the good features of both of the parabolic reflector antenna and the phased array (Mener et al., 2013). Compared with the conventional antennas, the reflectarray is much lighter as it requires less supporting fixtures, making it suitable for space-borne applications. Unlike the parabolic reflector antenna, the flat radiating surface of the reflectarray is much easier to manufacture (Huang, 1996), as presented in Figure 1.3. Unlike the phased array, the radiating elements of the reflectarray act as the phase shifters to compensate the phase differences between the neighboring elements. Also, reflectarray does not require any high loss and complex power divider networks as all of the radiating elements of the reflectarray are spatially excited by a feeding source (Pan et al., 2012). This can minimize the loss incurred in the reflectarray while improving its radiation efficiency. However, the metallic structure of the feeding horn may scatter the radiation beams. To

minimize the effects of the feeding horn, side-fed configuration is usually preferable (Han et al., 2006).

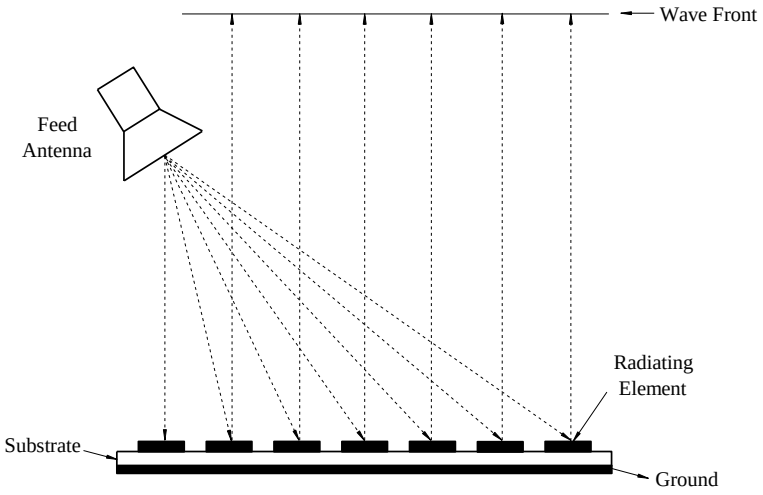

Figure 1.3: A typical side-fed reflectarray.

1.2 Key Performance Parameters for Reflectarray Unit Element

A good reflectarray unit element must be able to achieve a reflection phase range of 360° with a minimal reflection magnitude. In this section, this two crucial parameters are discussed in detail – reflection magnitude and reflection phase.

1.2.1 Reflection Magnitude

When designing a reflectarray unit element, it is usually desirable to achieve a low reflection magnitude (close to 0 dB) at the resonance. The

reflection magnitude can be contributed by two types of losses - metallic loss and dielectric loss (Bozzi et al., 2004). These losses are mainly introduced by the reflectarray elements when they reradiate the incoming wave beams in a certain direction. The metallic loss is the loss suffered from the metallic surfaces while the dielectric loss is caused by the dielectric substrate. The amount of the metallic loss can be varied if different geometrical shapes of the metallic resonators are used for reflectarray designs (Bozzi et al., 2004).To achieve a low reflection magnitude, the dielectric substrate has to be carefully chosen as its loss tangent and thickness affect the reflection magnitude, as stated in (Rajagopalan and Rahmat-Samii, 2010).

1.2.2 Reflection Phase

Reflection phase is the most crucial parameter in the unit element design. It is also known as S-curve, which indicates the reflection phase required for each of the reflectarray elements, and each reflection phase corresponds to a particular design dimension (phase-shifting parameter) (Niaz et al., 2010). In the reflectarray design, all of the reflectarray elements are necessary to have unequal design dimensions for compensating the phase shifts so that a co-phasal reradiated wave beam can be formed. Thus, it is desirable to have a slow changing rate of the reflection phase curve with a broad phase range (>360°). This is because a slow gradient of the phase slope can give a more distinguishable design dimension between the neighboring elements. However, this is usually a challenging task as a sharp phase change

may be introduced during the resonances of the metallic patch. Various reflectarray element designs have been proposed for reducing the gradient of the reflection phase slope. The proposed designs included the use of phase delay line (Carrasco et al., 2008), stacked patches (Encinar, 2001) and thick substrate (Karnati et al., 2011). In unit element design, it is also preferable to achieve a phase range of more than 360° so that it can be used for designing large-sized reflectarrays.

1.3 Key Performance Parameters for Reflectarray

For a linearly polarized reflectarray, the performances of the reflectarray can be analyzed based on its antenna gain and -1dB gain bandwidth. On the other hand, for a circularly polarized reflectarray, axial ratio bandwidth is considered the most important performance parameter. In designing a reflectarray, a high antenna gain and a broad operating bandwidth are always preferable.

1.3.1 Antenna Gain

Antenna gain measures the ability of an antenna to focus radiation beams into certain directions. It is expressed in dBi, which refers to the gain of an antenna with regard to the gain of an isotropic radiator. The antenna gain of a reflectarray mainly depends on its aperture dimension (Huang and Encinar,

2007). The reflectarray antenna gain increases with increasing its aperture size. This results in an increment of the total number of reflectarray elements. Also, a larger antenna gain can improve the aperture efficiency of the reflectarray, as defined in equation (1.1) (Yu et al., 2010).

$$n_a = \frac{G\lambda^2}{4\pi A_p} \tag{1.1}$$

where

n_a = aperture efficiency of a reflectarray

G = antenna gain of a reflectarray

λ = wavelength at the working frequency of a reflectarray, m

A_p = aperture area of a reflectarray, m^2

Spill-over losses can reduce the antenna gain of the reflectarray. To alleviate this, the feed horn must be positioned at a distance where it is just sufficient to cover the reflectarray aperture. Concurrently, all of the reflectarray elements must be located at the far-field of the feed horn. Another factor that affects the reflectarray antenna gain is the gap separation between two reflectarray elements. This factor may cause unwanted sidelobes in the reflectarray if it is not fully optimized. Sidelobes can significantly reduce the antenna gain of a reflectarray. To minimize this effect, the gap separation is usually designed to be between 0.5λ - 0.6λ.

1.3.2 Gain Bandwidth

When analyzing the performances of a reflectarray, the parameter of -1dB gain bandwidth is usually used. It is defined as the frequency range where the antenna gain of a reflectarray drops by 1 dB. The bandwidth of a reflectarray is mainly affected by the bandwidth of its element (Huang and Encinar, 2007).

1.3.3 Axial Ratio Bandwidth

Axial ratio (AX), usually expressed in dB, is an important performance indicator when designing a circularly polarized (CP) reflectarray. When characterizing a CP reflectarray, the 3-dB axial ratio bandwidth, which is defined as the frequency range where AX ≤ 3 dB (Toh et al., 2003), is used. The performance of a CP reflectarray primarily depends on the characteristics of the feeding source and the unit element. In (Huang and Pogorzelski, 1998), for the first time, element rotation technique was used for designing a CP reflectarray, which consisted of multiple microstrip patch elements rotated with different angles. To achieve left-handed CP, a conical feed horn with left-handed CP was used as the feeding source. The same technique was applied to obtain a right-handed CP reflectarray with the use of a right-handed CP feed (Strassner, Han and Chang, 2004).

Instead of using the CP feed, a linearly polarized (LP) horn can also be used as the feeding source of CP reflectarrays. In this case, the polarization of the LP feed must be set in such a way that it is parallel to the diagonal line of the CP reflectarray aperture, as demonstrated in (Wu et al., 2005). Also, the designed unit element must be able to provide CP operation so that it can convert LP to CP. The unit elements that are able to deliver CP performances have been proposed in (Zhao et al., 2010; Ren et al., 2011).

1.4 Research Objectives and Motivation

In this dissertation, different designs of unit elements will be used for designing one linearly- and one circularly polarized reflectarrays, which combine the good features of both of the conventional parabolic reflector and the phased array. The research objectives and motivations for both of the projects are clearly stated in this section.

In the first project, the research objectives and the motivation are:

- An E-shaped patch resonator will be deployed for designing a linearly-polarized (LP) broadband reflectarray for the first time. The lengths of its two arms will be varied simultaneously to provide a phase change, without the use of any dielectric substrate.
- To demonstrate that the design idea works, an 11×11 E-shaped patch reflectarray will be designed with the use of a total of 121 unit elements.
- The reflection and radiation characteristics of the unit element will be investigated to obtain low reflection magnitudes and wide phase ranges.

In the second project, the research objectives and the motivation are:

- With the use of the double-layered elliptical patches, a circularly-polarized (CP) reflectarray will be explored. The major axes of the elliptical patches will be varied to give a broad phase range.
- To demonstrate the design concept, an 11×11 reflectarray, which has a total of 121 unit elements, will be designed.

- With the use of a linearly-polarized feeding source, the reflectarray will be able to provide circularly-polarized waves with broad bandwidth.

1.5 Thesis Overview

In this dissertation, five chapters will be presented together with a complete reference list. In Chapter 1, the background of the parabolic antenna and the phased array will be reviewed, along with the issues faced by both types of the antennas. Here, the concept of reflectarray is introduced and its important performance parameters are studied. It is then followed by the research objectives and motivation of my research.

In Chapter 2, the development history of the reflectarray will be provided. Besides that, the reflectarray design techniques will be discussed in detail, together with the design procedures of both the LP and CP reflectarrays. Simulation methods for the reflectarray unit elements and their design limitations will also be introduced.

In Chapter 3, the linearly-polarized reflectarray will be presented with the use of the E-shaped patch resonator. Complete study will be performed on the reflectarray, along with the simulation and measurement results. Parametric analysis is also performed on some crucial design parameters.

In Chapter 4, a circularly-polarized reflectarray is designed using the elliptical patches. Description on the design procedure as well as the measurement setup will be provided. The simulated and measured results are comprehensively discussed.

In Chapter 5, my research works are summarized and some of the important findings are made.

CHAPTER 2

BACKGROUND AND DEVELOPMENT

2.1 Development History of Reflectarray Antenna

Reflectarray, a new type of antenna composed of an array of truncated waveguides, was first introduced by Berry et al. (1963). Waveguide elements of variable length were deployed for compensating the path differences so that a co-phasal reradiated wave beam could be achieved. Unfortunately, the waveguide-type reflectarray is very bulky and heavy, making it not suitable for practical wireless applications. Later, Phelan (1977) proposed a spiraphase reflectarray in which the boresight beam of the reflectarray could be electronically re-directed to any angles. To enable this function, the reflectarray was incorporated with switching diodes. In the 70s, the electronic components were very heavy. Moreover, undesired grating lobes were observed when the element spacing was made larger.

In 1978, the concept of microstrip reflectarray was first introduced by Malagisi (1978). Various designs of microstrip reflectarrays were later proposed for achieving small size and light weight. Two simple microstrip reflectarrays were demonstrated in (Kelkar, 1991; Zhuang et al., 1993; Chang and Huang, 1995), where a phase-delay line with variable length was attached to the rectangular microstrip patch. It was shown that varying the size of the

microstrip patch resonator (Pozar and Metzler, 1993) is a good way to generate phase shifts.

A circularly-polarized reflectarray can be easily designed using identical resonators which are displaced with variable rotations. A stub-loaded CP reflectarray, which consists of an array of identical square patches, was demonstrated in (Huang, 1995; Huang and Pogorzelski, 1998). The desired phase shift can be obtained by varying the angular rotation of the reflectarray element.

To enable beam scanning, the reflectarray has to be incorporated with the PIN diode or varactor diode. In (Colin, 1996), with the use of a PIN diode phase shifter, the reflectarray was able to achieve a beam scanning angle of ±45°. Low phase shifter loss was achieved when varactor diodes were used (Boccia et al., 2002; Hum and Okoniewski, 2004).

Since 2000, various types of reflectarrays were proposed to suit different kinds of applications. Multilayer reflectarrays such as stacked patches (Encinar, 2001; Encinar and Zornoza, 2003), annular rings (Han et al., 2004), and crossed dipoles (Huang and Zawadzki, 2003) were developed for improving the bandwidth of the microstrip reflectarray. Varying the sizes of the stacked patches can achieve a phase range much greater than 360°. Also, a smooth phase curve can be obtained. For signal amplification purpose, an amplifying reflectarray (Bialkowski et al., 2002) was developed.

2.2 Design Procedure of Reflectarray

For designing a reflectarray, two approaches can be employed - Direct Optimization Technique (DOT) and Phase Only Optimization Technique (POT). The DOT is a precise and optimal design method. Also, it is very flexible as it can be used for designing reflectarray elements with arbitrary shapes. However, to have optimal design, a longer computation time is required for the DOT implementation as the geometrical parameters of the reflectarray elements are simultaneously optimized to fulfill the design requirements. Designing reflectarray in this way is very troublesome as the design procedure involves complex computations which requires high computer resources (Zhou et al., 2013).

The POT is commonly used for designing reflectarrays as it is simple to implement and fast in computation (Zhou et al., 2013). A square unit element is usually deployed in order to have identical spacing between the adjacent elements. The design procedure of the POT is straightforward and accurate. When designing a reflectarray using the POT, the elements are optimized individually to match the phase distributions on the radiation aperture. Compared with the DOT, the POT is more effective, much simpler and it requires much lesser computation time. Due to these advantages, this technique has been widely adopted in various reflectarray designs (Encinar and Zornoza, 2004; Carrasco et al., 2007; Capozzoli et al., 2009; Capozzoli et al., 2010; Ucuncu, 2013).

In my dissertation, the POT method is used for both of the projects. Figure 2.1 shows the flowchart of the design procedure using the POT. Initially, the proposed E-shaped patch element (first project) is designed and it is simulated inside a Floquet cell for generating its reflection magnitudes and phases. The design parameter that generates phase shift is then identified, and the reflection phase curve (S-curve) is obtained by varying this design parameter, with an oblique incident wave supplied to the proposed element. The S-curve indicates the reflection phases of the proposed element at all design dimensions. Next, the proposed element is expanded into a linearly polarized (LP) reflectarray, where the locations of all of the elements are decided and the total dimension of the reflectarray is determined. By knowing the feeding angle of the reflectarray, the path distances propagated by the wave beams from the feed horn to all of the elements can be calculated. With the design frequency set, the phases propagated by the wave beams can also be computed.

By choosing the reference element which has the shortest propagation path length from the feed horn, the phase differences between the reference element and all the other elements are calculated. The phase shifts required for all elements can then be extracted from the simulated S-curve. Each reflection phase corresponds to a particular design dimension. After extracting the dimensions for all the elements, the complete reflectarray model can be constructed. It is then simulated and optimized using the CST Microwave Studio. In the reflectarray simulation process, the radiation patterns and antenna gain of the reflectarray are obtained. After optimizing the reflectarray,

its prototype is fabricated and measured for verification. For my second project, an elliptical patch element is proposed, and the same design procedure (Figure 2.1) is employed. With the use of the elliptical patch, a circularly polarized (CP) reflectarray is designed, simulated and fabricated.

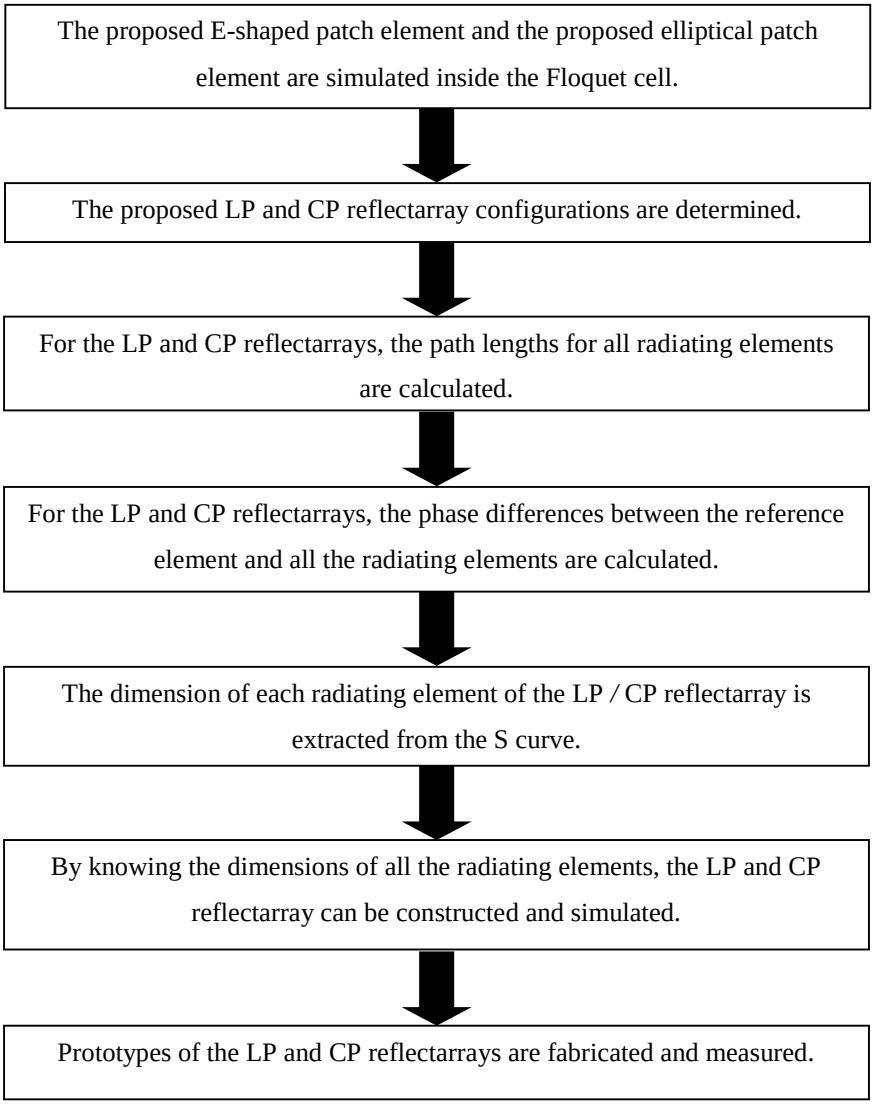

Figure 2.1: Design procedure of the reflectarrays by using the phase only optimization technique (POT).

2.3 Unit Element Simulation

In the unit element simulation, the reflection characteristics of the proposed element are analyzed. To simulate it, two methods can be used - Floquet method and Waveguide method. Both of the methods can be implemented using the CST Microwave Studio. The explanations for each of the methods are given in the subsequent subsections.

2.3.1 Waveguide Method

Waveguide method is usually used for simulating the unit element. The waveguide model consists of a unit element located at one end of the waveguide while an incident wave is supplied at the other end, as illustrated in Figure 2.2. In simulation, the four walls of the waveguide are defined to be perfect electric conductors (PEC). To analyze the reflection performances of the unit element, the waveguide model (with the unit element inside) is simulated using the CST Microwave Studio. The reflection phase curve is then obtained by changing the phase-shifting design parameter. Restricted by the waveguide dimension, this parameter cannot be changed much. Also, the angle of the incident wave cannot be altered as it depends on the operating frequency of the unit element. The weaknesses have made this method not convenient to be used for designing the whole reflectarray.

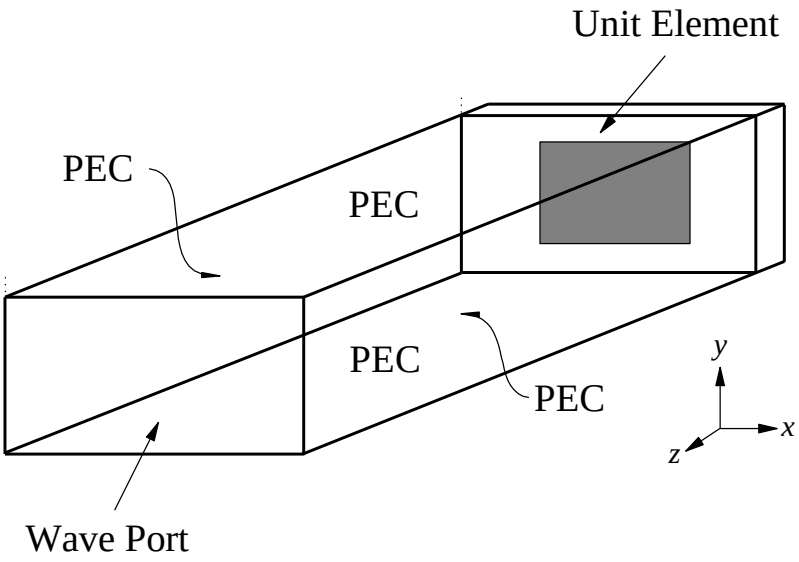

Figure 2.2: Waveguide model with its boundary conditions defined.

2.3.2 Floquet Method

Floquet method has been extensively used for designing various reflectarrays. This is because the boundary conditions of the Floquet model allow the duplications of the unit element, which can virtually form an infinite array, and include the mutual coupling between the adjacent elements. To enable this, the four side walls of the Floquet model are set to be periodic boundaries, as shown in Figure 2.3.

In simulation, more freedom is given to the unit element as there is no restriction on the element size. Unlike the waveguide method, the incident angle in the Floquet model can be freely chosen as it does not depend on the working frequency. Although this method is able to provide a fast simulation on a virtual infinite array, there remains shortcomings. For this method, as can

be seen from Figure 2.4, the mutual couplings are assumed to be contributed by identically sized nearby elements. In fact, this assumption is not accurate as the mutual couplings are caused by neighboring elements with unequal sizes. Unfortunately, this assumption cannot be avoided when using the Floquet method.

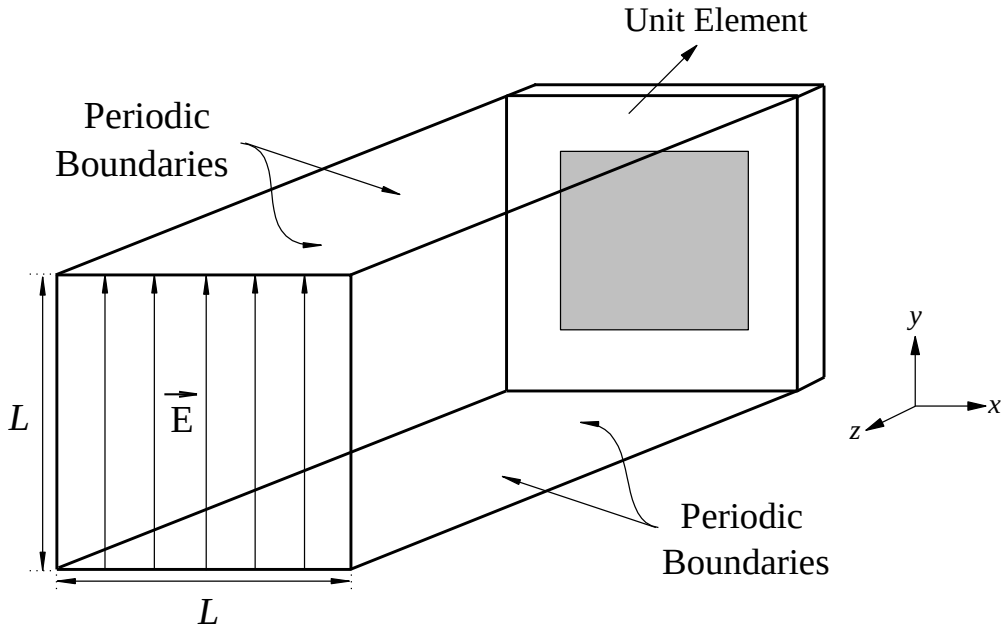

Figure 2.3: Floquet model with its boundary conditions defined.

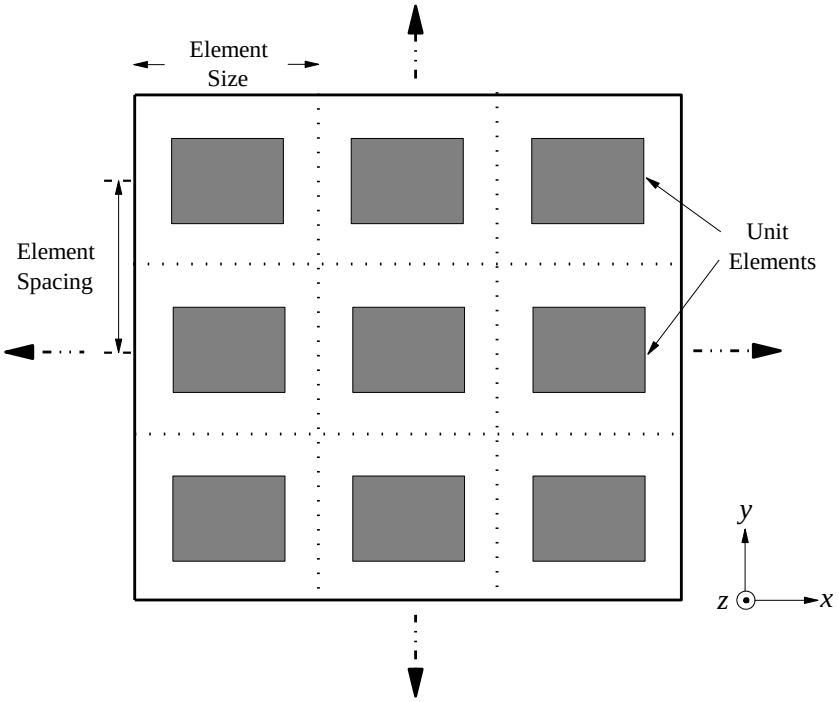

Figure 2.4: Virtual infinite array constructed using the Floquet method.

CHAPTER 3

BROADBAND SINGLE-LAYER E-PATCH REFLECTARRAY

3.1 Introduction

The first reflectarray, which was constructed using an array of truncated waveguides, was introduced by Berry et al. in 1963 (Berry et al., 1963). Such wave-guiding structure is nonplanar and bulky. It was followed by the implementation of microstrip reflectarray which consisted of multiple patch elements of varied sizes (Pozar et al., 1997). Although microstrip structure is planar, its conductor and dielectric losses at high frequencies can be severe and the achievable bandwidth is usually narrow. Over the years, much effort has been spent to enhance the bandwidth of microstrip reflectarrays. Multilayer technology has been proven to be the one of the popular alternatives that can effectively extend the bandwidth (Encinar, 2001). Exploration on broadband microstrip reflectarray elements continues because of the possible applications of the microstrip reflectarrays in space-related applications. Unit elements such as double hexagonal rings (Arshad et al., 2014), disk element with attached phase-delay lines (Hasani et al., 2010; Malfajani and Atlasbaf, 2012), triple square rings (Vosoogh et al., 2014), and square patch with dual gaps (Ismail and Sulaiman, 2011) were discovered to be able to produce broad frequency bandwidth. Although the single-layer reflectarray in (Hamzavi-Zarghani and Atlasbaf, 2015) was able to achieve

wide bandwidth in two passbands, optimization of the element was very tough and time consuming as six degrees of freedom needed to be attended to when designing the unit element. Lately, active elements such as varactor diode, capacitor, and amplifier are incorporated into reflectarrays so that they are able to perform beam steering (Zainud-Deen et al., 2012), and provide dual polarization (Makdissy et al., 2014) and amplification (Kishor and Hum, 2012).

Reflectarray elements that are able to produce wide phase range have also been of great interest recently, although a full cycle of phase angle (360°) is usually considered sufficient for designing a full-fledge reflectarray of any size. Having an S-curve with broad phase range and slow gradient is still much sought after to make the geometrical dimension of the element more distinguishable in the design. A variety of resonators have been explored for broad phase range on a single layer. It was found that a reflection phase range of greater than 360° was easily obtainable by placing multiple hexagonal rings (Arshad et al., 2014) concentrically. Dipole was also used for reflectarray design in (Florencio el al., 2013; Yoon et al., 2015), and it was found that placing a couple of dipolar strips in parallel can provide linear phase response with a phase range of more than 360°.

The E-shaped patch resonator was proposed for wireless communication applications (Yang et al., 2001; Ang and Chung, 2007; Razzaqi et al., 2013) in the early 2000's. Involvement of E-shaped patch was found to be able to achieve wide bandwidth performance. Such a resonator is

simple to design and its geometrical parameters can be easily optimized to achieve different specifications. In (Liu et al., 2016), it was found that dualband performance could be realized when a U-slot patch was stacked on top of another E-shaped patch with an air layer introduced in between. Integrating the E-shaped patch antenna with an LC circuit was found useful for bandwidth improvement (Chen et al., 2010). When deployed as transmitarray element, it requires 3 layers of identical E-shaped patches to achieve a transmission phase range of 270° (Luo et al., 2014), which is usually not sufficient for designing a full-fledge transmitarray. To our best knowledge, so far, no work is found on the use of E-patch resonator for reflectarray design.

In this chapter, the E-shaped patch is used for designing a linearly-polarized (LP) broadband reflectarray for the first time. In the proposed design, the two arms of the E-shaped patch are varied to generate a broad phase range of greater than 360°. To begin, the configuration of the proposed reflectarray element is first described in Part II. Floquet method will be used for simulating the reflection characteristics of the proposed reflectarray element. In Part III, the design guideline of the full-fledge reflectarray will be explained. Prototype has been fabricated and measurements were conducted to verify the simulated results. A full description of the measurement setup is provided in Part IV, followed by discussion of the measured and simulated results in Part V. To study the effects of some of the crucial design parameters on the reflection characteristics and radiation performances of the proposed reflectarray, a complete parametric analysis is given in Part VI. The proposed unit element

has a single-layer structure and it can be used for designing a large-scale reflectarray as it is able to provide a full reflection phase range.

3.2 Unit Element Analysis

The configuration of the proposed unit element is shown in Figure 3.1(a) and (b). It consists of an E-shaped metal patch etched on the top surface of a piece of square polystyrene foam ($L \times L$) with dielectric constant of $\varepsilon_r \sim 1$ and thickness of h. The bottom surface of the foam is laminated with ground plane. The center arm of the E-shaped patch is shorted to the ground through via (diameter of d). With reference to Figure 3.1(a), the shorting via is positioned at a distance, s from the edge of the arm. To analyze its reflection properties, the proposed element with a cell size of 25 mm × 25 mm ($L \times L$) is simulated using the CST Design Studio. In simulation, as shown in Figure 3.2, the proposed element is placed at one end of a square Floquet cell at a distance of 76 mm (in this case) from the wave port at another end, where a y-polarized plane wave with an incident angle of $\theta_i = 20°$ is launched. Since the reference plane is always de-embedded to the top surface of the unit element, the distance between the port and element does not affect the reflection performance much. With reference to Figure 3.2, the four side walls of the Floquet cell are defined to be periodic boundaries. In order to take the mutual coupling mechanism between the elements into account, the unit element inside the Floquet cell is simulated as an infinite periodic array repeating itself. Figure 3.3 shows the reflection phase ($\angle S_{11}$) curves at frequencies of 7.5 GHz

(0.625λ), 7.7 GHz (0.642λ), 7.9 GHz (0.658λ) and 8.1 GHz (0.675λ). With reference to the same figure, by varying the two arms (L_1) of the E-patch from 5 mm to 18 mm, a reflection phase range of ≥ 360° can be easily obtained at the frequencies of 7.9 GHz and 8.1 GHz. In this case, the reflection phase slope at 7.9 GHz (0.658λ) (Huang and Encinar, 2007) is selected for designing the reflectarray. The reflection magnitude is not shown as it is less than 10^{-4} in the entire range. The arm widths (W_1, W_3) and gaps (G_1 and G_2) are made to be equal (3 mm). Other design parameters are W_2 = 2 mm, L_3 = 3 mm, L_2 = 7 mm, s = 3 mm and d = 1 mm. The current distributions for the case of L_1 = 12 mm are plotted on the patch in Figure 3.4(a), and the corresponding electric fields in the cavity region between the patch and ground are depicted in Figure 3.4(b). Typical current and field distributions for E-patch have been observed in both, comparable with those in (Ang and Chung, 2007).

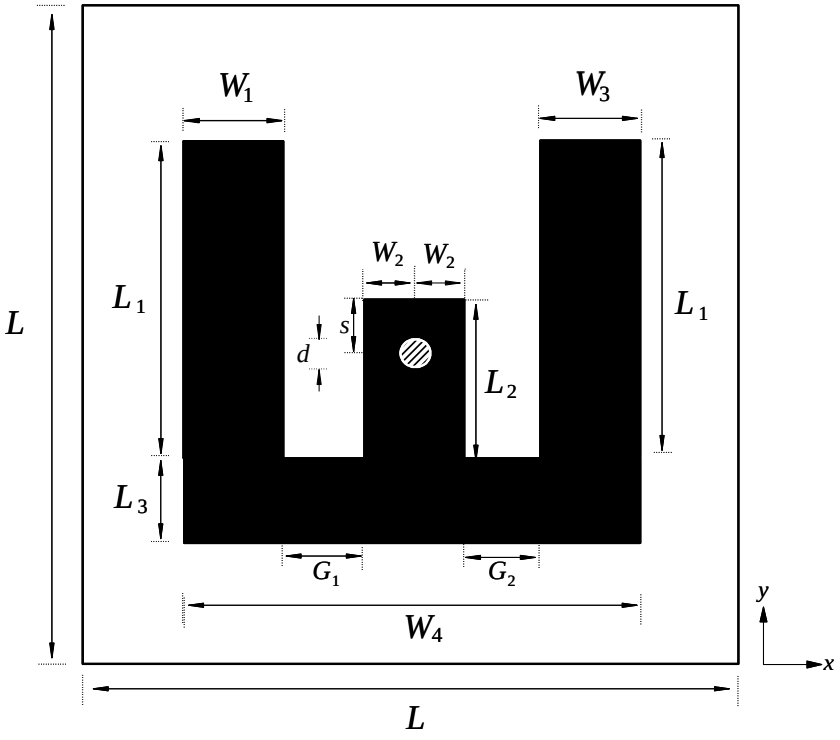

(a)

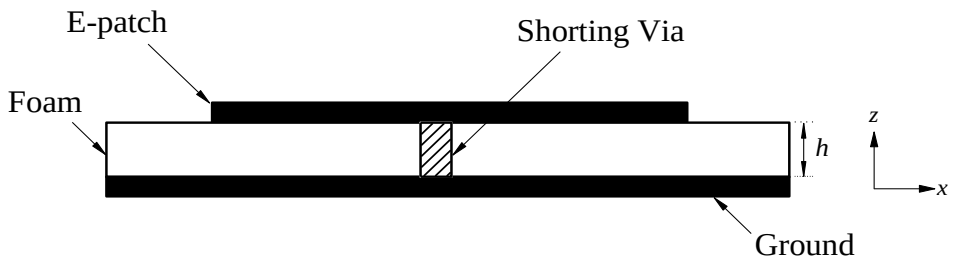

(b)

Figure 3.1: (a) Top view (b) Side view of the proposed E-patch unit element.

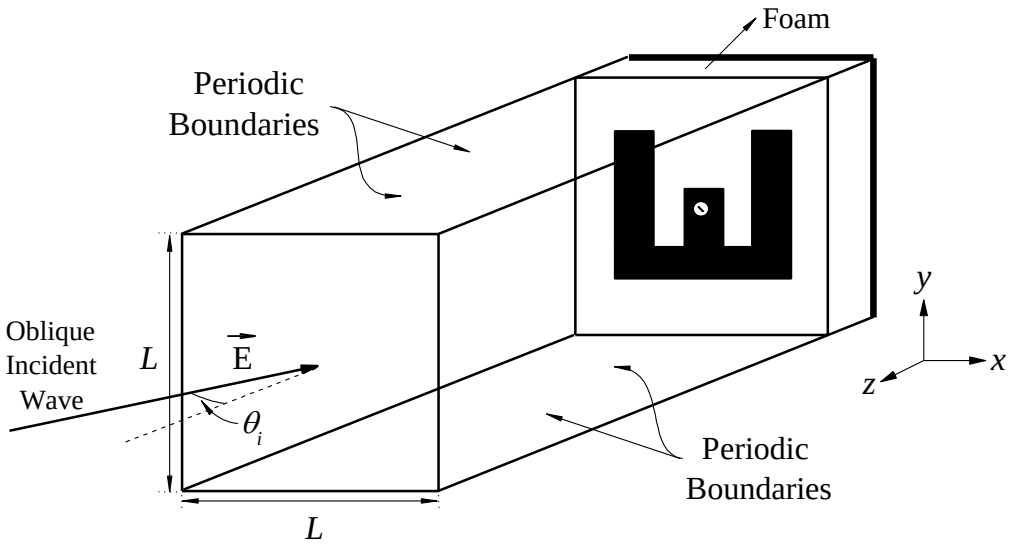

Figure 3.2: Simulation setting for the proposed unit element inside a Floquet cell.

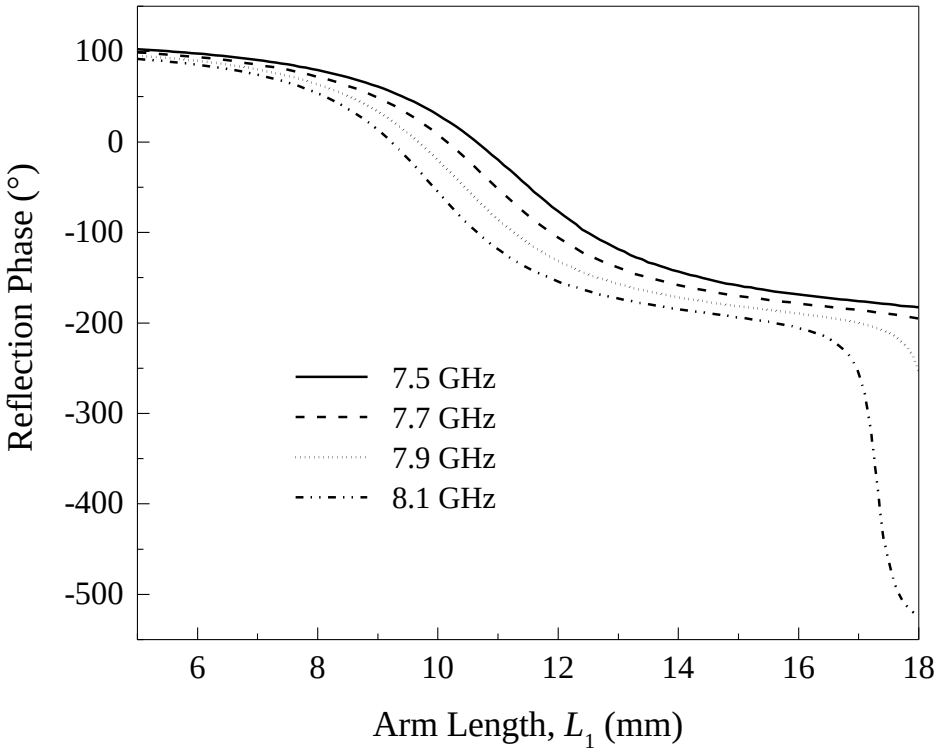

Figure 3.3: Reflection phase response as a function of arm length (L_1) of the proposed element at different frequencies.

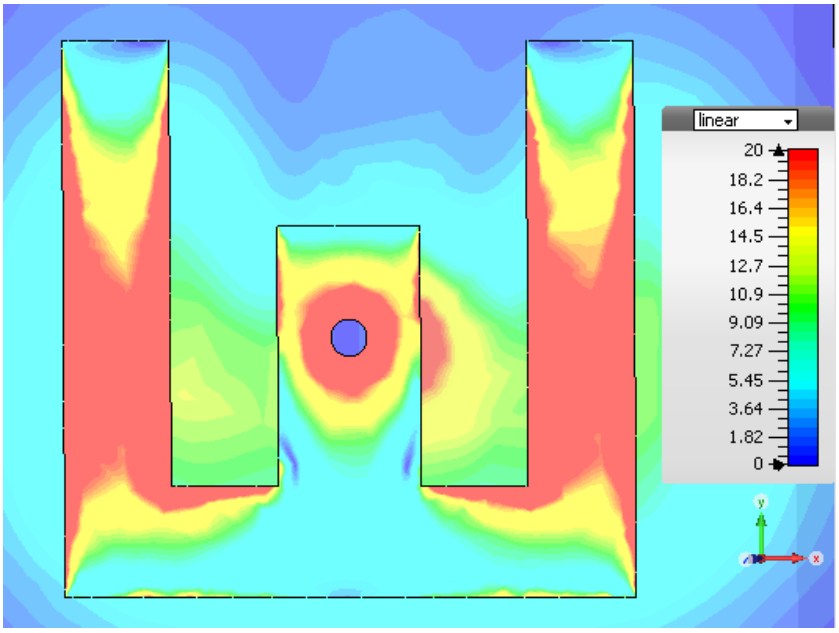

(a)

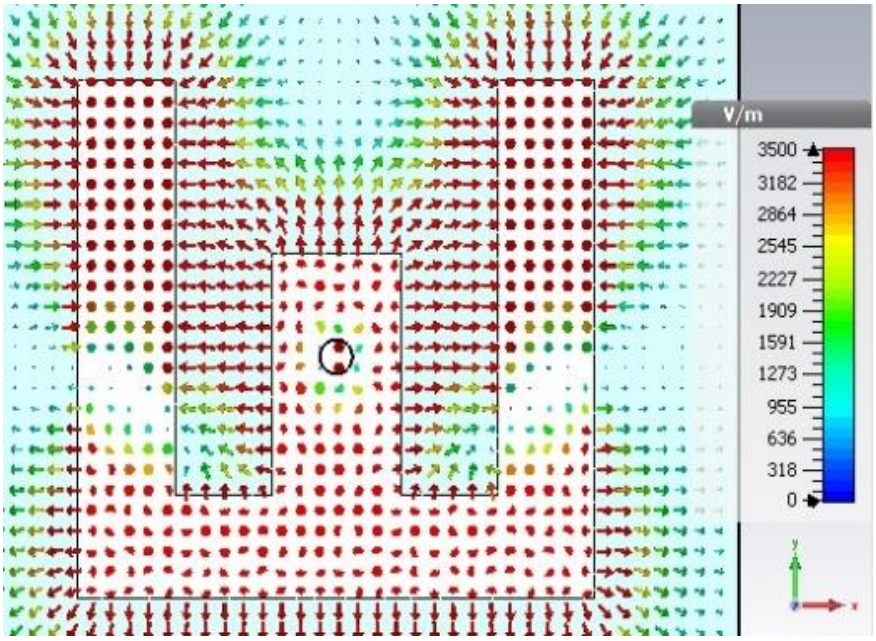

(b)

Figure 3.4: (a) Surface current on the E-shaped patch, and (b) electric field distribution in the cavity region between the patch and ground for the case of L_1 = 12 mm.

3.3 Reflectarray Configuration

With the use of the phase-length curve (also called S-curve) in Figure 3.3, an 11 × 11 linearly polarized (LP) reflectarray is designed. The elements are put into an array (shown in Figure 3.6), and the locations of the elements are represented as (*m*, *n*). The arrays are fed by a C-band pyramidal horn (5.85 GHz - 8.2 GHz), which is suspended at a focal distance F = 233.75 mm from the center point of the (6, 6) element with an incident angle of θ_i = 20°. Design procedure of the proposed reflectarray is briefly described here. With reference to Figure 3.5, wave propagating from the horn to the (6, 1) element is represented using path P_0 and its reflection phase is ϕ_0, which is taken to be a reference point. If the path length for another arbitrary element, say (6, 11)

element, is labelled as P_n, then the path difference between this particlar element and the reference can be denoted as $\Delta P_{n0} = P_n - P_0$. The phase difference is calculated as $\phi_{n0} = \Delta P_{n0} \frac{2\pi}{\lambda}$. To make the re-radiated wave from the (6, 11) element co-phasal with that from the (6, 1) element, the (6, 11) element is compensated with a phase ϕ_{n0}, which can be found from the *y*-axis of Figure 3.3, such that making it a constant at a certain phase $\phi_n = \phi_0 + \phi_{n0}$. From the same figure, also, ϕ_0 can be obtained from dimension L_1 on the *x*-axis. The design dimension (L_1) with its reflection phase for each radiating element of the proposed reflectarray is tabulated in a table, which can be found in Appendix A. The total dimension (D) of the proposed 11 × 11 (121 elements) LP reflectarray is 275 mm, and it has F/D ratio of 0.85. When fabricating the prototype of the proposed reflectarray, the adhesive side of the copper tape was stuck on the surface of a thin transparent paper. Next, the transparent paper with copper layer was laminated with dry film (photopolymer) and exposed to florescent light. It was then soaked in etching solution to remove all the unwanted parts of the copper layer. Then, the transparent paper with E-patches was stuck on a square polystyrene foam board, which was backed with a ground plane. Each of the patches was connected to its ground through a shorting via. It should be mentioned that the thickness and dielectric constant of the transparent paper were not included in simulation. The photograph of the fabricated prototype of proposed E-patch reflectarray is shown in Figure 3.6.

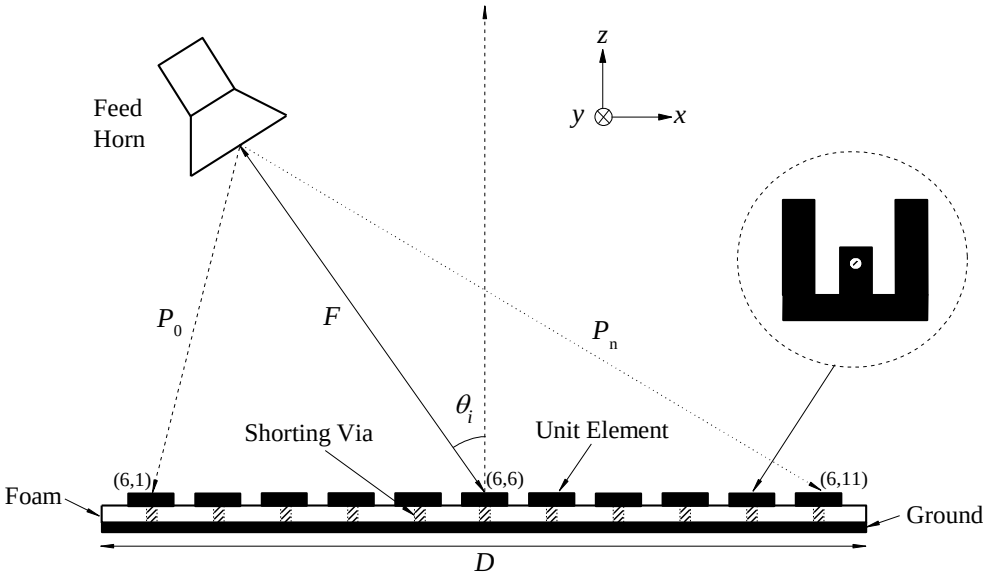

Figure 3.5: Configuration of the proposed linearly polarized reflectarray.

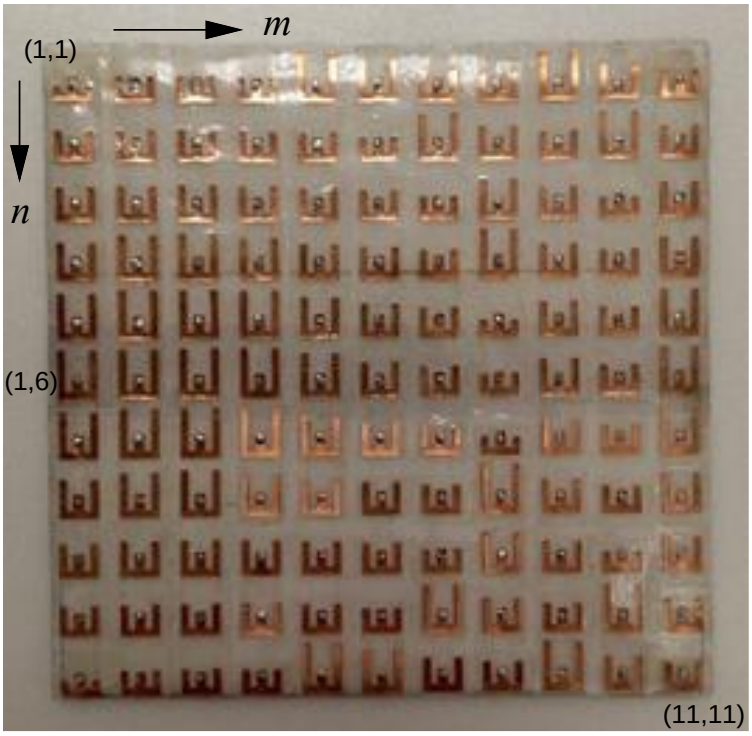

Figure 3.6: Photograph of the fabricated prototype of the linearly polarized E-patch reflectarray.

3.4 Measurement Setup

Measurement is conducted in free space environment for measuring the radiation patterns and antenna gain of the proposed reflectarray. Figure 3.7 shows the measurement setup. The reflectarray under test is placed on a rotating table and it is connected to a signal generator (Rohde & Schwarz SMB100A) for supplying a transmitting microwave signal with power (P_t) of 10 dBm at the desired frequency. Then, a linearly polarized C-band pyramidal horn (ATM PNR137-440-2, 5.85 GHz – 8.2 GHz) is placed at a far-field distance R = 8.5 m from the reflectarray and it is used to receive power (P_r) from the reflectarray. The receiving horn is connected to an Advantest U3771 spectrum analyzer for reading the received power. To enable measurement of radiation patterns at all angles, the reflectarray is directed facing +z, and it is rotated in the θ direction. At each elevation angle, the received power is directly recorded from the spectrum analyzer. The antenna gain can then be calculated using Friis Transmission equation.

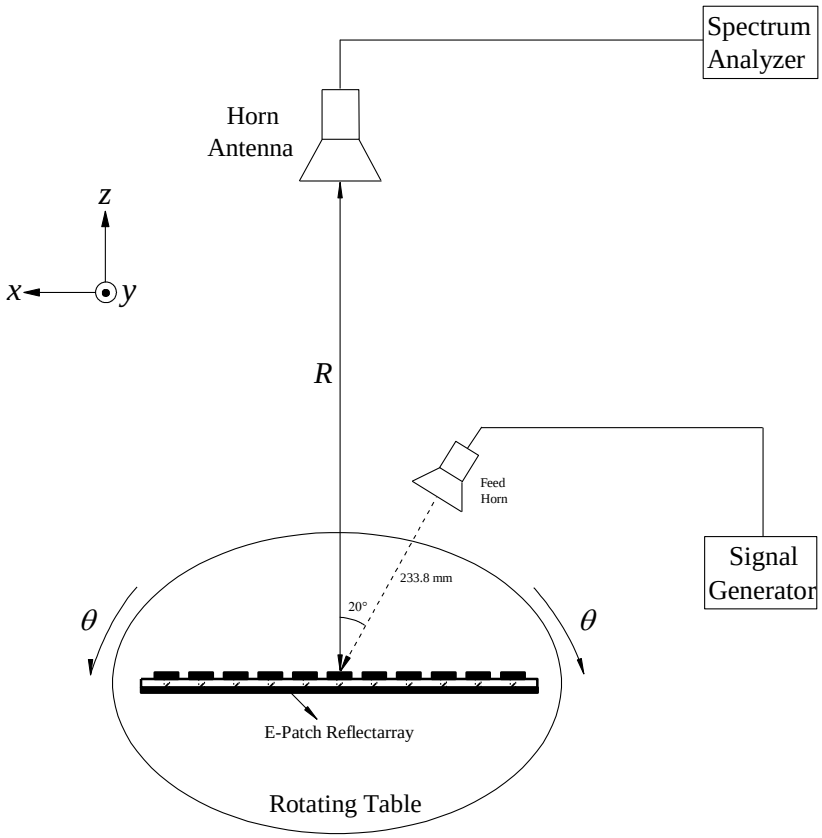

Figure 3.7: Measurement setup for the reflectarray.

3.5 Results and Discussion

Figure 3.8 shows the simulated and measured radiation patterns of the proposed E-patch reflectarray in the *E* (*yz*-plane) and *H* (*xz*-plane) planes. Good agreement is observed between the simulated and measured curves. A simulated peak gain of 24.56 dBi is observed in the boresight direction ($\theta = 0^0$) in both planes. With reference to the same figure, the measured peak gains for *E* and *H* planes are found to be ~23.7 dBi, which corresponds to an aperture efficiency of 36% (simulation 43.4%). The discrepancies can be caused by fabrication tolerances as it is very challenging to solder the vias accurately.

The simulated co-polarized fields are at least 20 dB larger than their cross-polarized counterparts in the boresight direction ($\theta = 0^o$). On the other hand, the measured co-polarized fields are found to be only ~18 dBi larger than their cross-polarized components in the boresight, which can be caused by imperfections in the experimental setup. Figure 3.9 shows the simulated and measured antenna gain (at $\theta = 0^o$) as a function of frequency. The measured -1 dB gain bandwidth covers the frequency range of 7.1 GHz - 7.7 GHz (simulation 7.4 GHz - 8.2 GHz), with a bandwidth of 8.1% (simulation 10.26%). Again, fabrication tolerances can be one of the issues that contribute to the shift. Table 3.1 compares the performances of the proposed reflectarray with some of the linearly polarized reflectarrays in literature. As can be seen from the table, our reflectarray has reasonable gain, bandwidth, and aperture efficiency.

Table 3.1: Performances of the linearly polarized reflectarrays.

Reference No.	**No. of Reflectarray Element**	**Reflectarray Aperture Size (mm^2)**	**Gain (dBi)**	**Gain Bandwidth**		**Aperture Efficiency (%)**
				-1dB (%)	**-3dB (%)**	
(Guo et al., 2013)	27 × 27 = 729	405 × 405	28.5	8	-	34.12 (measured)
(Malfajani and Atlasbaf, 2012b)	-	280 × 210	26.2	-	17	37 (measured)
(Abd-Elhady and Hong, 2010)	29 × 29 = 841	246.5 × 246.5	34	8	-	41 (simulated)
(Hasani et al., 2010)	21 × 31 = 651	190 × 270	24	-	18	35 (measured)
(Li et al., 2009)	11 × 5 = 55	660 × 300	14.2	-	14.1	22.6 (simulated)
This work	11 × 11 = 121	275 × 275	23.7	8.1	19.8	36 (measured)

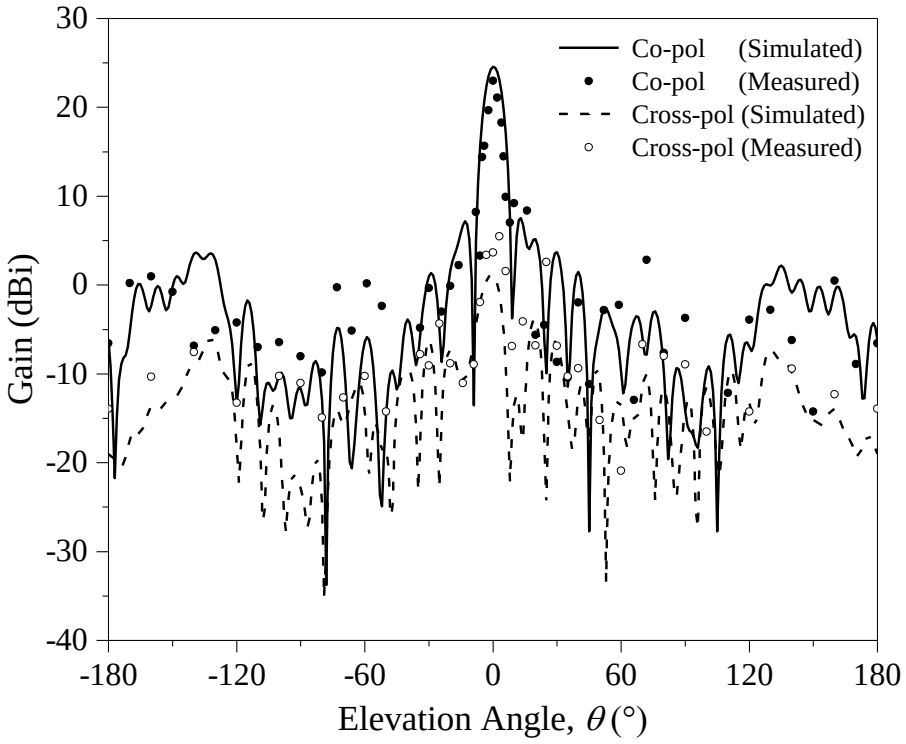

(a)

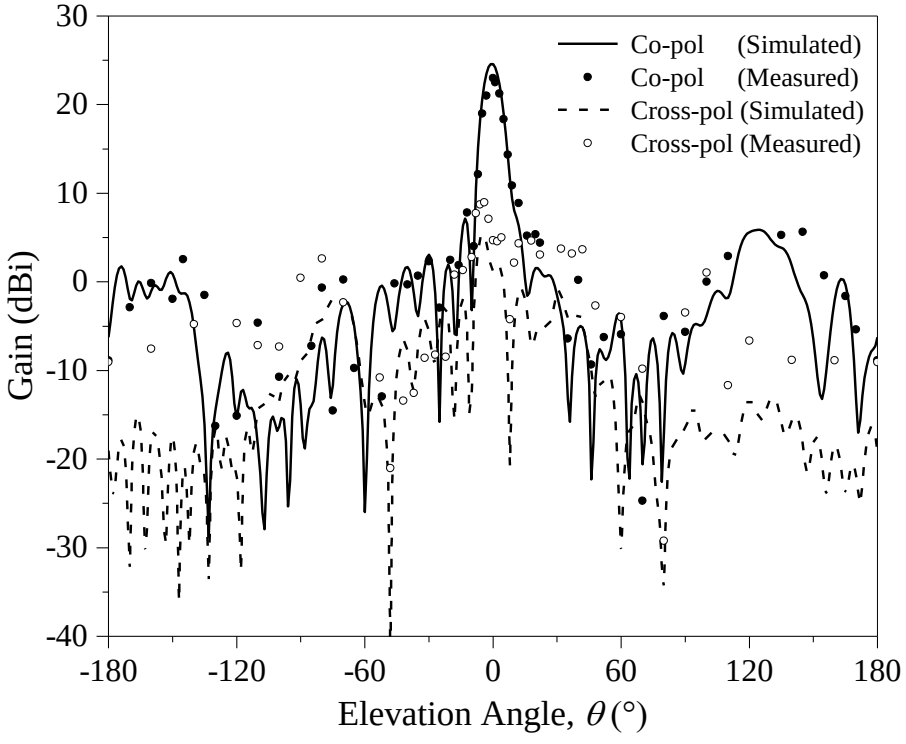

(b)

Figure 3.8: Measured and simulated (a) *E*- and (b) *H*- plane radiation patterns of the proposed E-patch reflectarray.

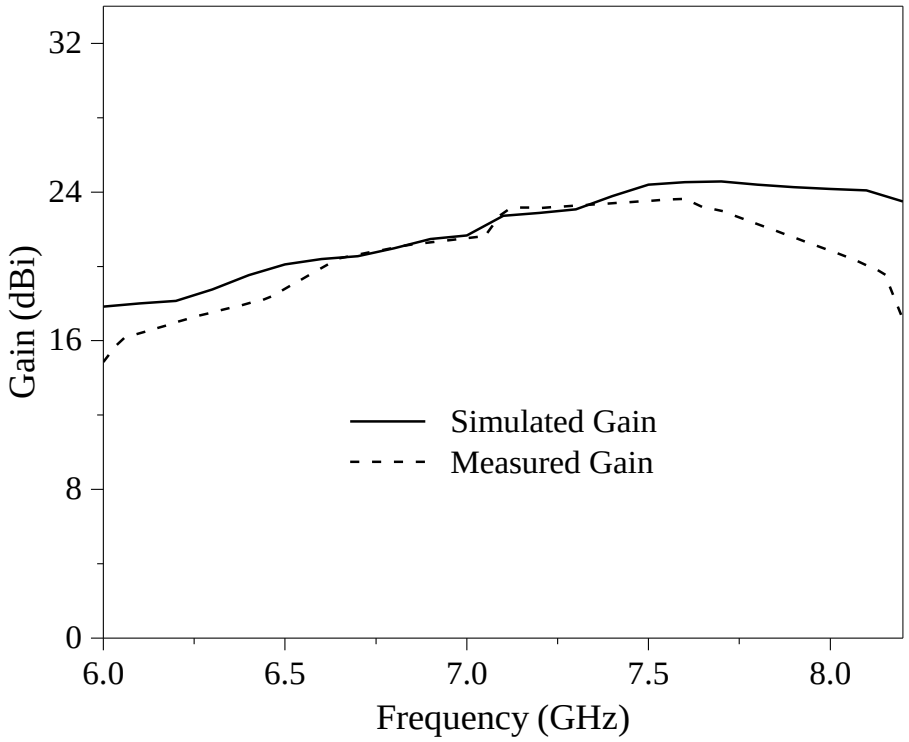

Figure 3.9: Measured and simulated antenna gain of the proposed E-patch reflectarray as a function of frequency.

3.6 Parametric Analysis

In this section, parametric analysis is performed to study the characteristics of the proposed unit element and the LP reflectarray. First of all, the effect of the shorting via is studied. Next, the effects of the arm widths of the E-shaped patch and the gap separations between the two adjacent arms on the reflection and radiation performances are studied. Lastly, analysis on some crucial design parameters such as foam thicknesses, centre arm widths and lengths, cell sizes, feeding angles, and etc. has been performed, with detailed description given in each parametric analysis.

3.6.1 E-Shaped Patch without Shorting Via

To begin with, the E-patch without a shorting via is simulated for comparison. Figure 3.10 shows the simulated reflection phases for the E-patch with and without a shorting via. With reference to Figure 3.10, a sharp change in gradient is observed in the phase curve in the range of L_1 = 6.2 mm - 6.4 mm when the via is removed, causing it to be unsuitable for use in reflectarray design. Although the gradient becomes slower beyond L_1 = 6.4 mm, the phase range is less than 360°. On the other hand, the E-patch with via is able to achieve a phase range of ~360° with slow gradient.

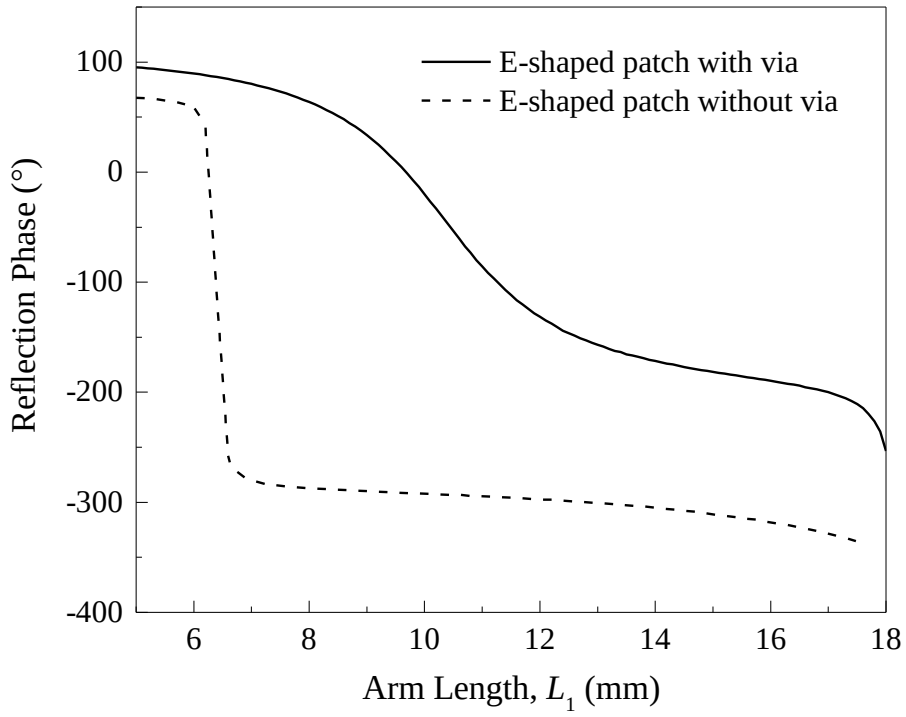

Figure 3.10: Reflection phases of the E-patch element with and without shorting via.

3.6.2 Widths of Two Sides Arm

Next, the effects of the arm widths (W_1 and W_3) are studied. The two arm widths (W_1 and W_3) are varied and the corresponding reflection phases are shown in Figure 3.11. W_1 and W_3 are made to be equal in this case. With reference to Figure 3.11, increase in phase range is observed when varying the parameters W_1 and W_3 from 1 mm to 5 mm. However, the usable L_1 length for the case of ($W_1 = W_3 = 4$ mm and 5 mm) is still in the range of 5 mm – 15 mm as the curve gradient becomes too steep beyond $L_1 = 15$ mm. For $W_1 = W_3 = 1$ mm, although the entire range of L_1 can be used, its achievable phase range is lesser than 360°. With reference to Figure 3.12, it is observed that the side and back lobes of the reflectarray become larger when the arm widths (W_1 and W_3) are varied from 3 mm to 5 mm. It causes the antenna gain to reduce at $\theta = 0^o$, as can be seen in Figure 3.12. In our design, the arm widths ($W_1 = W_3 = 3$ mm) are chosen as they enable the reflectarray element to produce a phase range of ~360°, with slow curve gradient and maximum antenna gain.

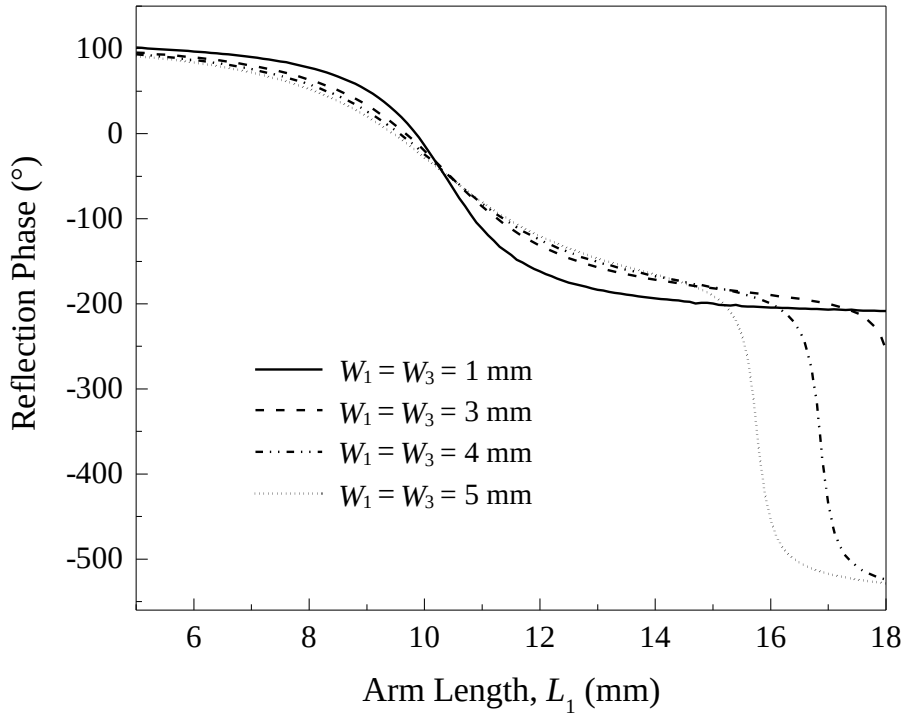

Figure 3.11: The effects of arm widths (W_1 and W_3) on the reflection phase of the E-patch reflectarray unit element.

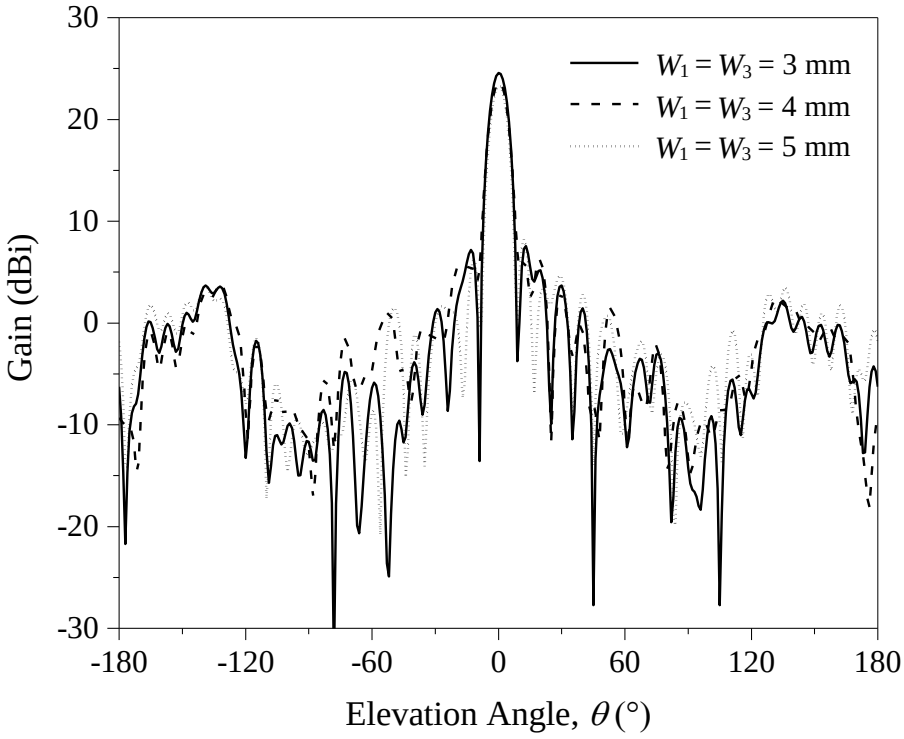

(a)

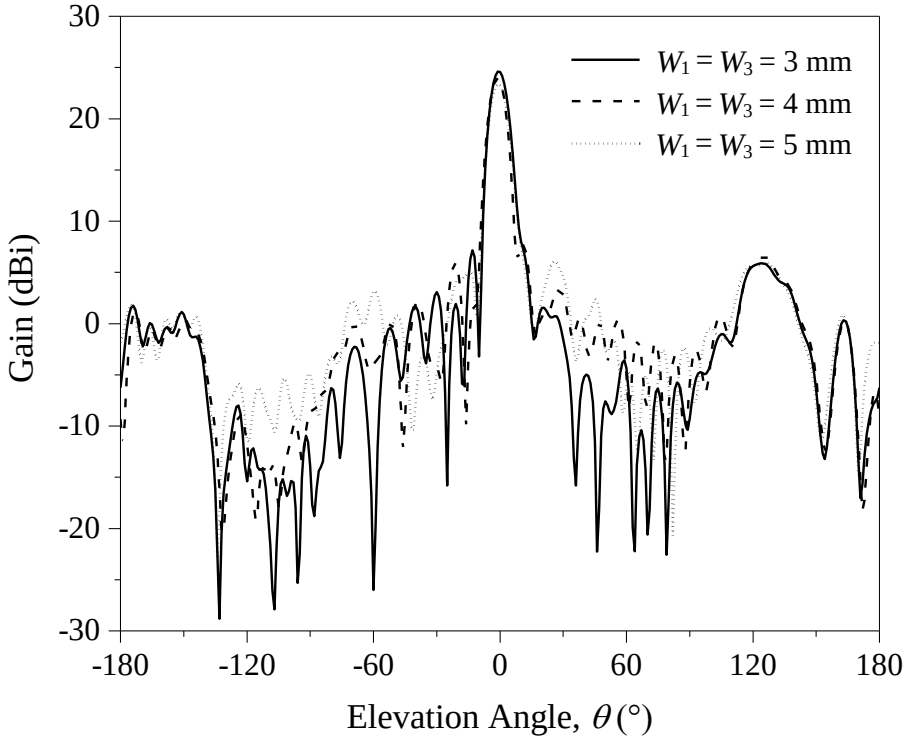

(b)

Figure 3.12: Radiation patterns of the proposed E-patch reflectarray with different arm widths (W_1 and W_3). (a) *E* - and (b) *H* - planes.

3.6.3 Gap Separation between Two Adjacent Arms

Subsequently, the effects of the separation gaps (G_1 and G_2) between two adjacent arms are studied, as depicted in Figure 3.13. In this case, G_1 and G_2 are set to be the same. As can be seen from the curve for (G_1 = G_2 = 5 mm and 6 mm), rapid phase change is observed for L_1 beyond 14 mm, introducing sudden increase in the total phase range, although it is too steep to be useful. Similar trend is observed when broadening the gap separations (G_1 and G_2) from 1 mm to 3mm. For the case of (G_1 = G_2 = 3 mm), minor increase is observed in the total phase range. With reference to the radiation patterns in Figure 3.14, the side lobes become larger in the *H*-plane when (G_1 and G_2) are

increased from 3 mm to 6 mm. Low side lobes and optimum antenna gain are observed for $G_1 = G_2 = 3$ mm.

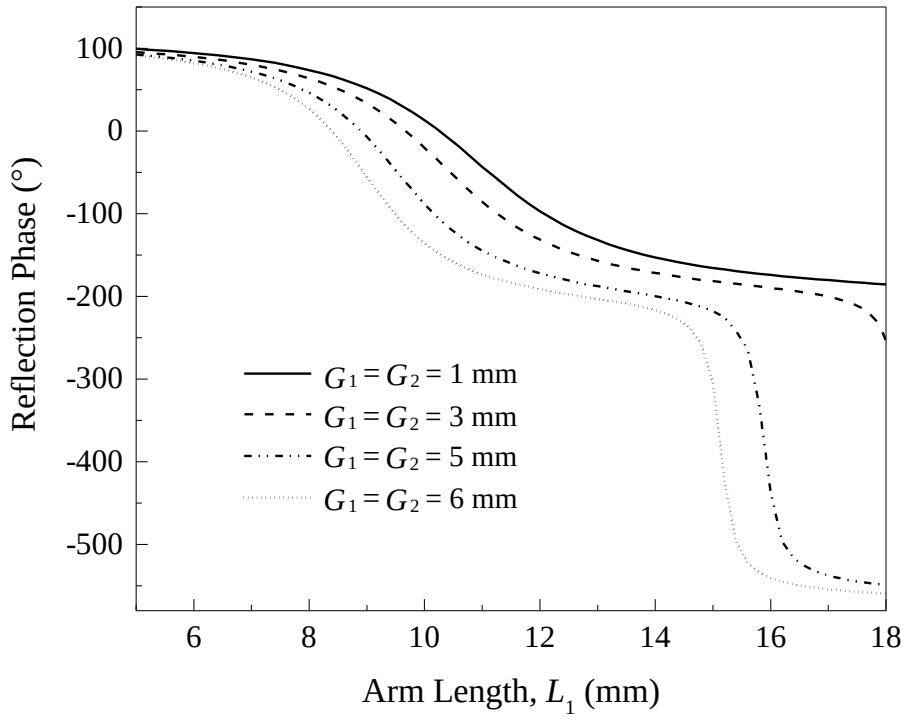

Figure 3.13: The effects of gap separations (G_1 and G_2) on the reflection phase of the E-patch reflectarray unit element.

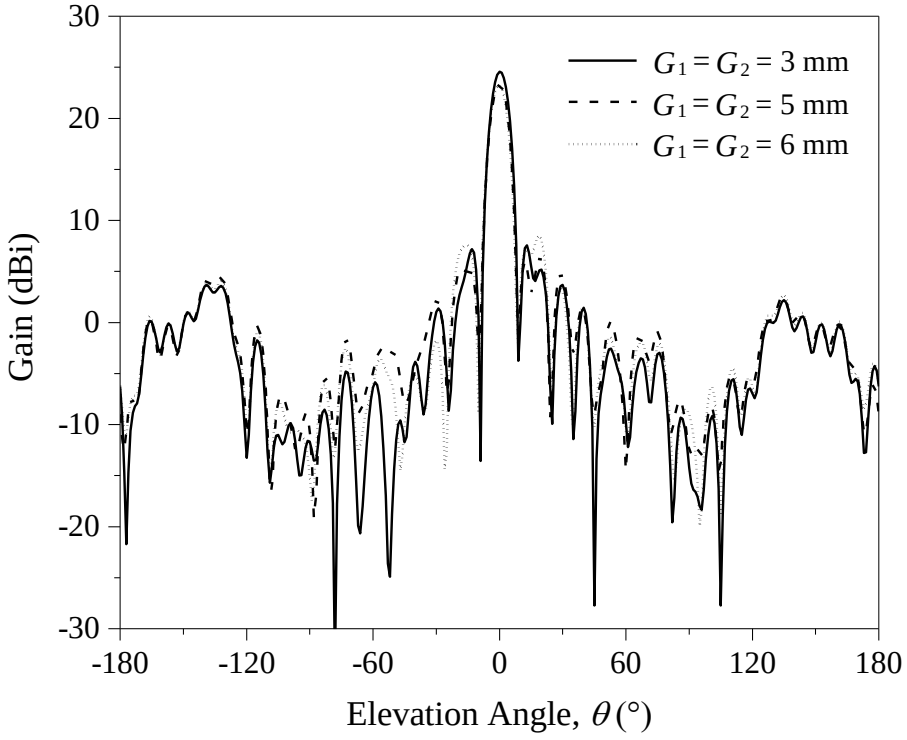

(a)

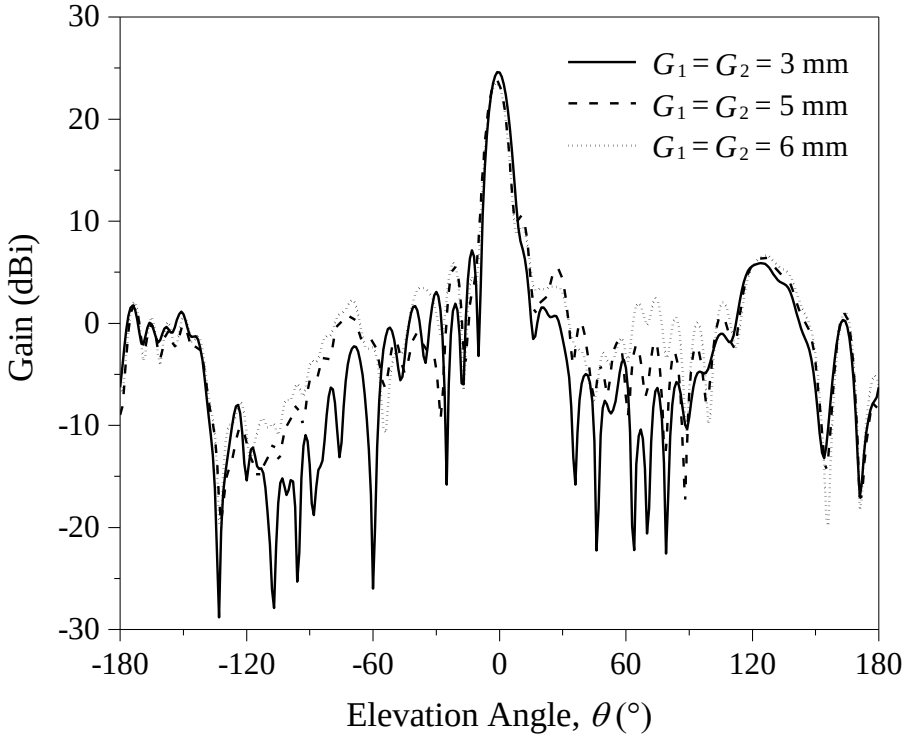

(b)

Figure 3.14: Radiation patterns of the proposed E-patch reflectarray with different gap separations (G_1 and G_2) between two adjacent arms. (a) *E* - and (b) *H* – planes.

3.6.4 Foam Thickness

The thickness of the foam (h) is now varied and its reflection phase response is shown in Figure 3.15. It is observed that the reflection phase range increases when h is increased from 2 mm to 7 mm. For the cases of h = 6 mm and 7 mm, the gradients of the phase curves become very steep when the arm length (L_1) goes beyond 16 mm, and this portion cannot be used for designing reflectarrays limited by our fabrication precision. As a result, the achievable phase range ~260° is not sufficient for designing a full-fledge reflectarray. On the other hand, for the case of h = 2 mm, the unit element is able to produce a phase range of 327°, which is slightly less than one full cycle (360°). The radiation patterns of the reflectarray with h = 4 mm, 6 mm and 7 mm are shown in Figure 3.16. As can be seen from the figure, the side lobes of the reflectarray increase when the thickness of the foam is increased from 4 mm to 7 mm. The highest antenna gain is observed when h is set to 4 mm. In this case, the reflectarray with foam thickness of 4 mm is selected as it has radiation with the lowest side- and back-lobes levels, resulting in high front-to-back ratio.

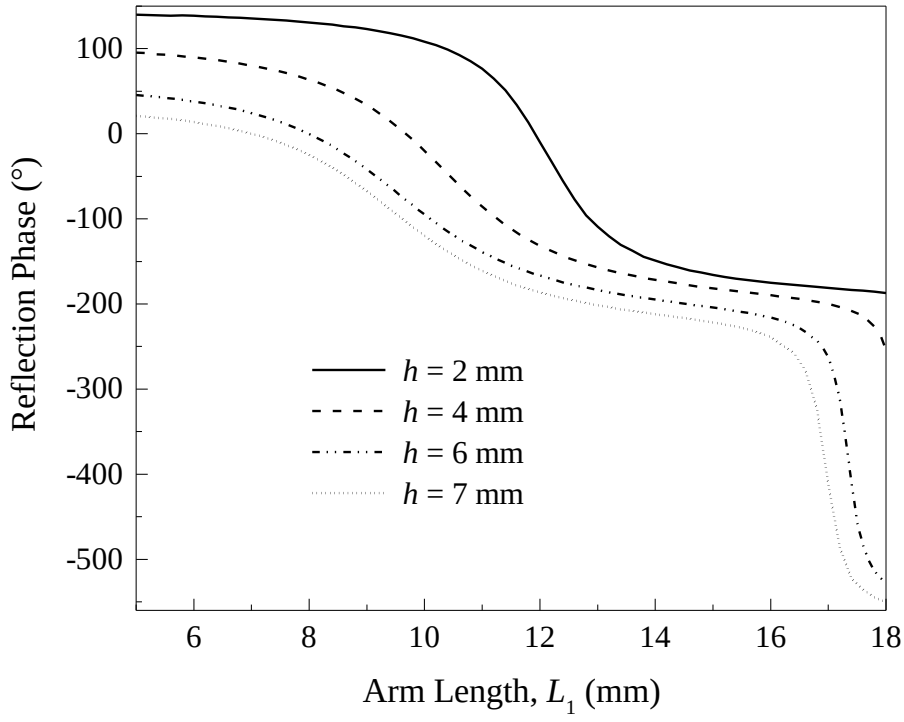

Figure 3.15: The effects of foam thickness (h) on the reflection phase of the E-patch reflectarray unit element.

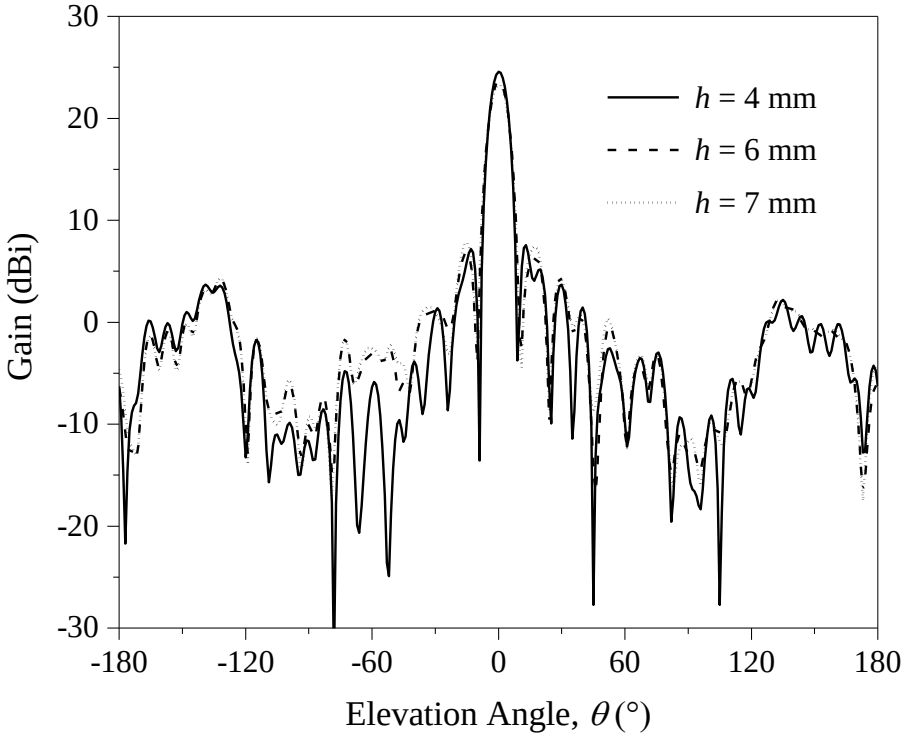

(a)

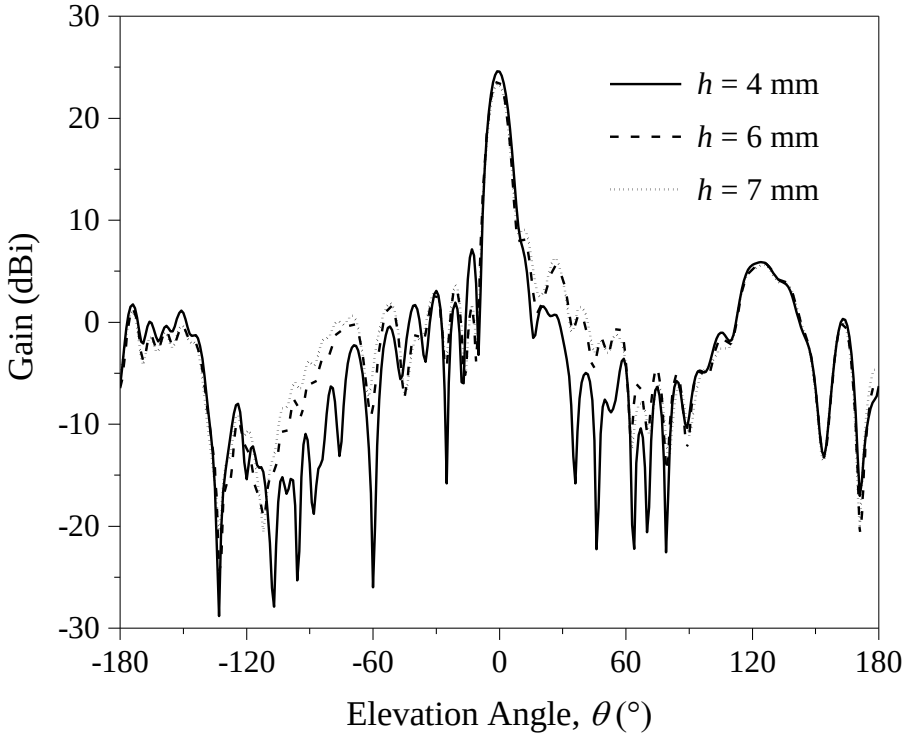

(b)

Figure 3.16: Radiation patterns of the proposed E-patch reflectarray with different foam thicknesses. (a) *E* - and (b) *H* - planes.

3.6.5 Centre Arm Width

Next, the effects of the centre arm width (W_2) on the reflection and radiation characteristics are studied. In this case, the centre arm width is changed from 1.5 mm to 4 mm and their reflection phase curves are plotted in Figure 3.17. With reference to Figure 3.17, it can be observed that the total phase range increases, and the gradient of the phase curve becomes steeper when W_2 is increased from 1.5 mm to 4 mm. Although a slow gradient of the phase curve is observed for W_2 = 1.5 mm, it has the total phase range of only 300° which is not sufficient for designing a large-size reflectarray. For W_2 = 4.0 mm, a very steep gradient of the phase curve is observed across the design

dimensions and thus, it is not suitable to be used for designing reflectarray as it requires very tight fabrication tolerances. For W_2 = 3.0 mm, although it has a total phase range of much larger than that for W_2 = 2.0 mm, a steeper gradient of phase curve is observed if compared with that for W_2 = 2.0 mm. The radiation patterns of the reflectarray with W_2 = 2 mm, 3 mm and 4 mm are depicted in Figure 3.18. As W_2 is varied from 2 mm to 4 mm, it is observed that the antenna gain at θ = 0° reduces with the backlobe increased. This results in lower front-to-back ratio which is undesirable in the reflectarray design. Also, an increment in the side lobe levels is observed when W_2 is increased.

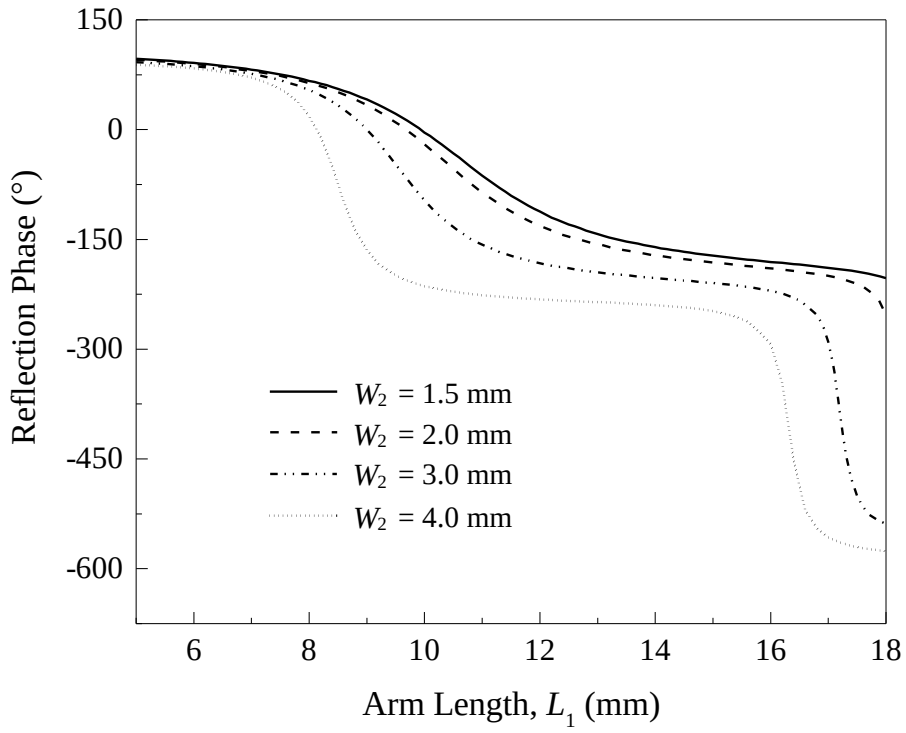

Figure 3.17: The effects of centre arm width (W_2) on the reflection phase of the E-patch unit element.

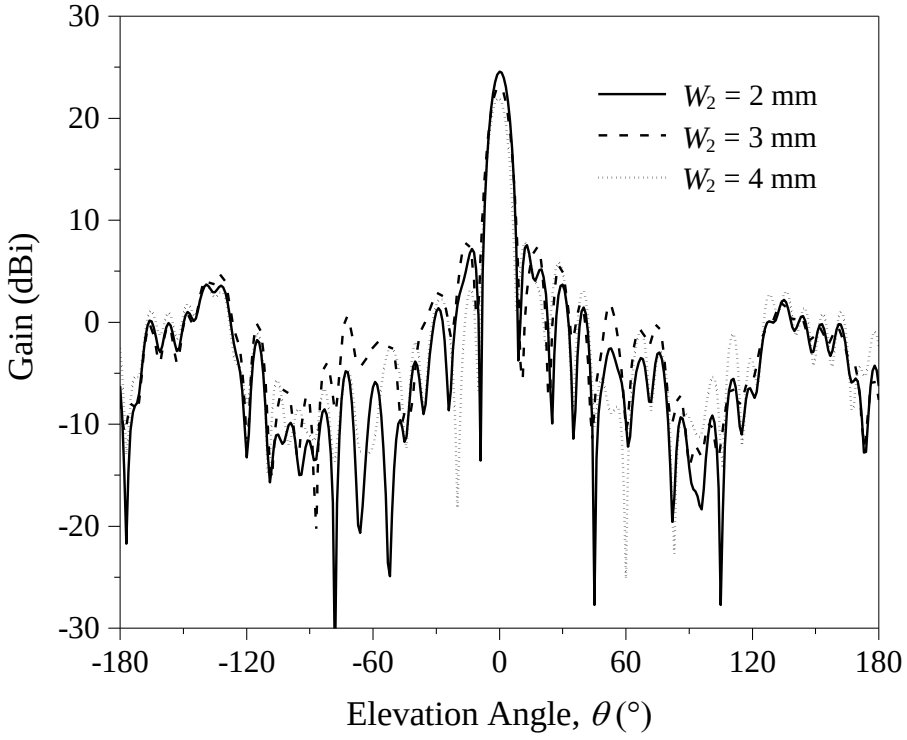

(a)

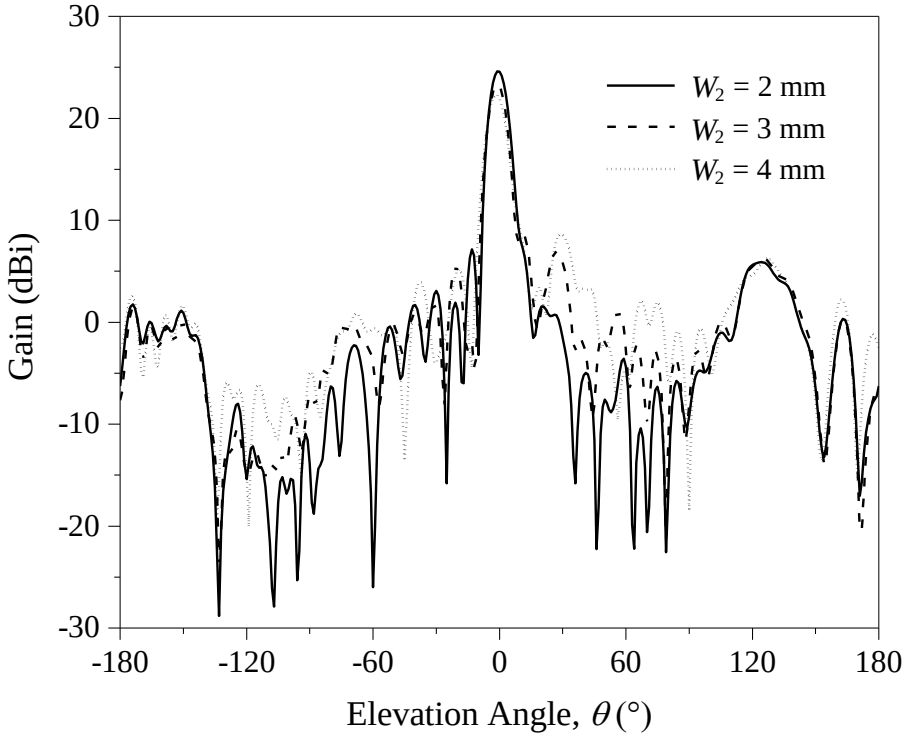

(b)

Figure 3.18: Radiation patterns of the proposed E-patch reflectarray for different centre arm widths (W_2). (a) *E* - and (b) *H* - planes.

3.6.6 Centre Arm Length

The centre arm length (L_2) is now varied from 5 mm to 11 mm and the reflection phase curves are illustrated in Figure 3.19. With reference to Figure 3.19, the gradient of the phase curve becomes steeper when L_2 is lengthened. It is noticed that an almost equal amount of total phase range is achieved for L_2 = 5 mm, 7 mm, 9 mm and 11 mm. On the other hand, a minor decrement in the antenna gain of the main lobe is observed when L_2 is increased from 7 mm to 11 mm, as depicted in Figure 3.20. For the case of L_2 = 9 mm and 11 mm, larger side lobes are observed when compared with that for L_2 = 7 mm.

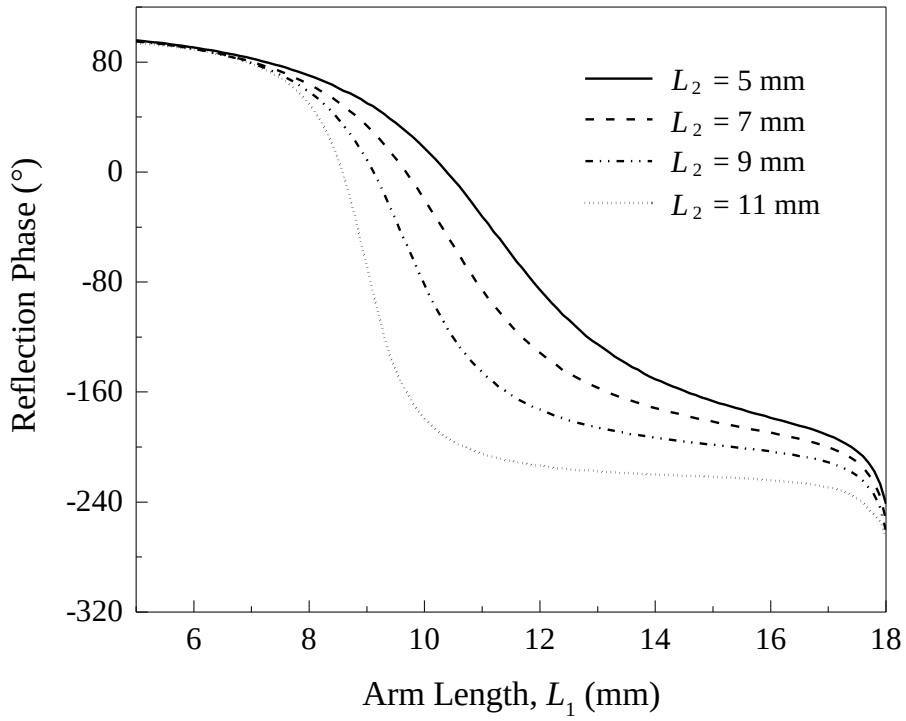

Figure 3.19: The effects of centre arm length (L_2) on the reflection phase of the E-patch unit element.

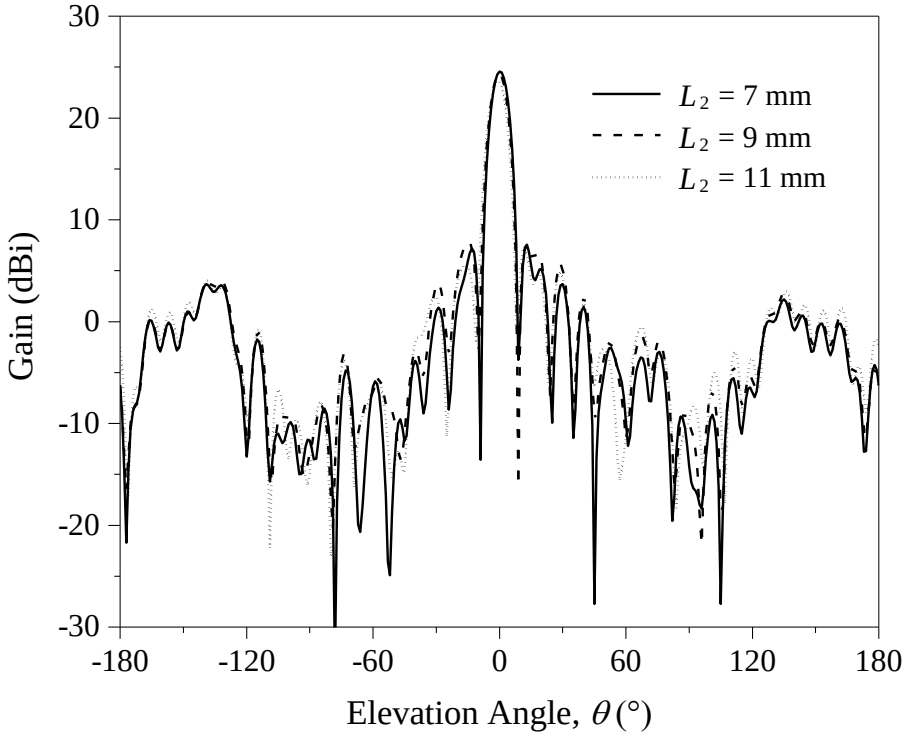

(a)

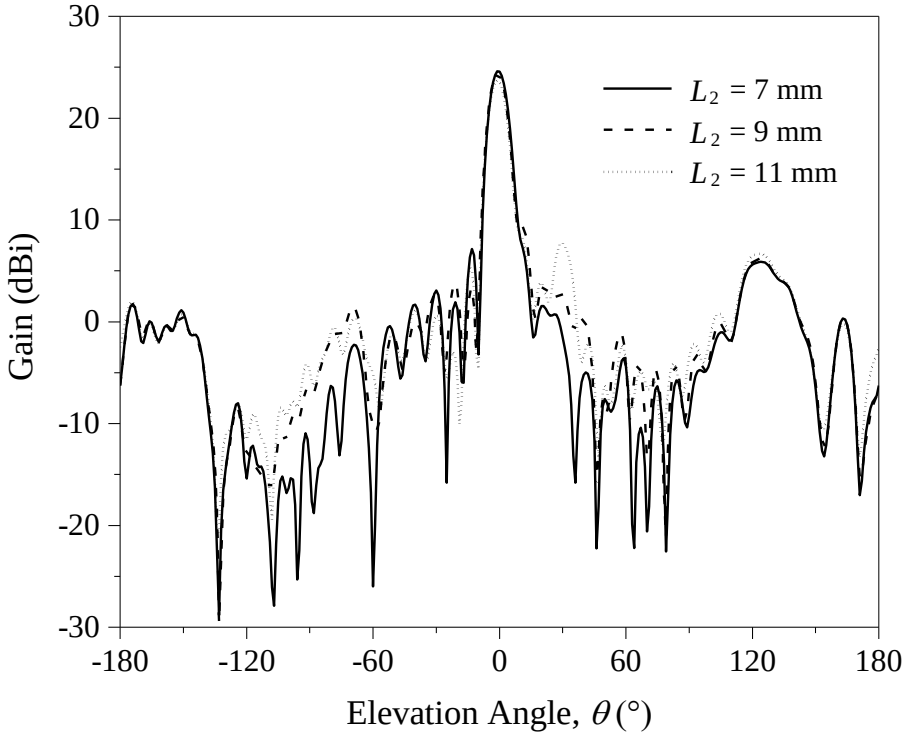

(b)

Figure 3.20: Radiation patterns of the proposed E-patch reflectarray for different centre arm lengths (L_2). (a) *E* - and (b) *H* - planes.

3.6.7 Unit Cell Size

The effects of the unit cell size (L) on the reflection characteristics are now studied. The reflection phase curves for L = 0.606λ, 0.658λ and 0.711λ are almost overlapping, as can be seen from Figure 3.21. The cell size is translated into separation distance between two adjacent elements when the unit element is employed for designing a full-fledge reflectarray. The radiation patterns for separation distances of 0.606λ, 0.658λ and 0.711λ are depicted in Figure 3.22. Antenna gain in the boresight direction is found to be larger with lower backlobe level when the separation distance is increased. This can further improve the front-to-back ratio, which is much desirable. In our design, however, the separation distance is selected to be L = 0.658λ as the side lobes are lower for this case.

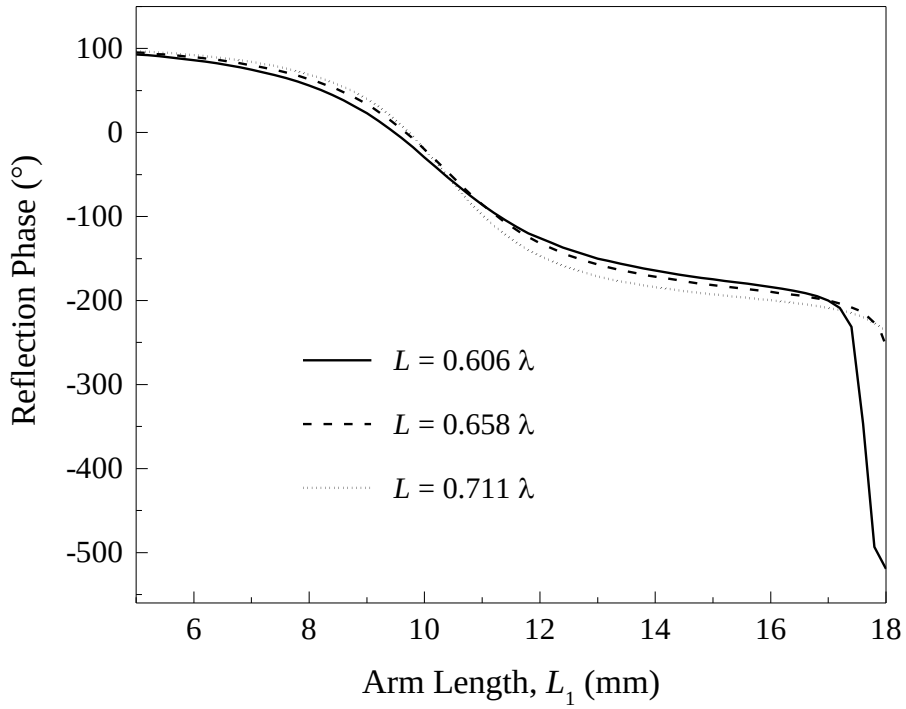

Figure 3.21: The effects of the unit cell size (L) on the reflection phase response of the proposed unit element.

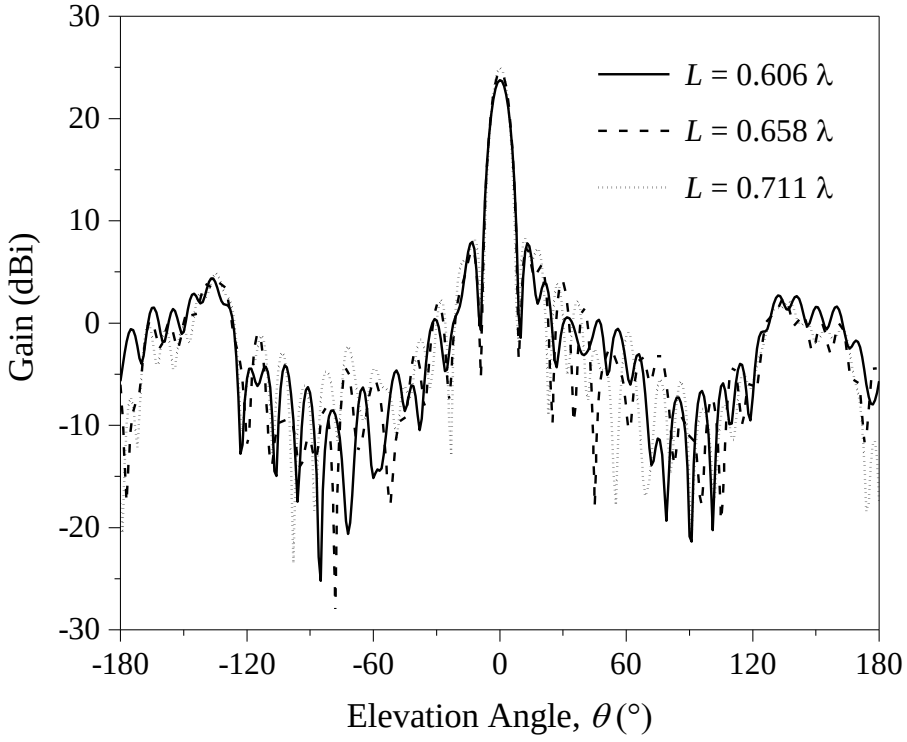

(a)

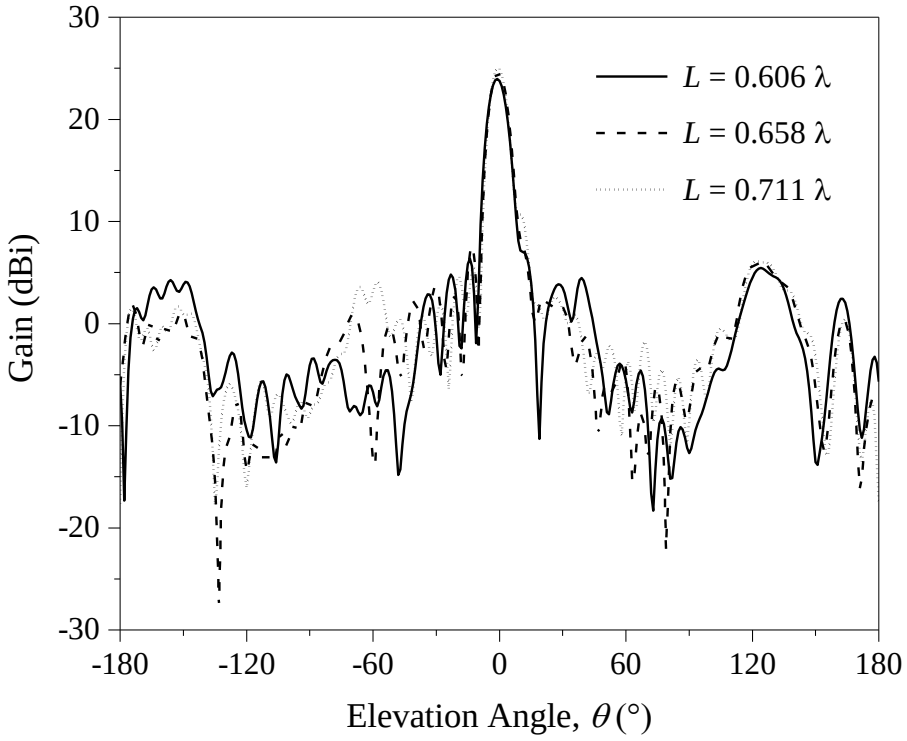

(b)

Figure 3.22: Radiation patterns of the proposed E-patch reflectarray with different unit cell sizes. (a) *E* - and (b) *H* - planes.

3.6.8 *F/D* Ratio

With the use of $L = 0.658\lambda$ and the reflectarray dimension of $D = 11L = 275$ mm, the radiation patterns of the reflectarray for different *F/D* ratios are illustrated in Figure 3.23. It is obvious that the front-to-back ratio decreases when the *F/D* ratio is increased from 0.85 to 0.95. This can be caused by spill-over losses when the focal distance is increased. However, the ratio can't be made too small as it has to satisfy the far-field criterion. In our case, it is found that the reflectarray design with *F/D* = 0.85 and focal distance of 233.75 mm has given the best radiation performance.

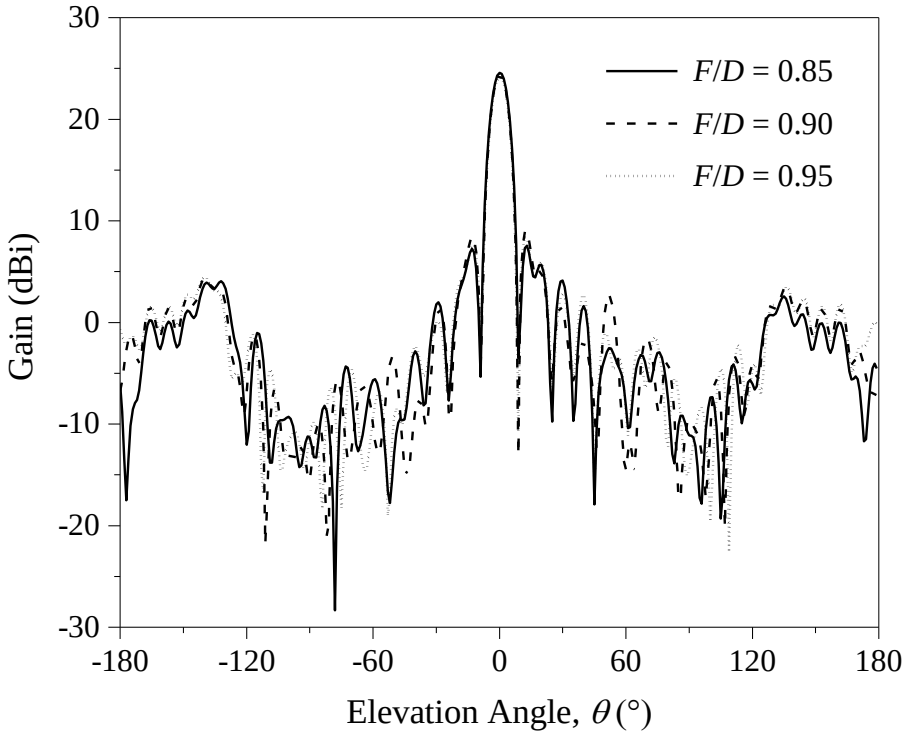

(a)

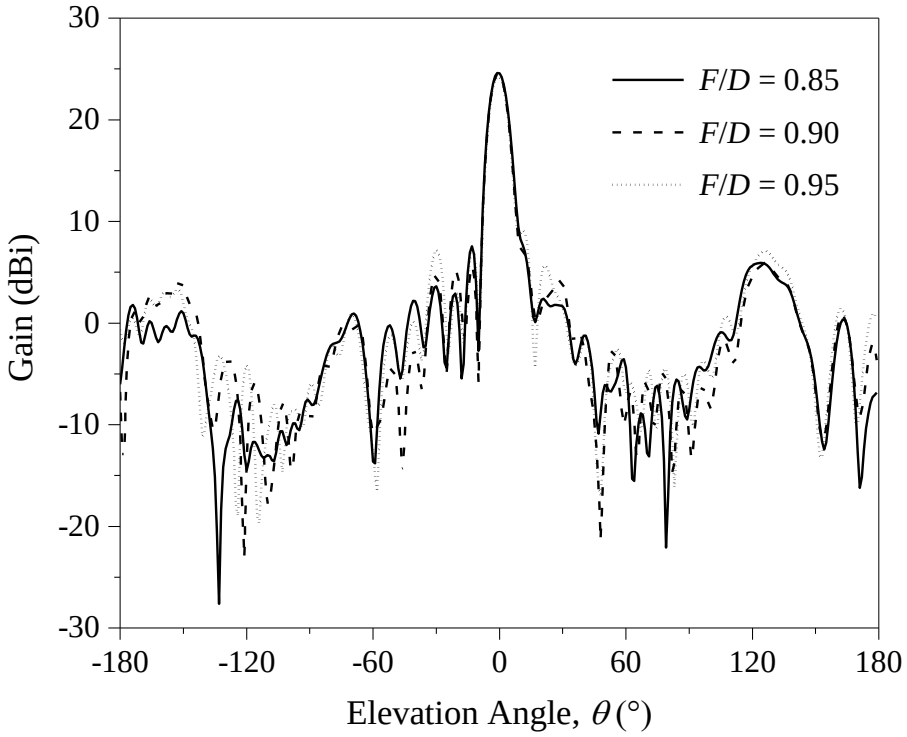

(b)

Figure 3.23: Radiation patterns of the proposed E-patch reflectarray with different *F*/*D* ratios. (a) *E* - and (b) *H* - planes.

3.6.9 Feeding Angle

Next, the feeding angle (θ) is studied. It can be observed from the unit cell simulation that the reflection phase does not vary much when the proposed unit element is fed with an incident angle of 10°, 20° and 25°, as shown in Figure 3.24. But it has much effect on the radiation patterns. With reference to Figure 3.25, it is noticed that the side and back lobes of the reflectarray become larger when the feeding angle is increased from 10° to 25°. To reduce the effect of feeder blockage, the feeding angle of 20° is selected for our design.

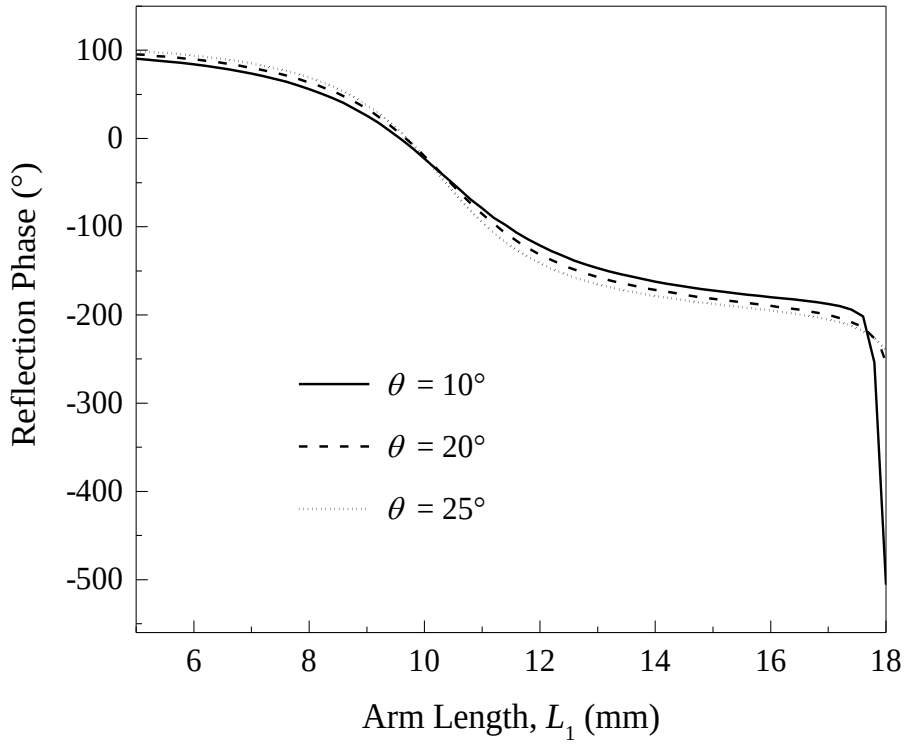

Figure 3.24: The effects of feeding angle (θ) on the reflection phase of the E-patch unit element.

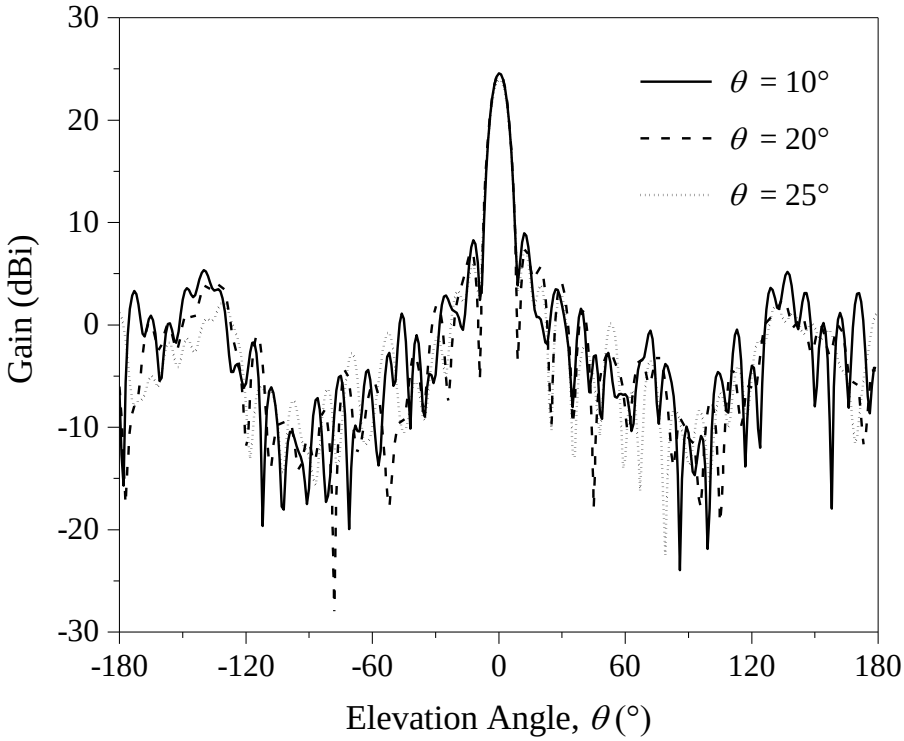

(a)

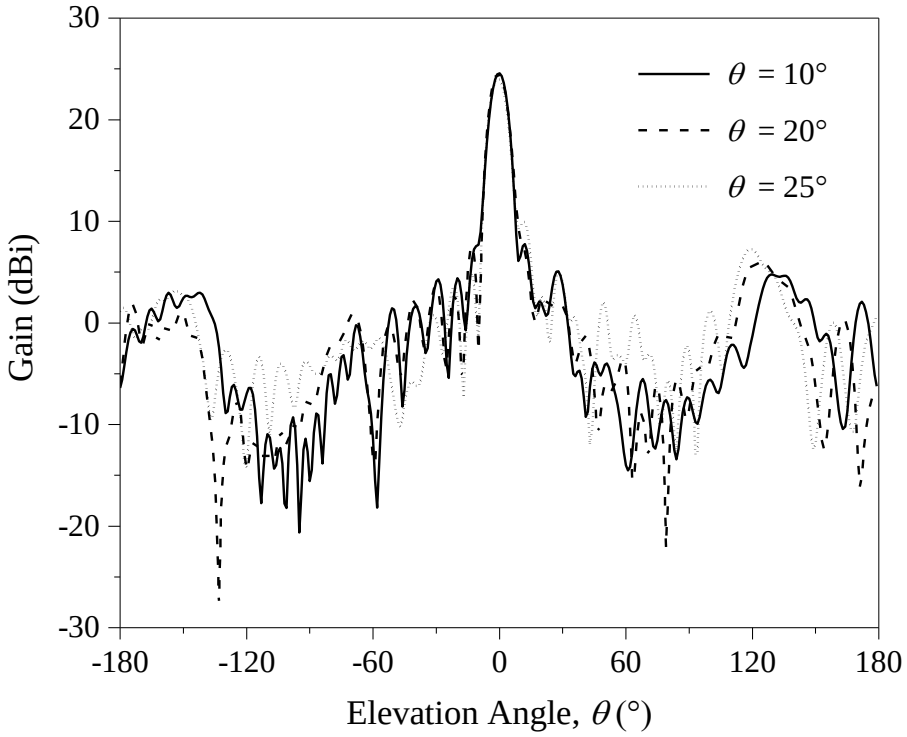

(b)

Figure 3.25: Radiation patterns of the proposed E-patch reflectarray for different feeding angles (θ). (a) *E* - and (b) *H* - planes.

3.6.10 Position of Shorting Via

Lastly, the effects of the position of the shorting via on the reflection performances are studied. Shifting the via in the *x*-direction (S_X) is first analyzed. When the via is offset by S_X = 0.5 mm and 1 mm, it can be observed that it has no effect on the reflection phase curve, as illustrated in Figure 3.26. On the other hand, moving the via in the *y*-direction (S_y) has effect on the reflection phase curve, as depicted in Figure 3.27. In this case, the via position is varied vertically (S_y) from 2 mm and 4 mm from the top edge of the centre

arm. As can be seen from Figure 3.27, varying S_y introduces minor change in the gradient of the phase curve. Figure 3.28 shows the radiation patterns of the reflectarray with S_y = 2 mm, 3 mm and 4 mm. With reference to Figure 3.28, it can be observed that shifting the via position vertically causes larger side lobes and a reduction in the main lobe gain by ~0.5 dBi.

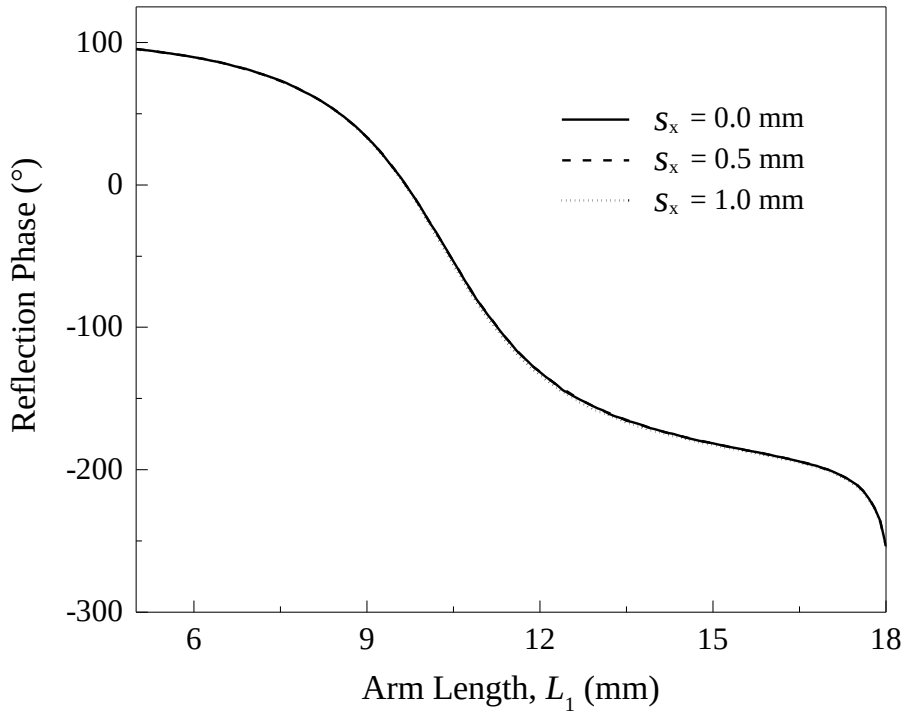

Figure 3.26: The effects of shift in via position (to *x*-direction, S_x) on the reflection phase of the E-patch unit element.

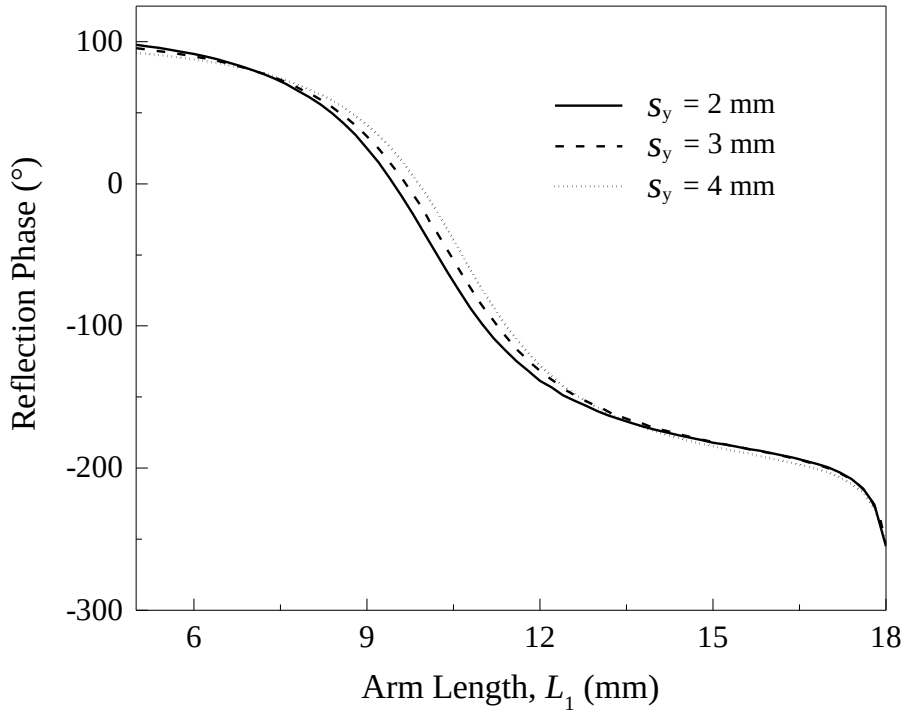

Figure 3.27: The effects of shifting the via position (to the *y*-direction, s_y) on the reflection phase of the E-patch unit element.

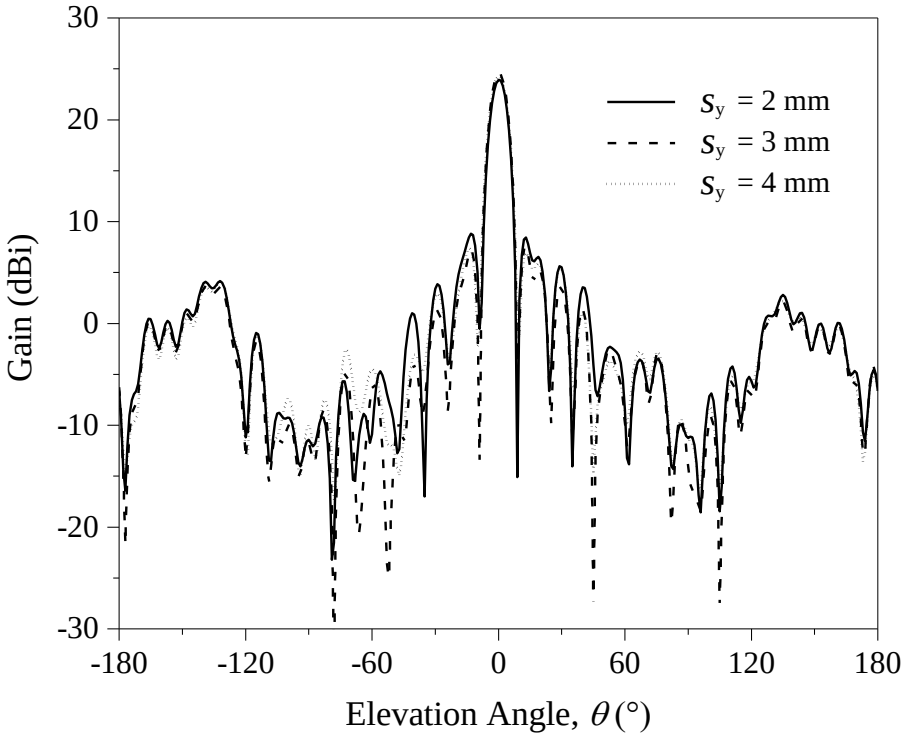

(a)

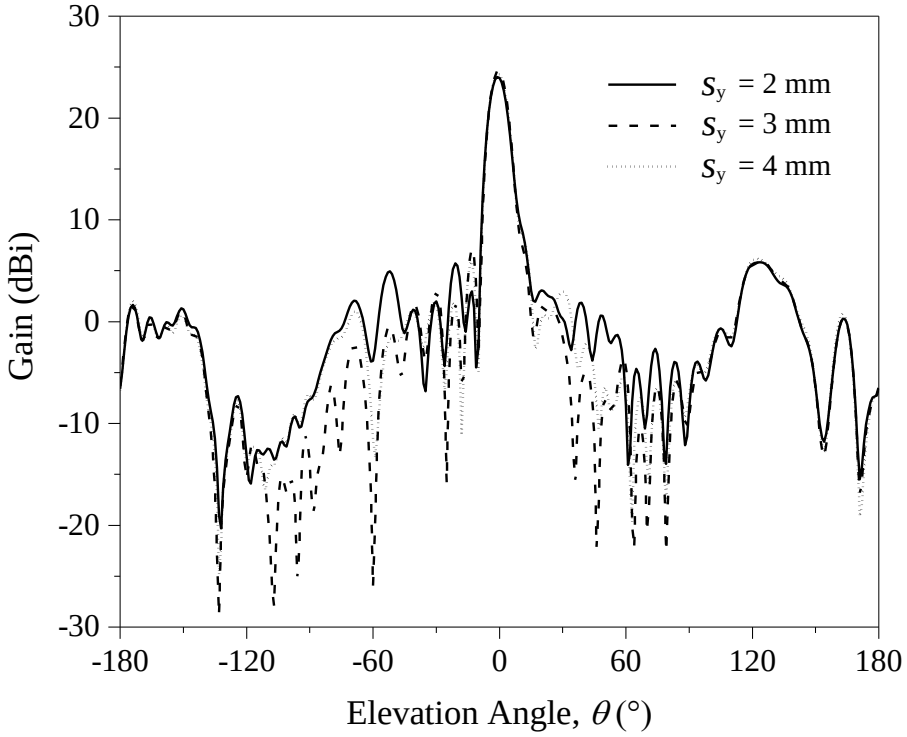

(b)

Figure 3.28: Radiation patterns of the proposed E-patch reflectarray for different via positions (to *y*-direction, S_y). (a) *E* - and (b) *H* - planes.

3.7 Conclusion

A single-layer E-patch reflectarray has been proposed for broadband applications. The unit element has extremely small reflection magnitude and a phase range of ~360º. With the use of this element, a full reflectarray has been designed and fabricated. Measurement shows an antenna gain of ~23.7dBi and a -1dB gain bandwidth of 8.1%. Parametric analysis was conducted and it was found that the radiation performance of the full reflectarray can be further optimized by manipulating some of the design parameters such as foam thickness, arm length, *F*/*D* ratio, and incident angle. The proposed reflectarray is very simple as it does not require the use of any dielectric substrate. It can provide sufficient phase range using one layer. Also, the antenna is lightweight and it can be manufactured with minimum cost.

CHAPTER 4

CIRCULARLY POLARIZED ELLIPTICAL MICROSTRIP PATCH REFLECTARRAY

4.1 Introduction

Reflectarray has multiple radiating elements arranged in an array form, with equal space between any two adjacent elements. The concept was first presented by Berry et al. in 1963 (Berry et al., 1963), where a non-planar reflectarray was formed by an array of truncated waveguides. However, it is bulky and nonplanar, making the fabrication very troublesome. Later, in (Pozar et al., 1997), a planar microstrip patch-type reflectarray, which consisted of microstrip patch elements of different sizes, was proposed. Its advantages such as flat reflecting surface, light in weight, and easy to manufacture have been of great interest to researchers. Over the years, a myriad of reflectarray elements have been proposed for achieving different specifications. Reflectarray elements that involve sub-wavelength (Liu and Guo, 2012) and multi-resonant element (Deng et al., 2015) are found to be able to achieve broadband characteristics. In (Ghorbani et al., 2015), open-loop patches are used for designing a linearly polarized reflectarray that has dual polarization. Other additional functions, such as beam scanning, can also be performed by integrating varactor diode (Mahmoud et al., 2014) and oscillator (Georgiadis and Collado, 2010) into the reflectarray. Low reflection

magnitude can be easily realized (Yang et al., 2015) by incorporating MEMS switches into the reflectarray design.

Reflectarray elements that can generate circularly polarized (CP) waves are usually preferable. This is because they are less susceptible to interferences and are able to receive any microwave signals regardless of their polarizations. A reflectarray can generate CP waves with either a linearly polarized (LP) or a CP feeding source. To begin with, reflectarrays with CP feeder are reviewed. A reflectarray composed of microstrip ring elements with different rotation angles was found to be able to radiate CP waves (Strassner et al., 2004). Another two CP-fed reflectarrays were proposed by (Huang and Pogorzelski, 1998). Their designs are almost similar where the first design has a variable phase-delaying line attached to the square patch; whereas the second design has an identical phase-delaying line connected to the square patch with variable rotation angle. Instead of rotating the unit element itself, in (Yu et al., 2012), the slot of a split square ring element is rotated to generate phase change. CP reflectarrays that are fed with a LP source are reviewed next. In (Chaharmir et al., 2002), a CP reflectarray element is built from the cross slot with its two arms varied such that the phase difference is always 90°. Then, square patches are placed right on top of the slot, enabling the signals to couple through it. To generate circular polarization in the reradiated waves, the electric field vector of the excitation LP wave source must be aligned in parallel along the 45° line with respect to the arms of the cross slot. This has caused the radiation efficiency to reduce as the elements have to be fed at the

boresight. A detailed explanation on the transformation of LP to CP waves can also be found in (Wu et al., 2005).

Recently, much attention is given to designing CP reflectarray elements that are able to achieve broadband characteristics. However, this task is usually very challenging due to the narrow bandwidth nature of the microstrip element. A unit element consisting of four circular microstrip patches loaded with phase-delaying lines (Malfajani and Atlasbaf, 2012a) is found to be able to produce low axial ratio. Nevertheless, the element design becomes very complex as it requires proper arrangement of the four circular patches. Later, in (Zhao et al., 2013), it was discovered that single-layer multiple-resonance elements, such as double-ring and I-ring shaped elements, are able to produce broadband CP operation. In (Malfajani and Atlasbaf, 2012a; Zhao et al., 2013), the angular rotation technique has been employed for achieving wide CP performance. Similar technique has also been applied on the slotted hollow ring element (Chen et al., 2015), the ring-with-stub element (Guo et al., 2015), and the single slot-ring element (Yu et al., 2009). In (Zhao et al., 2010), the dimension of the subwavelength element was varied and it was found that the reflectarray was able to offer an axial ratio bandwidth of 11%. But it was very troublesome to tune that reflectarray element as it involved two design parameters. Later, it was demonstrated in (Ren et al., 2011) that a dual-layer T-shaped element with one length varied can also provide wideband CP bandwidth.

In this chapter, for the first time, the TM_{11} modes of two stacked elliptical microstrip patches are employed for designing a broadband circularly polarized (CP) reflectarray. A linearly polarized horn is used as the excitation source. Instead of using the conventional angular rotation technique, in the proposed design, the major axes of the elliptical patches are varied to provide a wide reflection phase range of 550^{o}. To start, the structure of the proposed element is shown in Part II. The Floquet method has been adopted for simulating the reflection performances of the proposed element. Design procedure of the full-fledge reflectarray will be given in Part III. And finally, discussions on the simulated and measured results are provided in Part IV.

4.2 Unit Element Analysis

The proposed reflectarray element, shown in Figure 4.1, consists of two elliptical microstrip patches, which are fabricated on two dielectric substrates (RO4003C) with dielectric constant of $\varepsilon_{r1} = \varepsilon_{r2} = 3.38$ and thicknesses of $h_1 = h_2 = 1.524$ mm. It has a square cell size of $L \times L$, where L is 14 mm in this case. The top and middle patches, aligned to their center points, are designed to have (major axis: $2a_1$ and minor axis: $2b_1$) and (major axis: $2a_2$ and minor axis: $2b_2$), respectively. With reference to Figure 4.1(a), the top patch is rotated anticlockwise (θ_t) while the middle patch is rotated clockwise (θ_b). The bottom surface of Substrate 2 is laminated with a copper layer to act as ground. In our design, θ_t and θ_b are made to be equal (45°) while $2a_1 = 2a_2$ and $2b_1 = 2b_2$. The major axes of the top and middle patches are changed in

the range of 2 mm – 14 mm to generate phase shifts and their minor axes are varied simultaneously following $2b_1 = 2a_1 / r_1$ and $2b_2 = 2a_2 / r_2$, where r is the ratio of major and minor axes ($r_1 = r_2 = 2$ in this case). In other words, the minor axes of $2b_1$ and $2b_2$ are changing with ($2a_1$, $2a_2$).

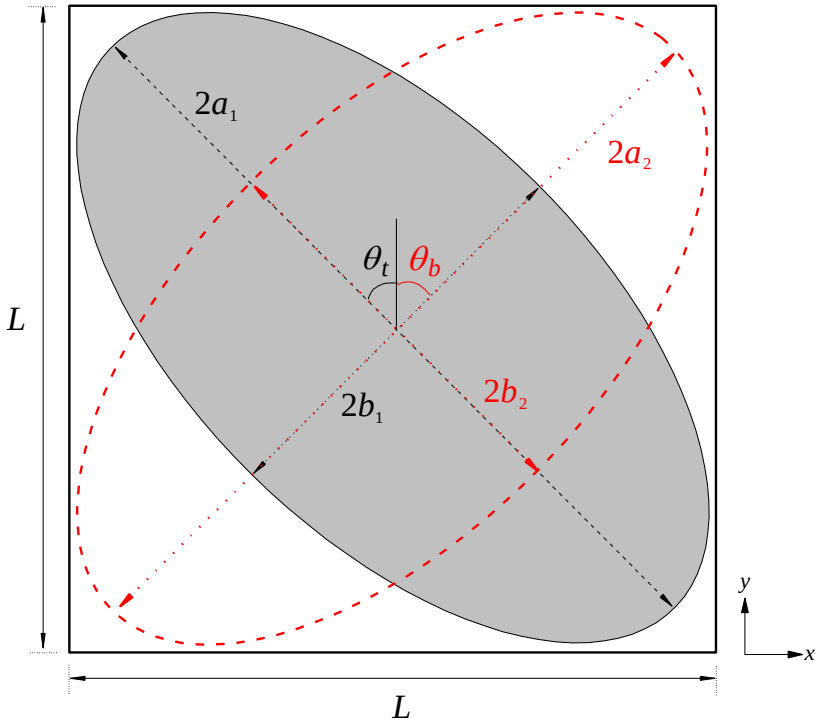

(a)

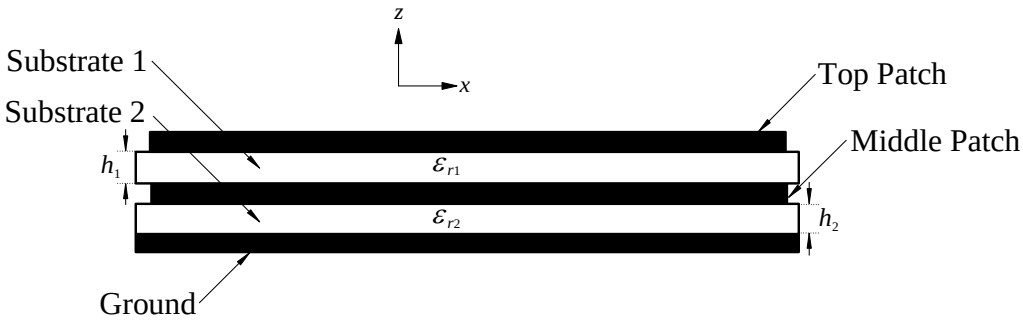

(b)

Figure 4.1: (a) Top view, where the middle patch is highlighted in dotted lines. (b) Side view of the proposed double-layered elliptical patch element.

To study its reflection characteristics, the proposed unit element is simulated inside a Floquet cell using the CST Microwave Studio, shown in Figure 4.2. A *y*-polarized plane wave is launched at the wave port on one end of the Floquet cell while the proposed reflectarray element is placed on the other end at a distance of 76 mm (in this case) from the wave port. Varying the distance will not affect the reflection performance much, as the reference plane is always de-embedded near to the top surface of the proposed element. In simulation, the unit element is duplicating itself in a periodic manner so that the mutual coupling effect between the elements is accounted for. The four side walls of the Floquet cell are defined to be periodic boundaries, as depicted in Figure 4.2.

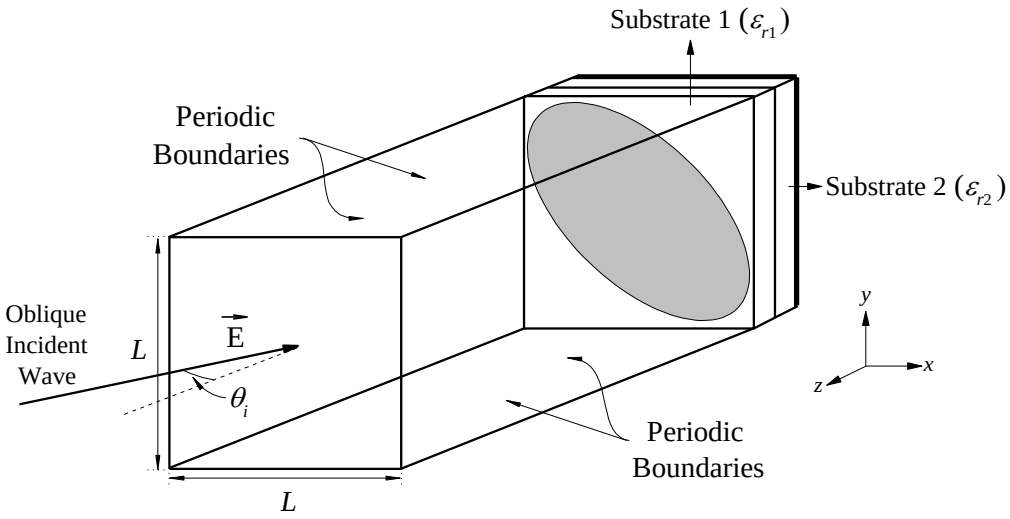

Figure 4.2: Floquet cell for simulating the proposed reflectarray element.

The simulated reflection magnitude and the corresponding phase response of the proposed element are presented in Figure 4.3. As can be seen from Figure 4.3, a reflection phase ($\angle S_{11}$) range of ~550° is achieved at the operating frequency of 10.5 GHz (0.49λ), with its reflection magnitude kept well above ~ -0.5 dB when the major axis ($2a_1$) is changed from 2 mm to 14 mm. To illustrate, the electric field distributions on the top and middle patches are plotted at the geometrical dimensions of $2a_1$ = 7.5 mm and 12.5 mm, as shown in Figure 4.4 and 4.5, respectively. It is observed that the even TM_{11} mode (Wang et al., 1994; Chakrabarty et al., 2012) has been excited in the elliptical patch elements in Figure 4.4(a) and 4.5; while the odd TM_{11} mode is observed on the top patch in Figure 4.4(b). Simultaneous excitation of the two modes has enabled broad phase range.

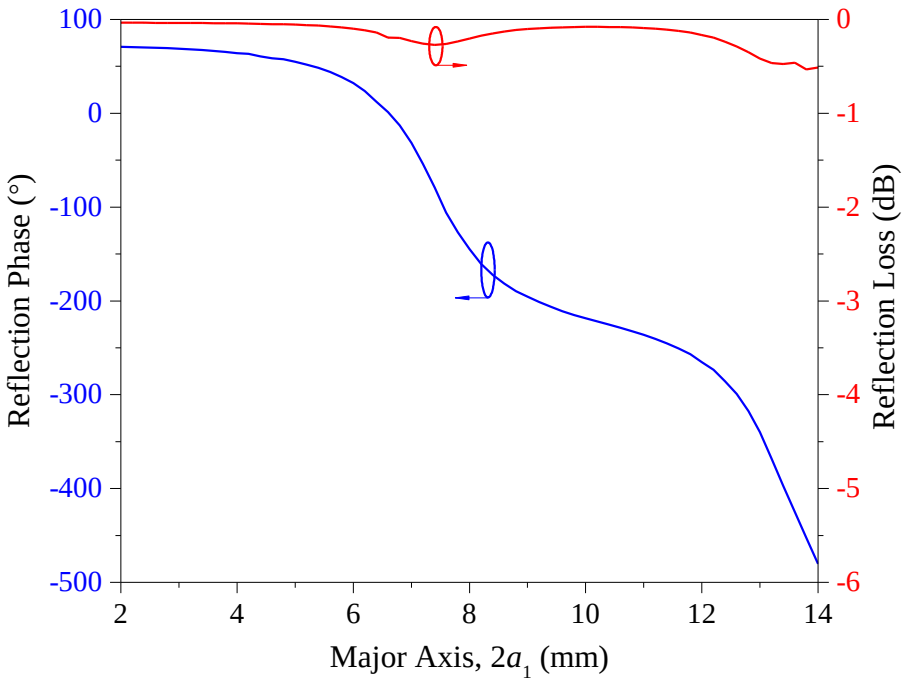

Figure 4.3: Reflection magnitude and its phase response as a function of the major axis ($2a_1$) at 10.5 GHz.

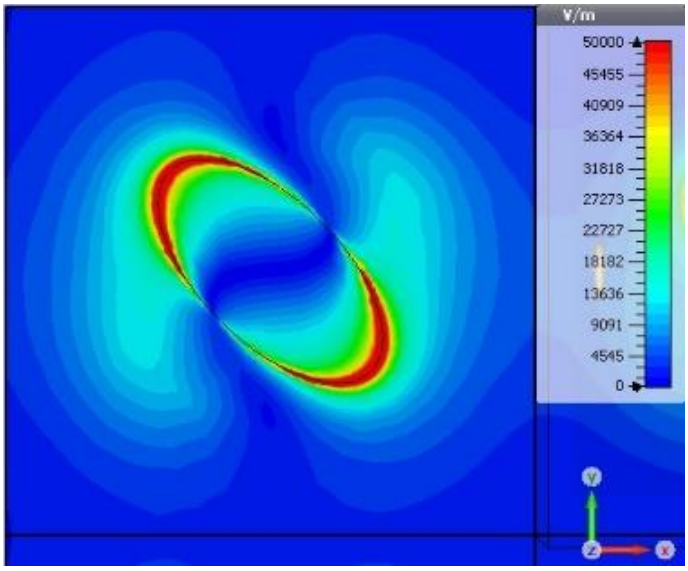

(a)

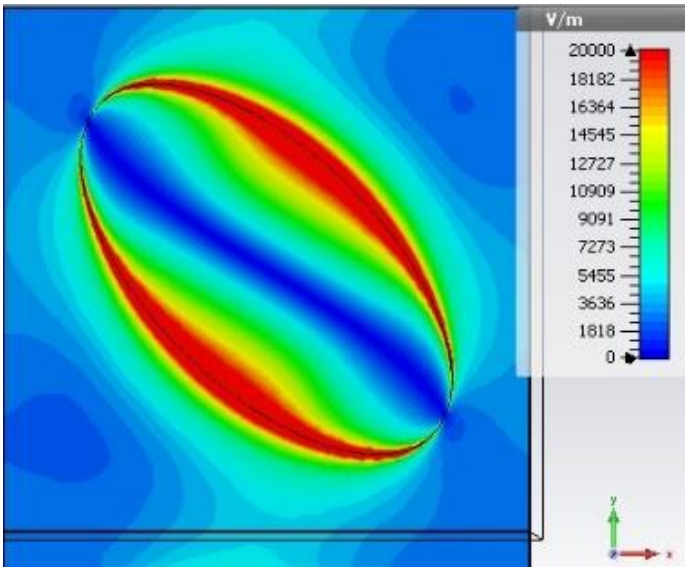

(b)

Figure 4.4: Electric field distributions on the top patch with the major axis of (a) $2a_1$ = 7.5 mm and, (b) $2a_1$ = 12.5 mm at 10.5 GHz.

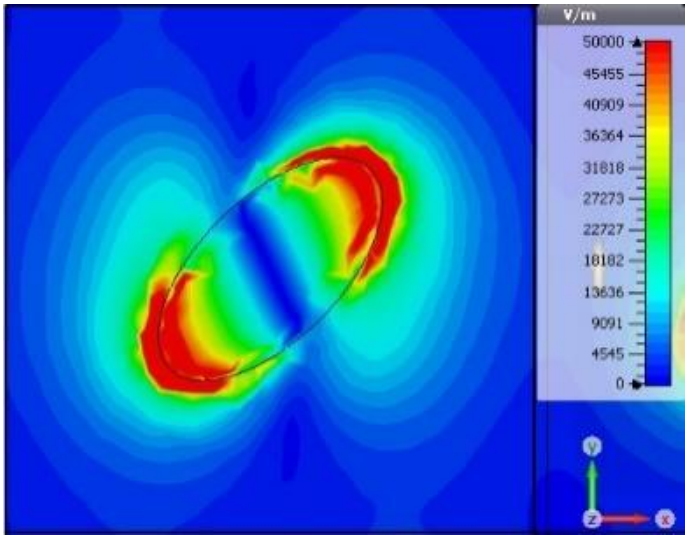

(a)

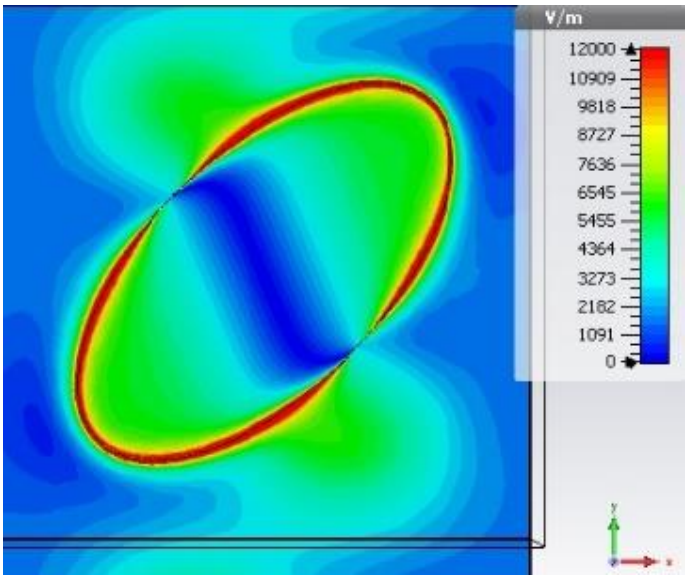

(b)

Figure 4.5: Electric field distributions on the middle patch with the major axis of (a) $2a_1$ = 7.5 mm and, (b) $2a_1$ = 12.5 mm at 10.5 GHz.

4.3 Reflectarray Configuration

With the use of the phase curve in Figure 4.3, the proposed unit element is expanded into an 11 × 11 (121 elements) circularly polarized (CP) reflectarray operating at 10.5 GHz. The CP reflectarray is fed by an X-band (9 GHz – 11.5 GHz) linearly polarized pyramidal horn, which has a measured gain of 10.5 dBi in both the *E*- and *H*- plane at 10.5 GHz. Its 3-dB beamwidth is 46^{o} in both planes. The feed horn is positioned at an incident angle (θ_i) of 20° and a focal distance (F) of 184.8 mm from the center point of reflectarray. The design procedure is briefly described here. First of all, as shown in Figure 4.6, the path P_0 is used as the reference path length and it has a reflection phase of ϕ_0. The wave beam from the feeder has travelled a path length of P_n before reaching the n^{th} element. Path difference between the n^{th} element and the reference can therefore be denoted as ($\Delta P_{n0} = P_n - P_0$) and the corresponding phase difference can be expressed as $\phi_{n0} = \Delta P_{n0}\frac{2\pi}{\lambda}$, which is the extra phase needed by the n^{th} element so that its re-radiated wave ($\phi_n = \phi_0 + \phi_{n0}$) is in-phase with that of the reference element. The geometrical dimension ($2a_1$) that is required to generate the phase ϕ_n can be easily found on the x-axis of the curve in Figure 4.3. Also, the geometrical dimensions for all the radiating elements of the proposed CP reflectarray can be found in Appendix B, along with their reflection phases. The full-fledge CP reflectarray has a total dimension (D) of 154 mm (=11L) and a F/D ratio of 1.2. The reflectarray prototype is fabricated and its photograph is shown in Figure 4.7.

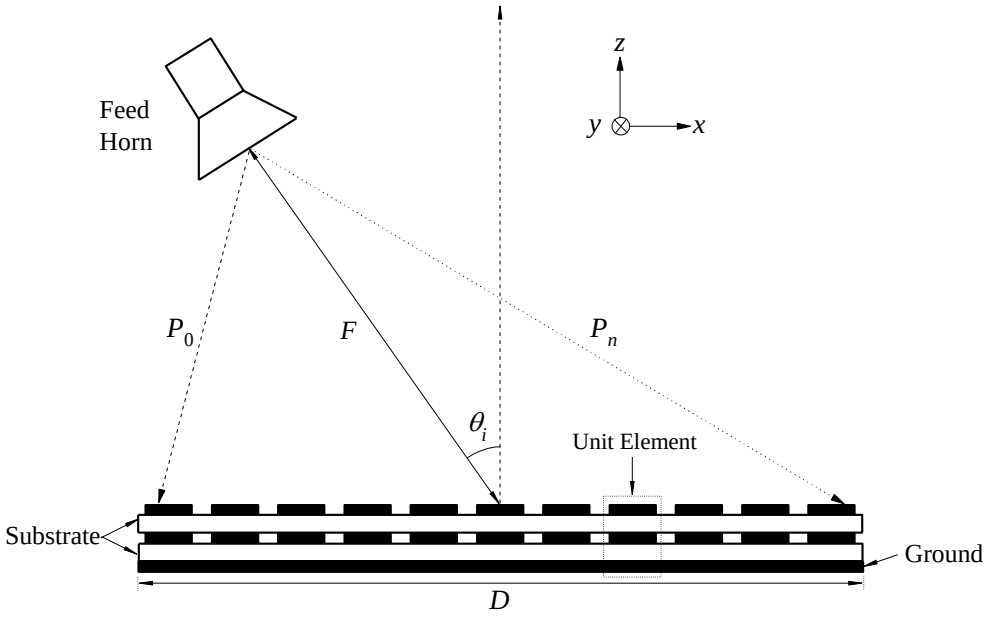

Figure 4.6: Configuration of the proposed circularly polarized reflectarray.

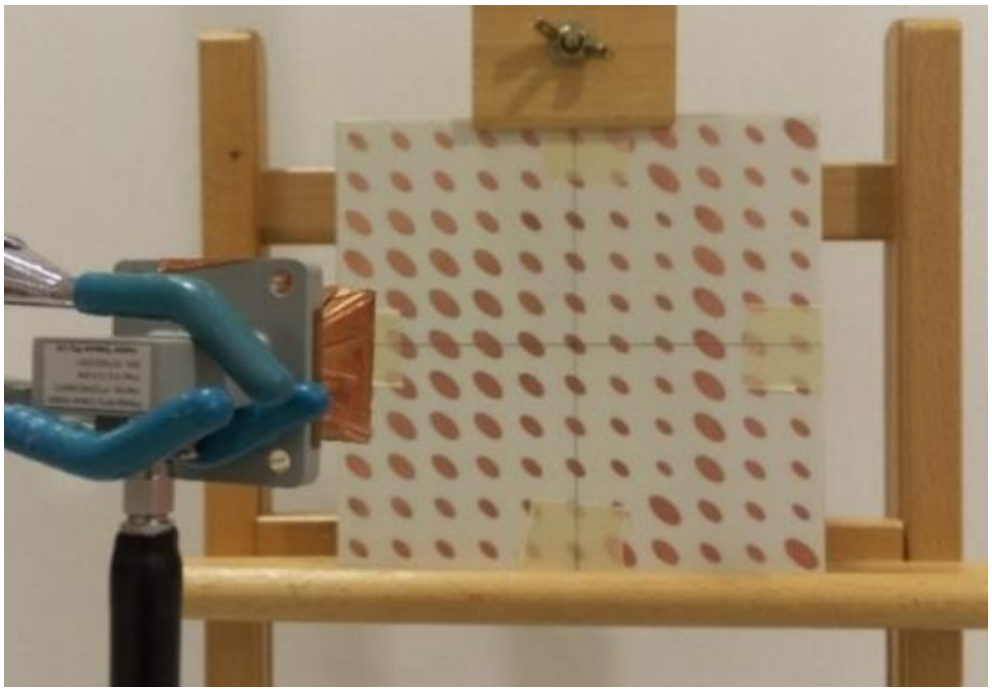

Figure 4.7: Photograph of the fabricated prototype.

4.4 Measurement Setup

Figure 4.8 shows the measurement setup for the CP reflectarray. Measurement is carried out in free space for measuring the antenna gain, axial ratio and radiation patterns of the proposed reflectarray. First, the measurement procedure for the axial ratio is briefly described. A 10.5 GHz transmitting signal with power (P_t) of 10 dBm, which is generated by a signal generator (Rohde & Schwarz SMB100A), is supplied to the reflectarray under test. A linearly polarized (LP) X-band (XB-HA90-18-SMA, 8.2 GHz – 12.9 GHz) pyramidal horn is used as the receiving horn and it is placed at a far-field distance (R) of 4 m from the reflectarray. The horn is connected to a spectrum analyzer (Advantest U3771) for recording the vertical (P_{rv}) and horizontal (P_{rh}) field components radiated by the reflectarray in the direction of θ = 0°. Then, axial ratio is obtained by comparing the P_{rv} and P_{rh} components. Next, the LP horn is replaced by a left- or right-handed polarized conical horn (XB-CPHA- L/R89) for measuring the antenna gain and radiation patterns of the reflectarray. Radiation pattern is measured by changing the angle (θ) of the rotation table and the corresponding antenna gain is calculated using the Friis transmission equation.

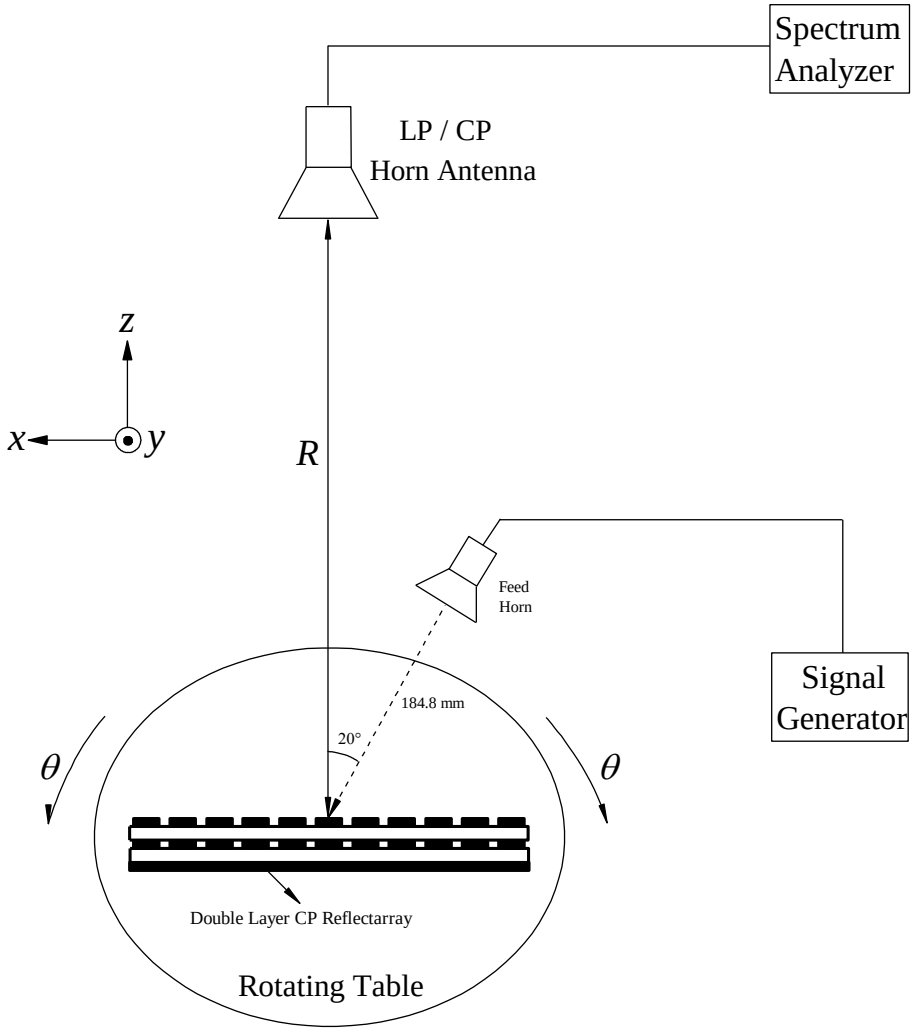

Figure 4.8: Measurement setup for the CP reflectarray.

4.5 Results and Discussion

Simulated and measured radiation patterns of the proposed CP reflectarray are depicted in Figure 4.9 in both the *xz*- and *yz*-planes. It can be seen from the measured radiation patterns that this is a left-handed circularly polarized (LHCP) reflectarray with a measured antenna gain of 20.38 dBi (simulation 20.69 dBi) in the boresight (θ = 0°). The radiation efficiency of the CP reflectarray is found to be 98%. With reference to the figures, the measured and simulated LHCP fields are at least 19 dBi larger than their RHCP components in the boresight direction. The measured aperture efficiency is 30% (simulation: 33%). Figure 4.10 shows the measured and simulated antenna gain at θ = 0° as a function of frequency. A measured -1dB gain bandwidth of 11.6% (simulation 17.8%) is obtained, and it covers the frequency range of 10.2 GHz – 11.45 GHz (simulation 9.7 GHz – 11.6 GHz). The axial ratio performance of the proposed CP reflectarray is illustrated in Figure 4.11. It is observed that the measured 3-dB axial ratio bandwidth covers the frequency range of 10.15 GHz – 11.5 GHz (simulation 10 GHz – 11.3 GHz), with a bandwidth of 12.47% (simulation 12.21%). The discrepancy can be caused by the minor misalignment between the top and middle elliptical patches, which is unavoidable during sample preparation.

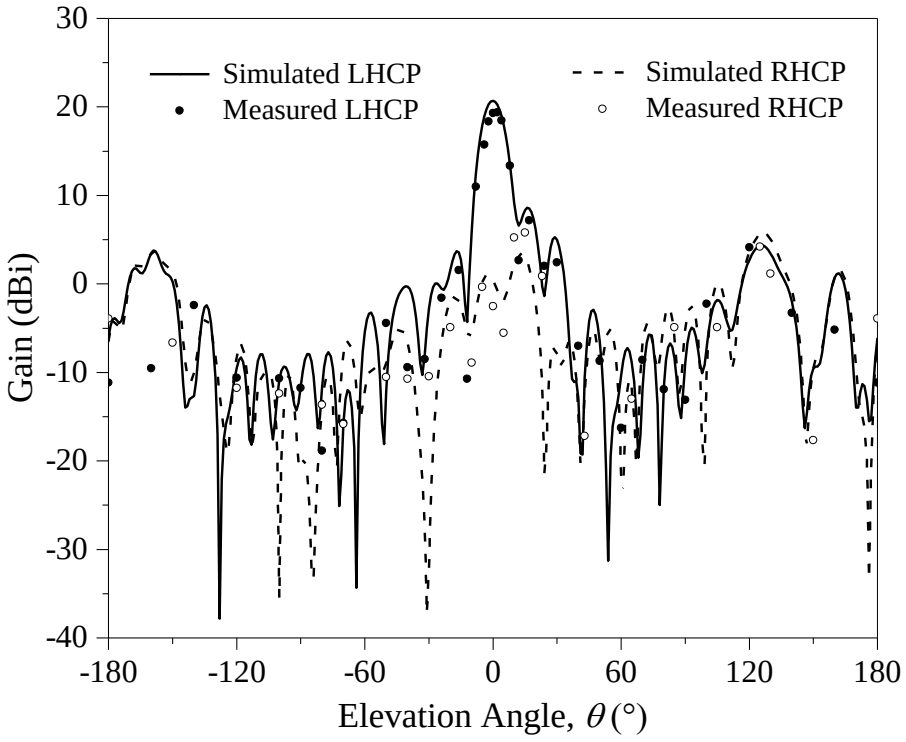

(a)

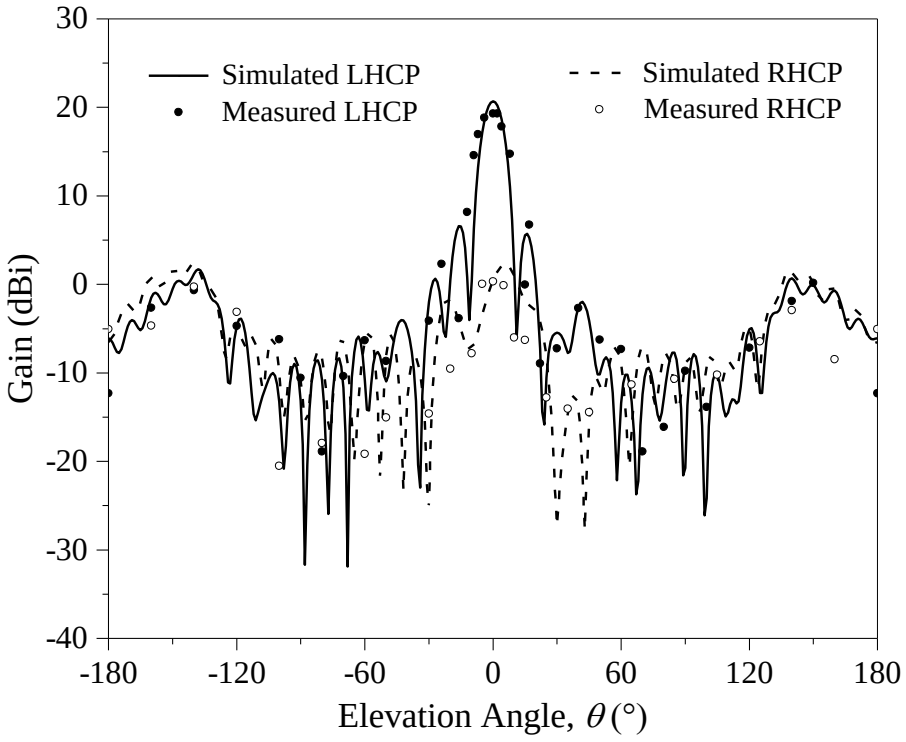

(b)

Figure 4.9: Simulated and measured (a) *xz*- and (b) *yz*- plane radiation patterns of the proposed CP reflectarray.

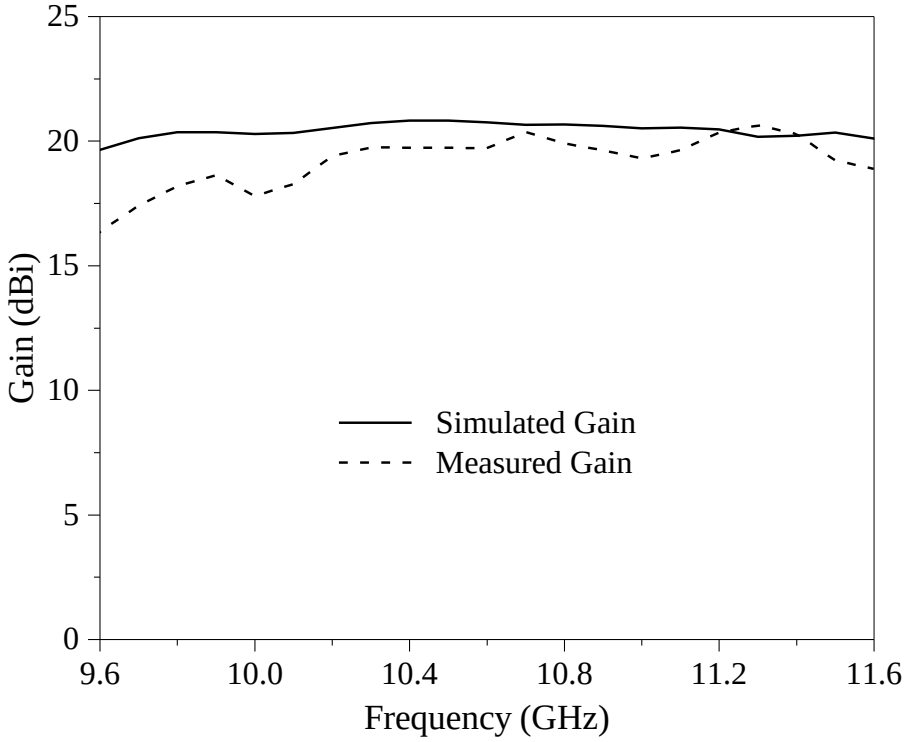

Figure 4.10: Measured and simulated antenna gain of the proposed CP reflectarray as a function of frequency.

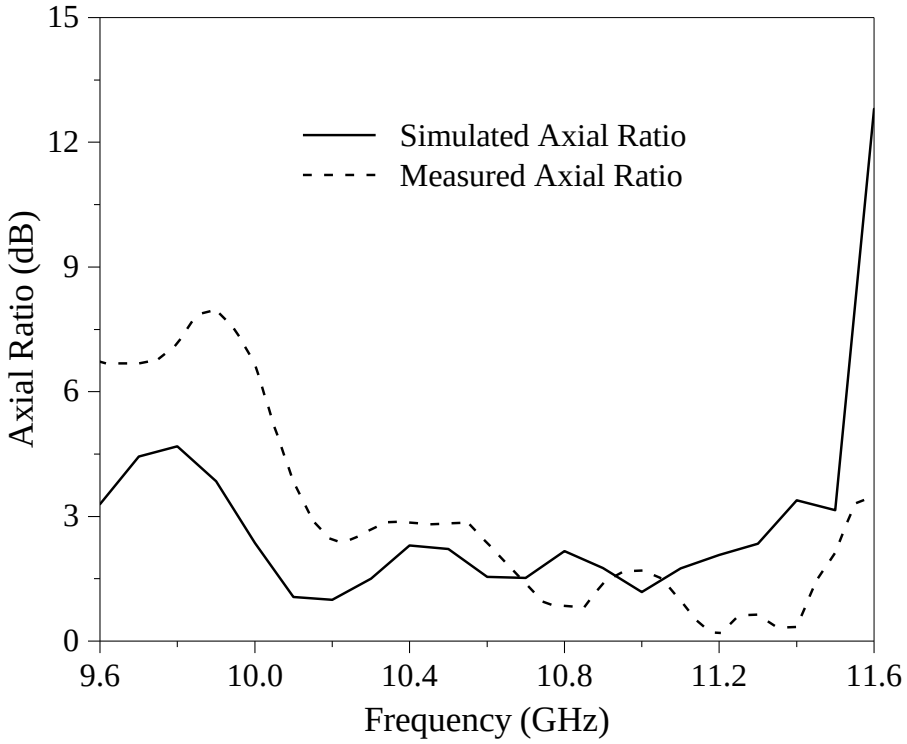

Figure 4.11: Measured and simulated axial ratios of the proposed CP reflectarray.

4.6 Parametric Analysis

Parametric analysis is now performed on some of the critical design parameters for analyzing their effects on the reflection characteristics of the unit element and the radiation performances of the reflectarray. The design parameters such as major to minor axis ratio, elliptical patch inclination angle, unit cell size and etc. are varied and the effects are discussed in detail in the following subsections.

4.6.1 Axis Ratio

To begin, the major to minor axis ratios (r_1 and r_2) of the elliptical patches are varied from 1.9 to 2.1 and the reflection characteristics are analyzed in Figure 4.12. In this case, r_1 and r_2 are set to be equal. Increasing the ratios (r_1 and r_2) from 1.9 to 2.1 causes the gradient of the phase curve to become slower for $2a_1$ beyond 10 mm. For all ratios, the reflection magnitude is less than -1.6 dB and the reflection phase is ~550°. Figure 4.13 shows the radiation patterns of the proposed reflectarray for different major to minor axis ratios. It is observed that the boresight antenna gain for $r_1 = r_2 = 1.9$ is lower by ~ 2.2 dBi than those for $r_1 = r_2 = 2$ and 2.1. Also, side lobes increase when r_1 and r_2 are varied from 1.9 to 2.1. Antenna gain and axial ratio of the proposed reflectarray are illustrated in Figure 4.14. Obviously, the reflectarray with $r_1 = r_2 = 1.9$ is not a good CP antenna as the axial ratio is much larger than 3-dB across the frequency range of 9 GHz to 11.5 GHz. Although the

reflectarray with $r_1 = r_2 = 2.1$ has broader 3-dB axial-ratio bandwidth, it has lower antenna gain across the -1dB bandwidth and higher side lobes compared with that for $r_1 = r_2 = 2$.

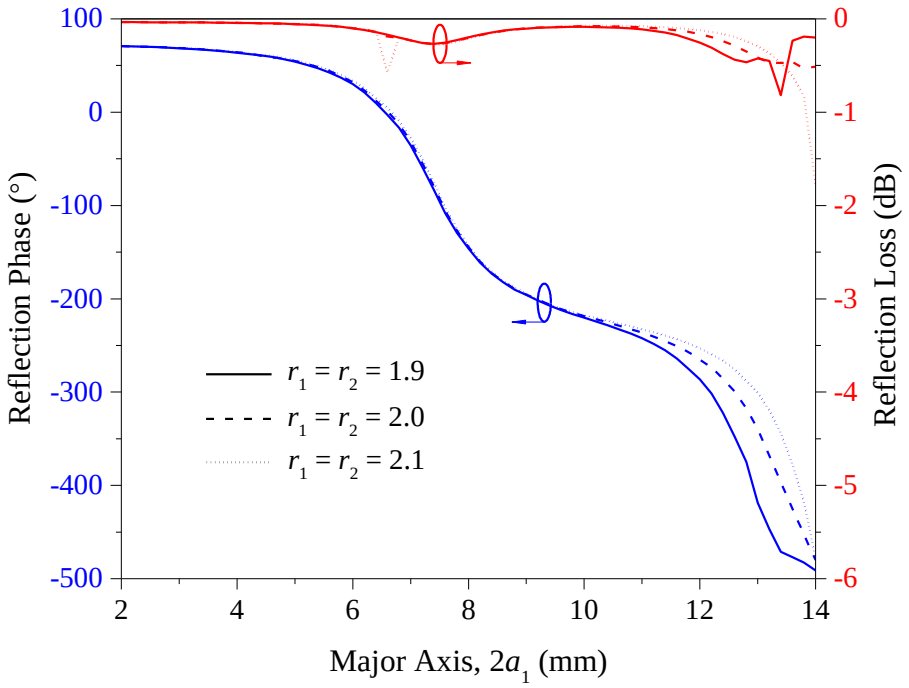

Figure 4.12: Effects of the major to minor axis ratio ($r_1 = r_2$) on the reflection magnitude and reflection phase of the unit element.

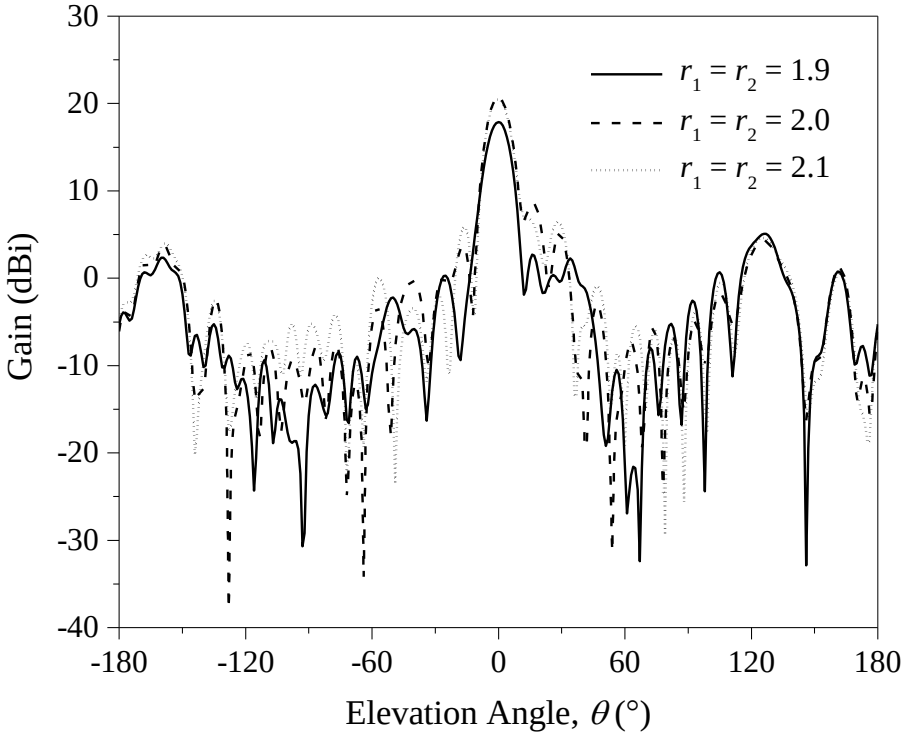

(a)

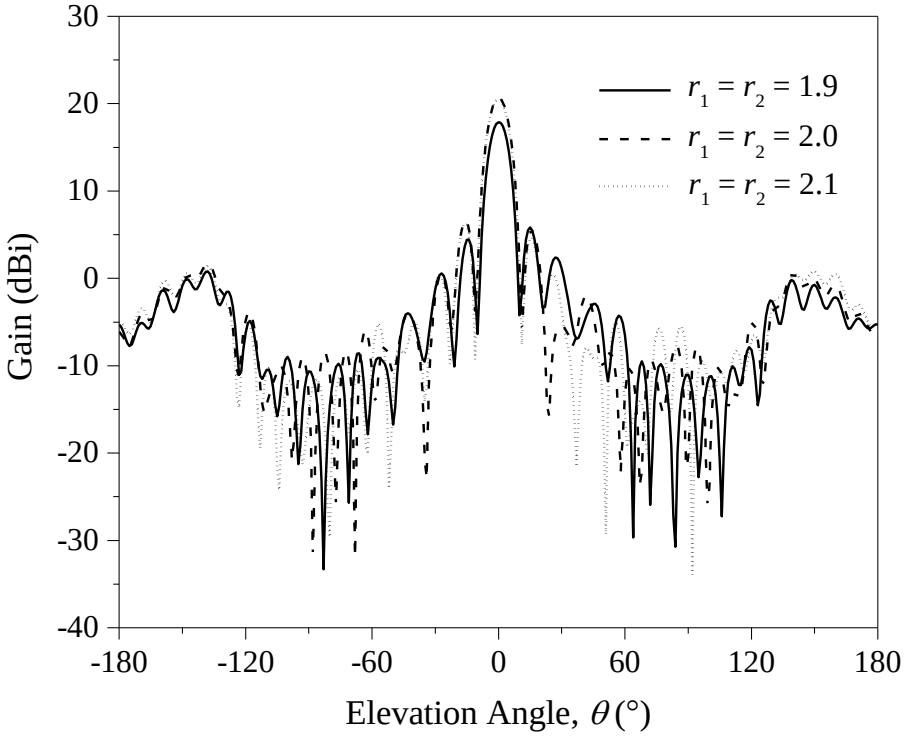

(b)

Figure 4.13: Radiation patterns of the proposed CP elliptical patch reflectarray with different major to minor axis ratios ($r_1 = r_2$). (a) *xz*- and (b) *yz*- planes.

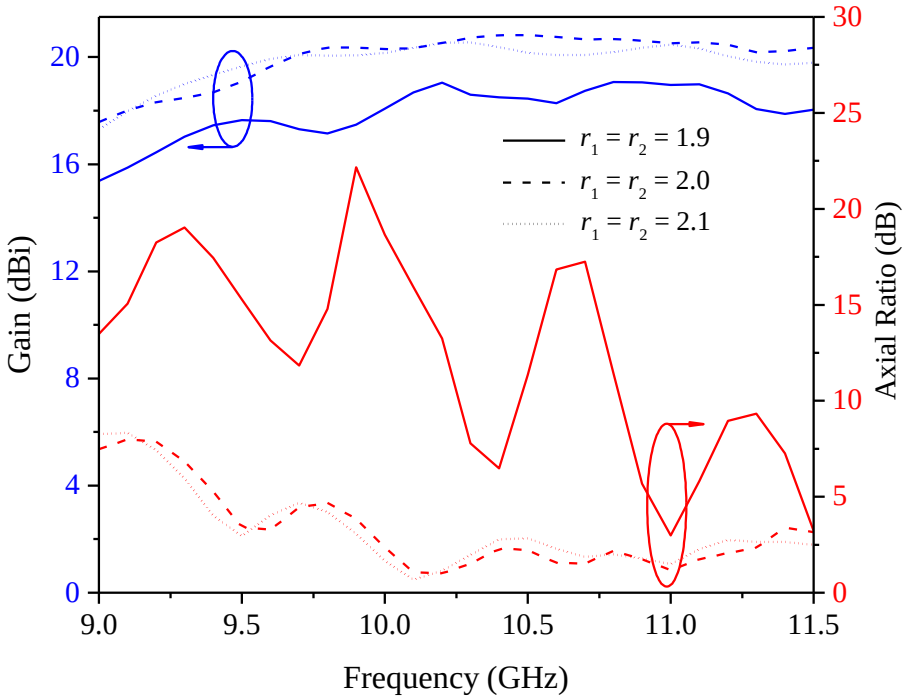

Figure 4.14: Effects of the major to minor axis ratio ($r_1 = r_2$) on the antenna gain and axial ratio of the CP elliptical patch reflectarray.

Unequal major to minor axis ratios (r_1 and r_2) of the top and middle patches are now defined. At first, the axis ratio of the top patch, r_1 is varied from 1.8 to 2.2; while the middle patch is fixed at $r_2 = 2$. It is observed that the elliptical patch with $r_1 = 2.2$ has the largest reflection magnitude at $2a_1 = 6.6$ mm and beyond $2a_1 = 13.8$ mm, as depicted in Figure 4.15. With reference to the same figure, a steeper gradient of the phase curve is observed beyond $2a_1 = 9$ mm when r_1 is increased, with the total phase range remains unchanged. Figure 4.16 shows the radiation patterns of the reflectarray for different r_1. For $r_1 = 1.8$, the lowest antenna gain is observed at the boresight direction, with the largest side lobes obtained in *xz*-plane. Although the reflectarray with $r_1 = 2.2$ has lower side lobe levels than that for $r_1 = 2.0$, its antenna gain at $\theta = 0°$ is still lower than that for $r_1 = 2.0$. The antenna gains and axial ratios of the reflectarray across all frequencies are illustrated in Figure 4.17. It is obvious

that the reflectarray with r_1 = 1.8 has poor axial ratios and low antenna gains across 9 GHz - 11.5 GHz. Compared with r_1 = 2.0, the reflectarray with r_1 = 2.2 has achieved better axial ratio with lower antenna gain. In this case, the reflectarray with r_1 = 2.0 is selected as it has the broadest -1dB gain bandwidth with good axial ratio.

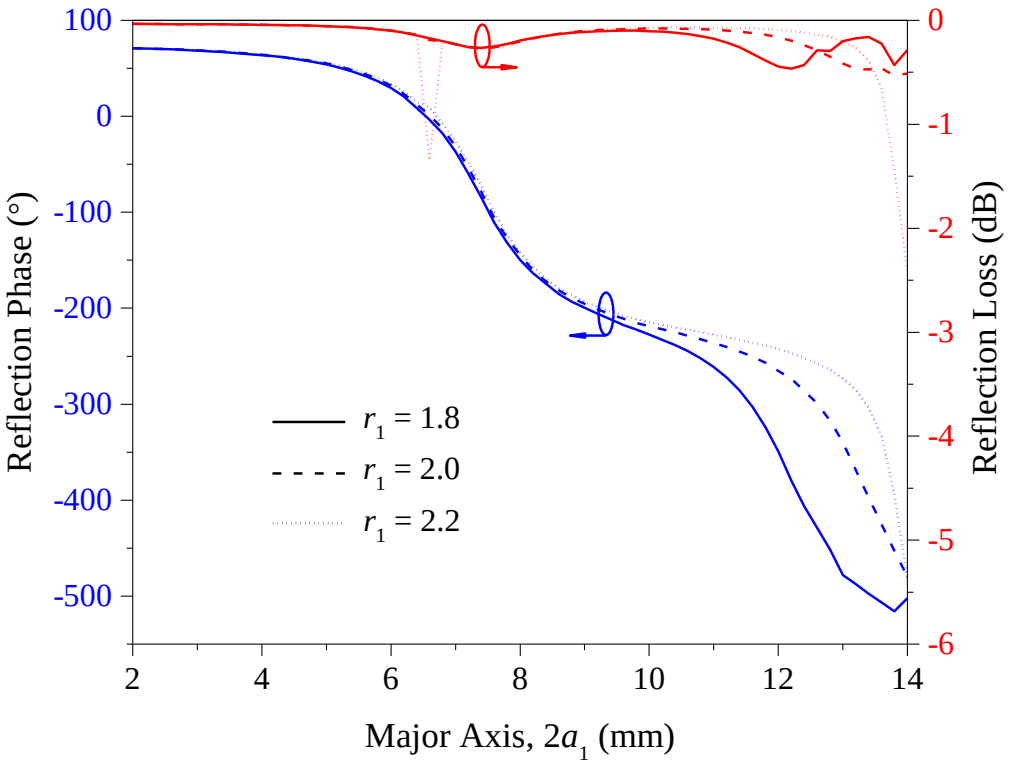

Figure 4.15: Effects of the major to minor axis ratio of the top patch (r_1) on the reflection magnitude and reflection phase of the unit element.

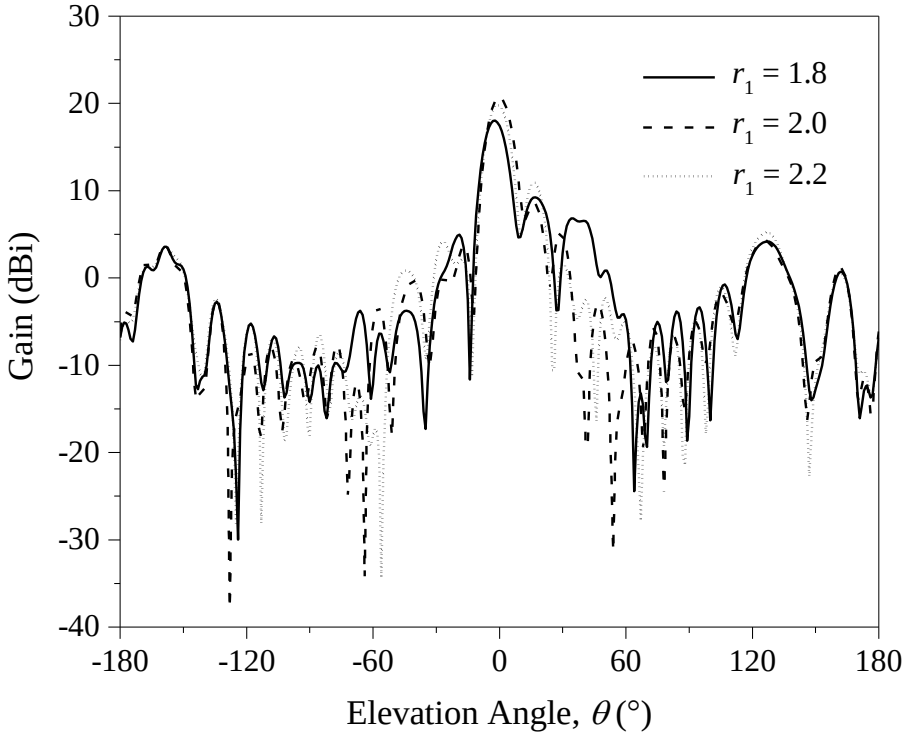

(a)

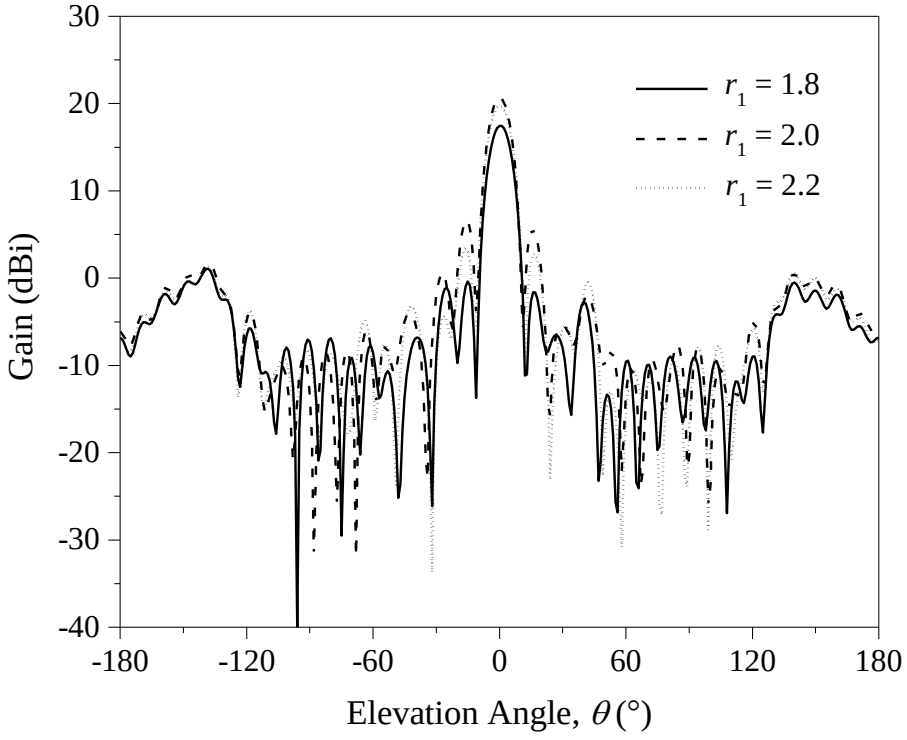

(b)

Figure 4.16: Radiation patterns of the proposed CP elliptical patch reflectarray with different major to minor axis ratios of the top patch (r_1). (a) *xz*- and (b) *yz*- planes.

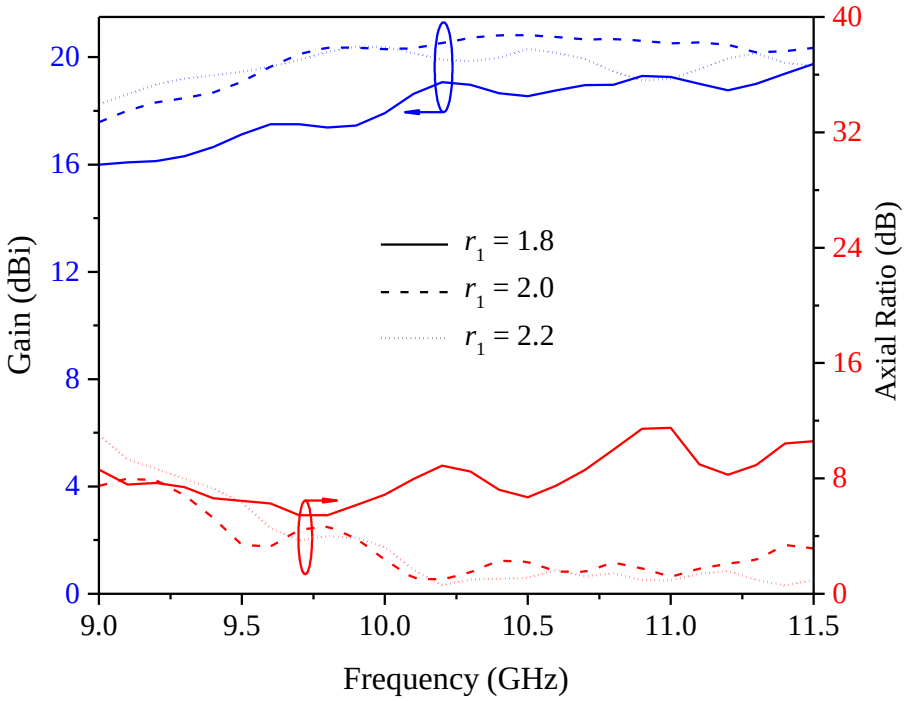

Figure 4.17: Effects of the major to minor axis ratio of the top patch (r_1) on the antenna gain and axial ratio of the CP elliptical patch reflectarray.

The axis ratio of the middle patch, r_2 is now varied and the effects on the reflection performances are shown in Figure 4.18. In this case, the top patch is fixed at $r_1 = 2$. The same gradient is observed in the phase curve when varying r_2 from 1.8 to 2.2. For all r_2, as can be seen from Figure 4.18, an equal amount of the phase range is achieved. On the other hand, the effects on the radiation performances are plotted in Figure 4.19. The lowest antenna gain (at $\theta = 0°$) is observed at $r_2 = 2.2$ with large side lobes. The antenna gain at $\theta = 0°$ is maximized when r_2 is reduced to 2.0. The antenna gains and axial ratios of the reflectarray for $r_2 = 1.8$, 2.0 and 2.2 are shown in Figure 4.20. For $r_2 = 1.8$ and 2.2, the reflectarray is absolutely not a good CP antenna as it is not able to get the axial ratio to be lower than 3-dB. Conversely, the reflectarray with $r_2 = 2.0$ has achieved good axial-ratio bandwidth with high antenna gain.

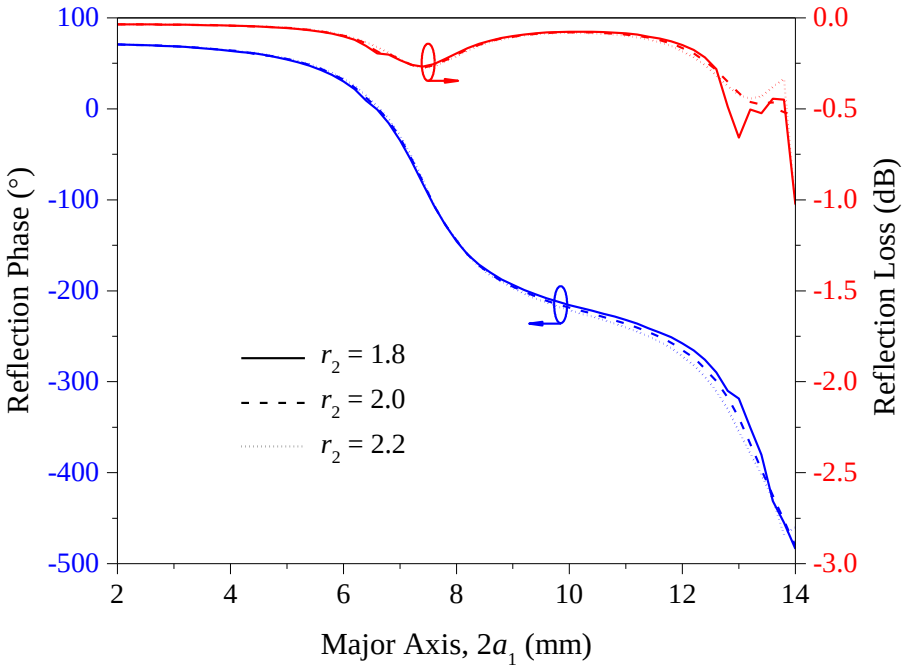

Figure 4.18: Effects of the major to minor axis ratio of the middle patch (r_2) on the reflection magnitude and reflection phase of the unit element.

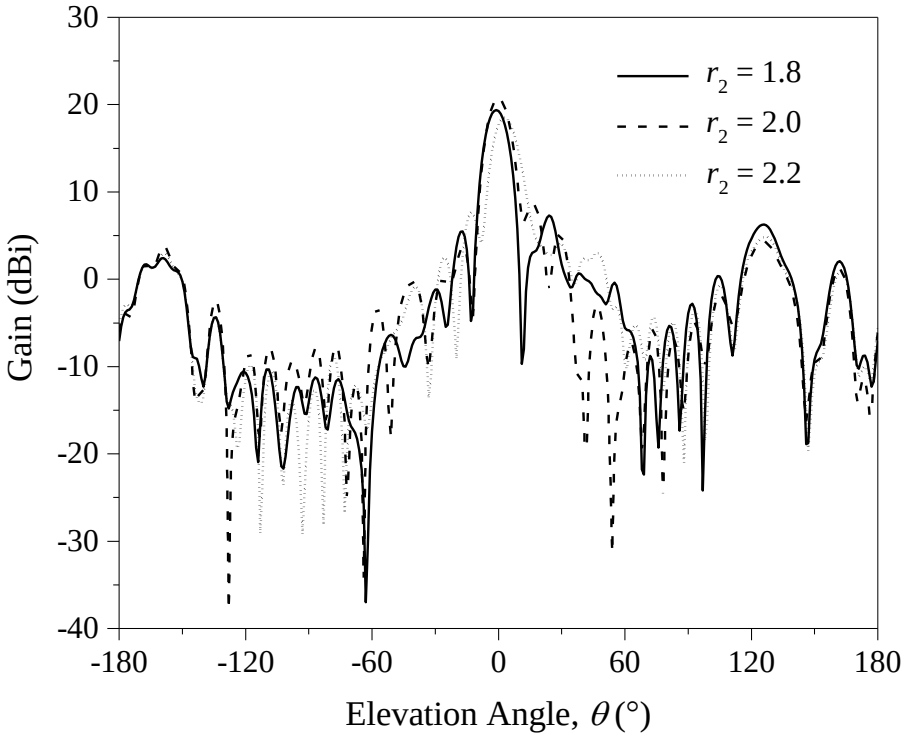

(a)

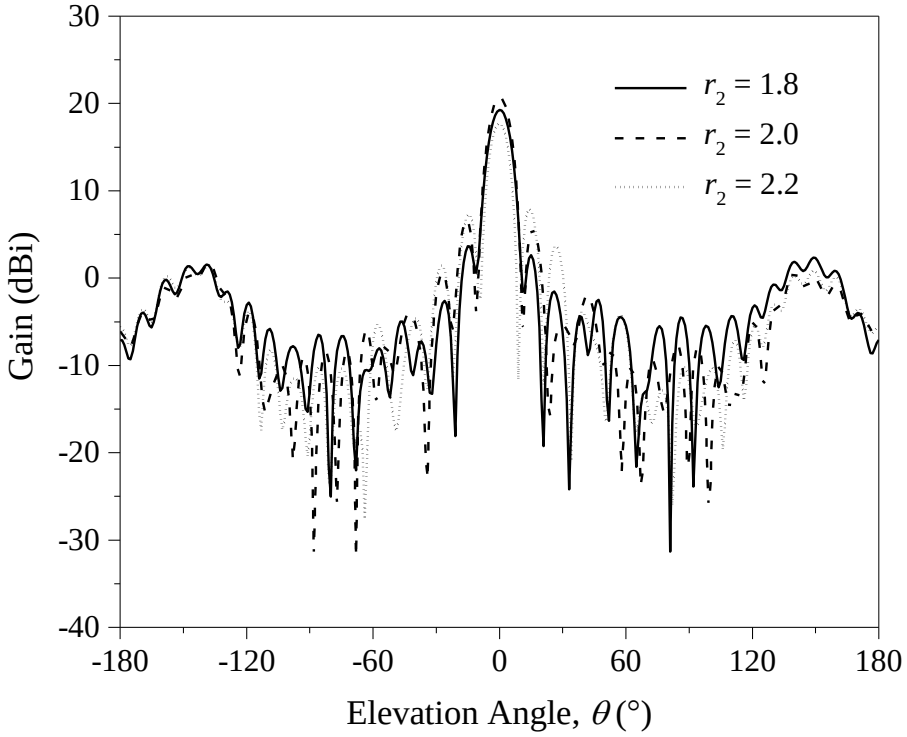

(b)

Figure 4.19: Radiation patterns of the proposed CP elliptical patch reflectarray with different major to minor axis ratios of the middle patch (r_2). (a) *xz*- and (b) *yz*- planes.

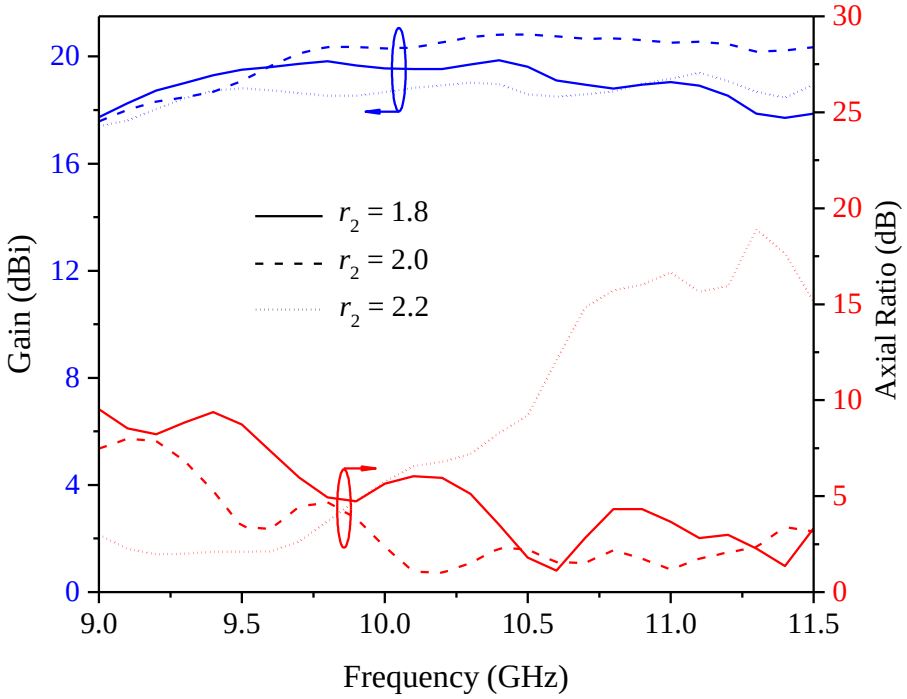

Figure 4.20: Effects of the major to minor axis ratio of the middle patch (r_2) on the antenna gain and axial ratio of the CP elliptical patch reflectarray.

4.6.2 Patch Inclination Angle

Next, effects of the patch inclination angle (θ_t and θ_b) on the reflection and radiation characteristics are studied. The results are shown in Figures 4.21 and 4.22. In this case, θ_t and θ_b are set to be the same and they are varied from 35° to 55°. It can be seen that elliptical patch with the inclination angle of 35° has the largest reflection phase range, as depicted in Figure 4.21. However, the phase slope becomes steeper beyond $2a_1$ = 9 mm, making this portion unusable for reflectarray design. For the case of θ_t (= θ_b) = 45° and 55°, they have similar reflection phase range. On the other hand, as can be seen from Figure 4.22, the boresight antenna gain reduces significantly when the patch inclination angle is increased from 35° to 55°. Although elliptical patch with θ_t (= θ_b) = 35° has the lowest sidelobes in the *yz*- plane, its boresight antenna gain is still lower than that for θ_t (= θ_b) = 45°. Axial-ratio and antenna-gain performances of the proposed reflectarray are analyzed in Figure 4.23. It is found that the case for θ_t (= θ_b) = 55° is not able to generate low (< 3dB) axial ratio across all frequencies. To achieve broad axial-ratio bandwidth and high antenna gain, the reflectarray with the inclination angle of 45° is selected.

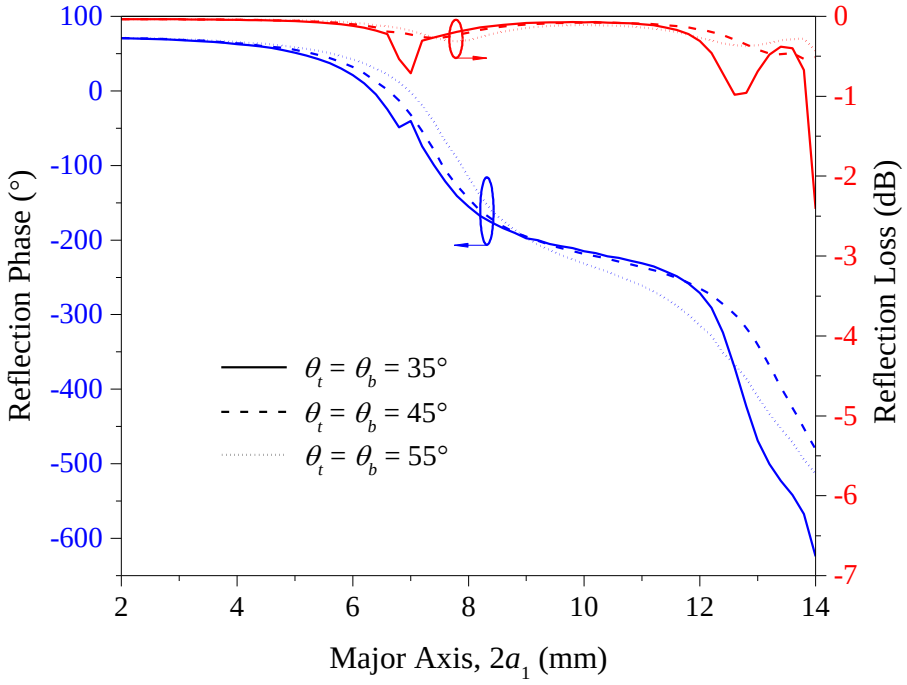

Figure 4.21: Effects of the patch inclination angle ($\theta_t = \theta_b$) on the reflection magnitude and reflection phase of the unit element.

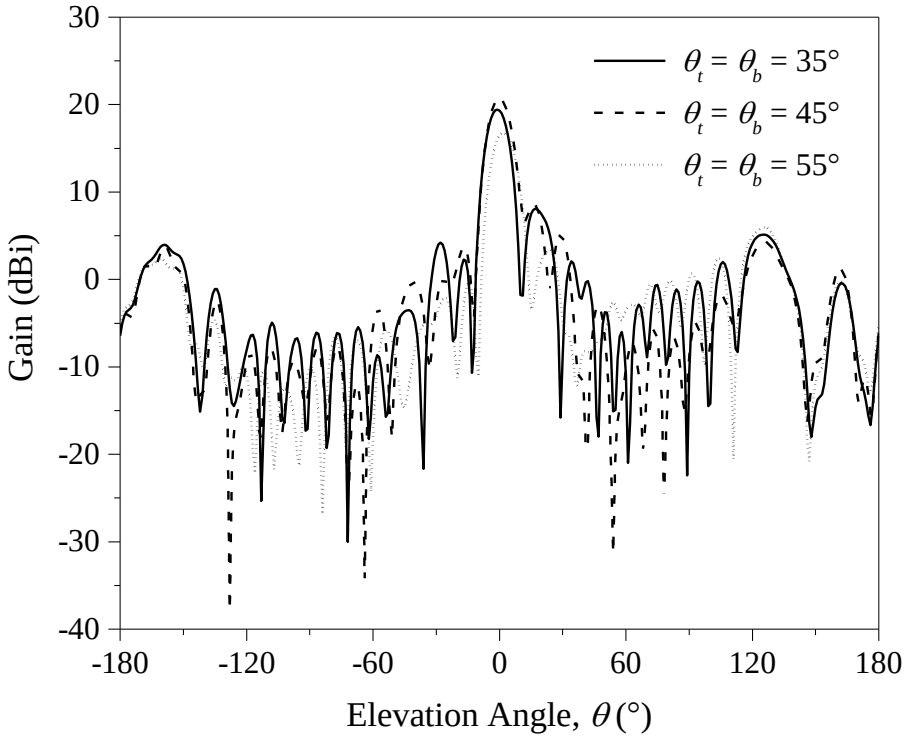

(a)

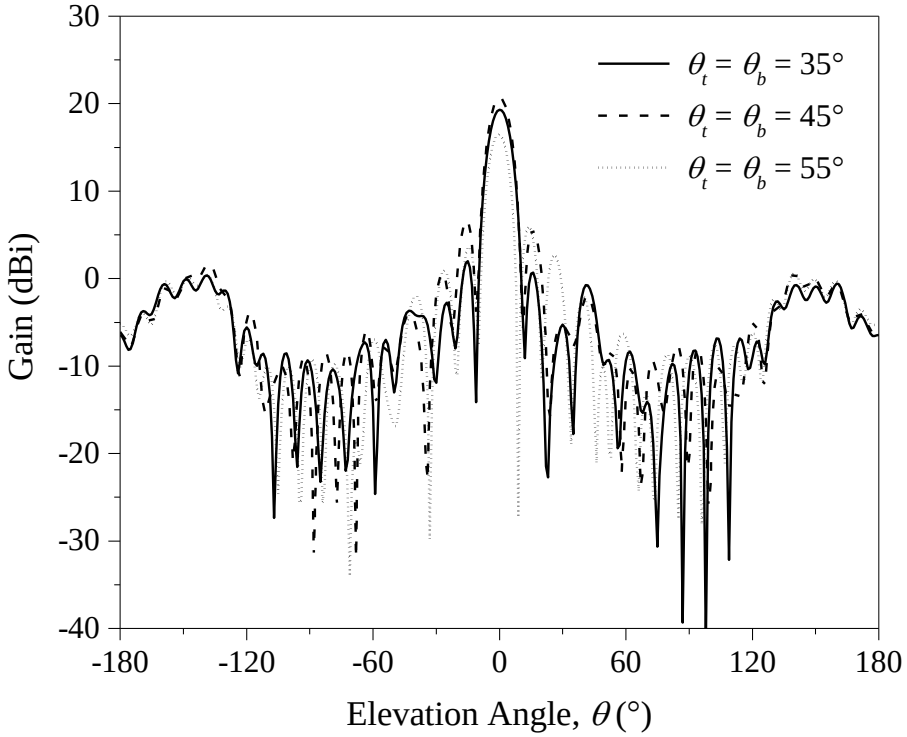

(b)

Figure 4.22: Radiation patterns of the proposed CP elliptical patch reflectarray with different patch inclination angles ($\theta_t = \theta_b$). (a) *xz*- and (b) *yz*- planes.

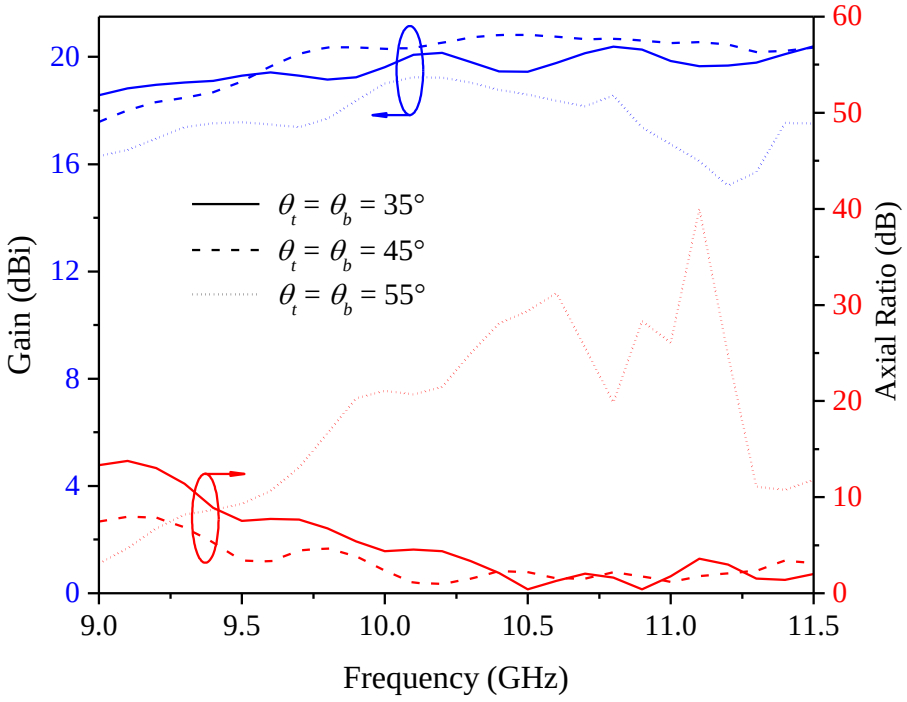

Figure 4.23: Effects of the patch inclination angle ($\theta_t = \theta_b$) on the antenna gain and axial ratio of the CP elliptical patch reflectarray.

4.6.3 Unit Cell Size

The effects of the cell size (L) are now studied and the reflection responses are shown in Figure 4.24. It is noticed that the gradient of the phase curve does not vary much when the unit cell size is changed from 0.42λ to 0.56λ. When the proposed unit cell is expanded into a full-fledge reflectarray, the cell size is translated into the gap separation between the adjacent elements. Radiation patterns of the proposed reflectarray are illustrated in Figure 4.25. High antenna gain (>21.2 dBi) is observed for L =0.49λ and 0.56λ. A ~5 dB gain decrease is observed when the gap separation is 0.42λ. As can be seen from the same figure, the backlobe level becomes larger when the gap separation is increased. Axial ratios and antenna gains for the gap separations of 0.42λ, 0.49λ and 0.56λ are depicted in Figure 4.26. The 3-dB axial-ratio bandwidths for the case of 0.42λ and 0.56λ read 0.7 GHz and 0.5 GHz, respectively. A broader 3-dB axial ratio bandwidth (1.3 GHz) is observed when the gap separation is set to 0.49λ, with a -1dB gain bandwidth of 1.8 GHz.

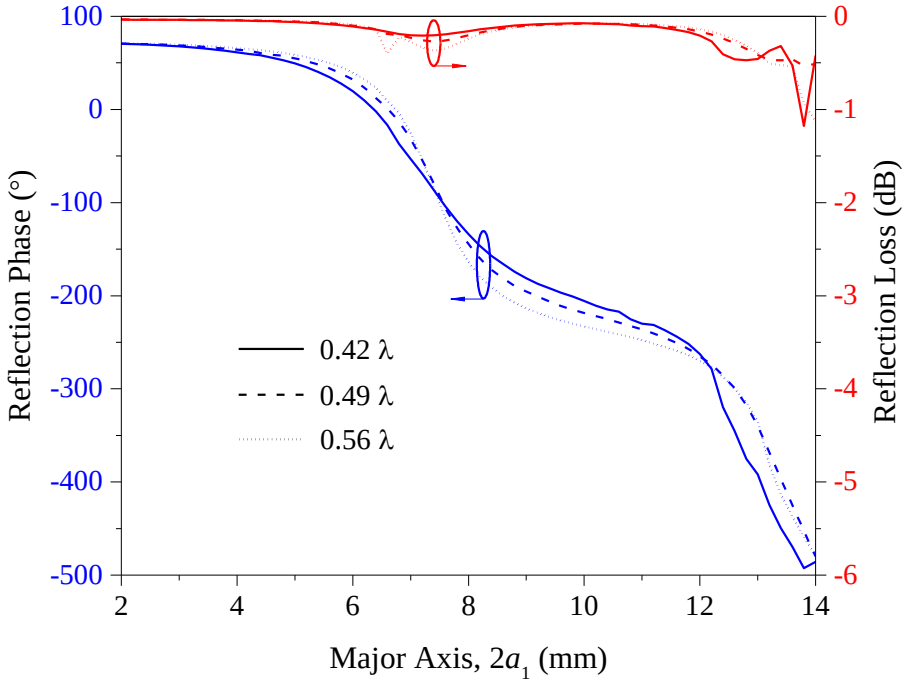

Figure 4.24: Effects of the cell size (L) on the reflection magnitude and reflection phase of the unit element.

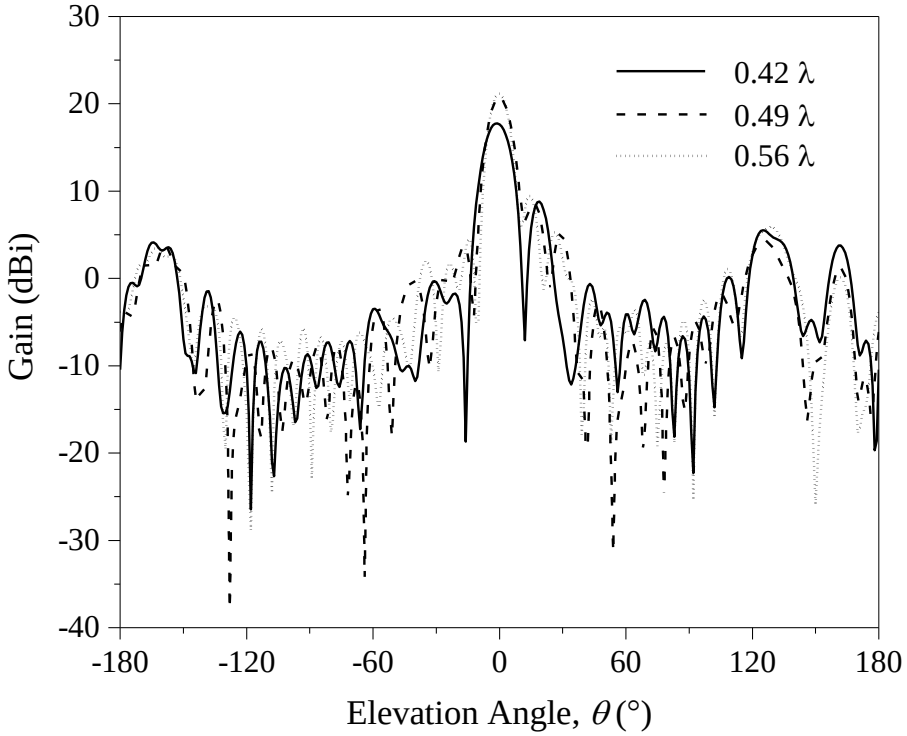

(a)

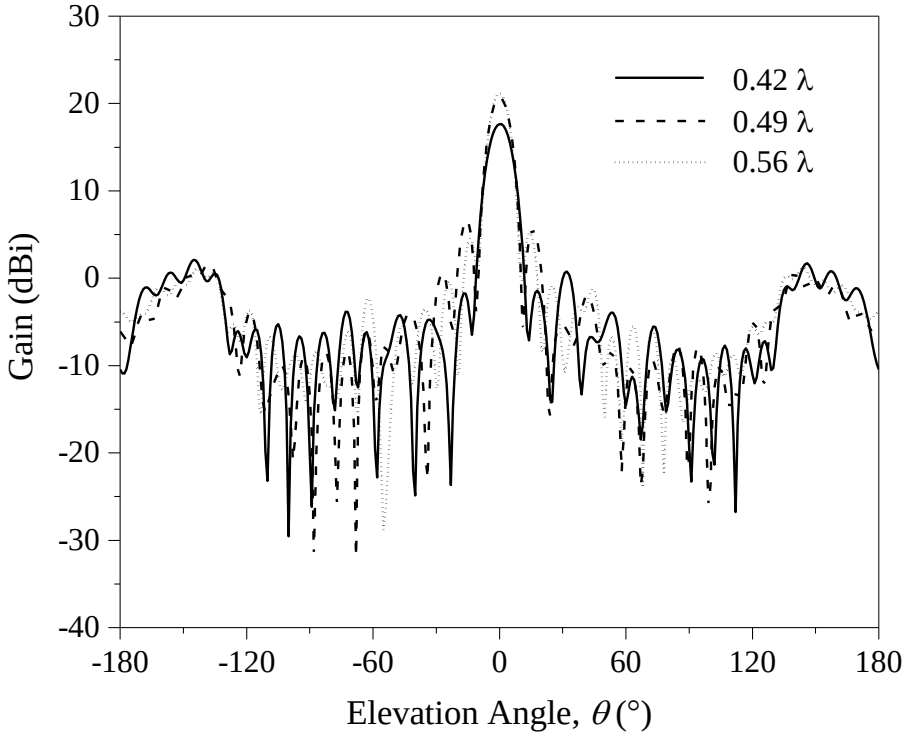

(b)

Figure 4.25: Radiation patterns of the proposed CP elliptical patch reflectarray with different unit cell sizes (L). (a) *xz*- and (b) *yz*-planes.

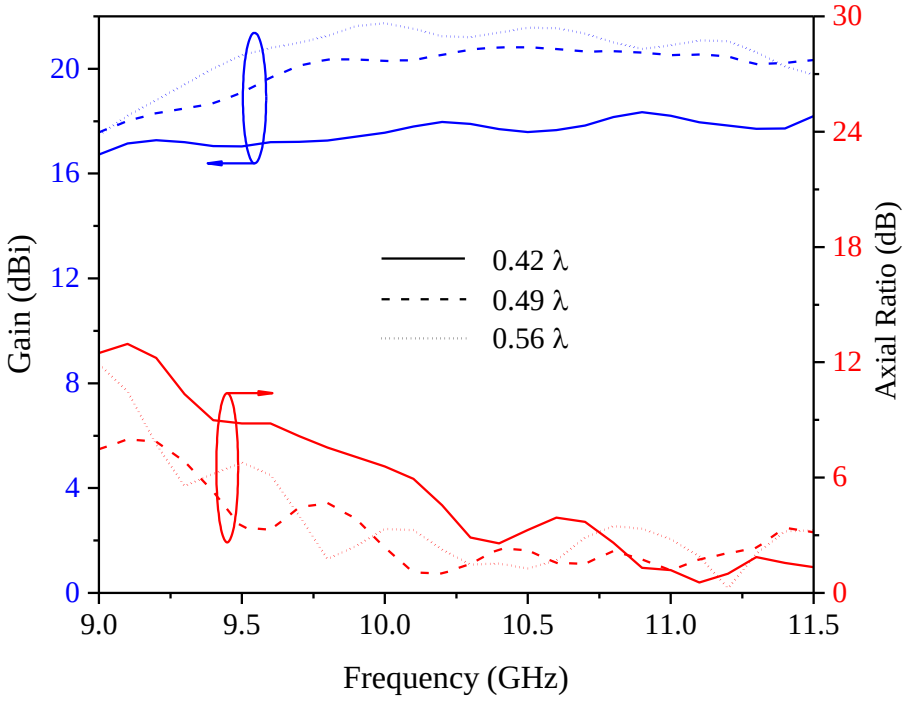

Figure 4.26: Effects of unit cell size (L) on the antenna gain and axial ratio of the CP elliptical patch reflectarray.

4.6.4 *F/D* Ratio

The effects of *F/D* ratio on the radiation characteristics are now studied. The boresight antenna gain stays almost the same for the case of *F/D* = 1.1, 1.2, and 1.3, as illustrated in Figure 4.27. With reference to the same figure, the reflectarray with *F/D* = 1.1 has larger a sidelobe level than those for *F/D* = 1.2 and 1.3. Also, for the case of *F/D* = 1.1, a narrower 3-dB axial ratio bandwidth is observed. For *F/D* ratio of 1.2 and 1.3, as can be seen from Figure 4.28, the trends of the axial-ratio curves are approximately the same across all frequencies. In our design, the proposed reflectarray is designed with *F/D* = 1.2 as it is able to provide higher antenna, lower sidelobes, and broader 3-dB axial-ratio bandwidth than those for the *F/D* = 1.3.

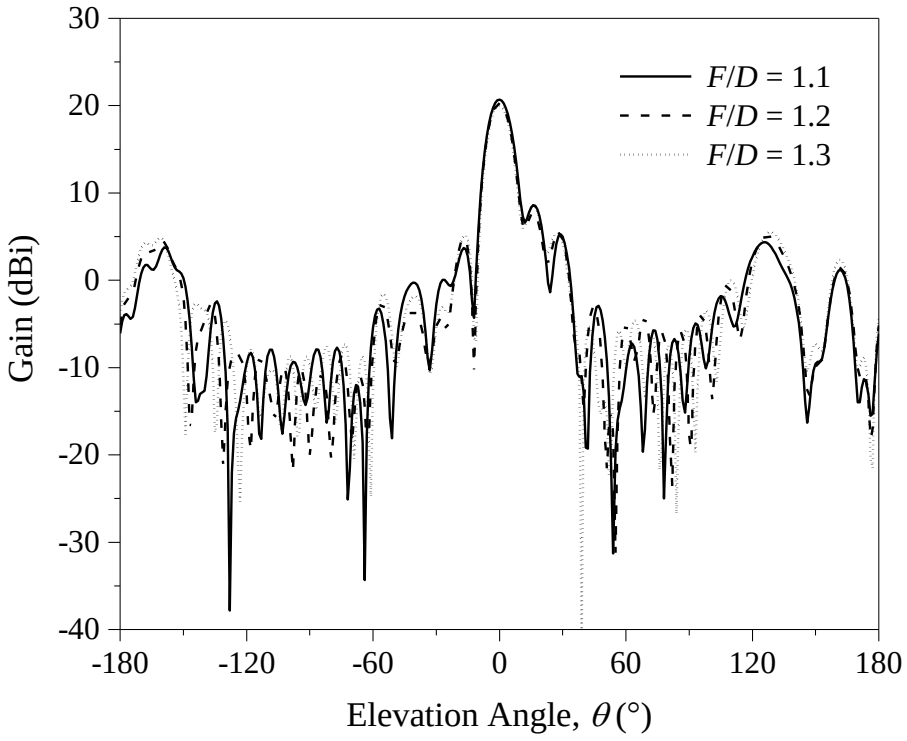

(a)

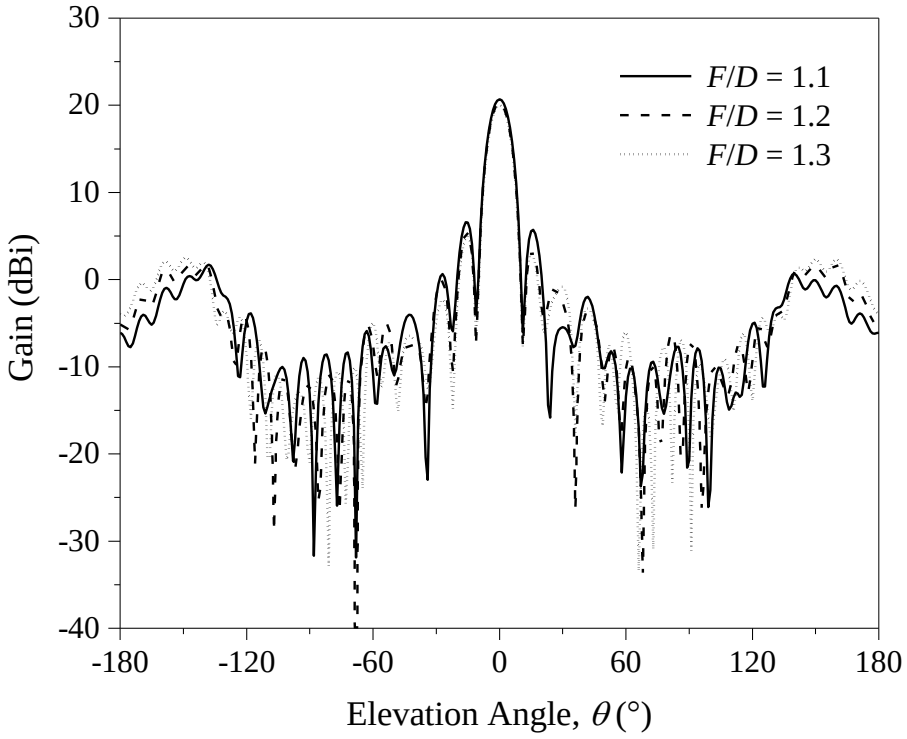

(b)

Figure 4.27: Radiation patterns of the proposed CP elliptical patch reflectarray with different *F*/*D* ratios. (a) *xz*- and (b) *yz*- planes.

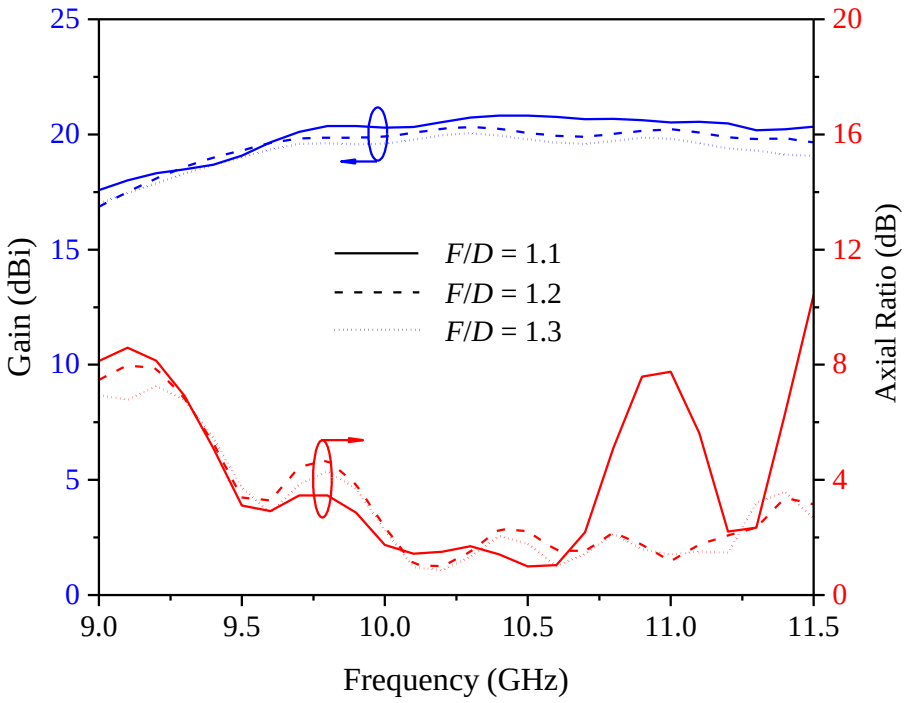

Figure 4.28: Effects of *F*/*D* ratio on the antenna gain and axial ratio of the CP elliptical patch reflectarray.

4.6.5 Substrate 1 Thickness

Subsequently, the effects of the top substrate (substrate 1) thickness (h_1) on the reflection performances are analyzed. In this case, the thickness of substrate 1 is varied from 0.8128 mm to 2.33 mm and the effects are illustrated in Figure 4.29. It is observed that a thin substrate 1 with h_1 = 0.8128 mm can provide very broad phase range. Nevertheless, it is not suitable to be used for designing the reflectarray as it has very sharp gradient with huge reflection magnitude. In the meanwhile, an almost linear phase slope is observed for h_1 = 2.33 mm, with its total phase range maintained at ~550°. The radiation patterns of the proposed reflectarray are depicted in Figure 4.30. An equal amount of antenna gain (θ = 0°) is observed for the cases of h_1 = 0.8128 mm and 2.33 mm, with large side lobes obtained for h_1 = 0.8128 mm. The reflectarray with h_1 = 1.524 mm has the largest boresight antenna gain than the other two. It also has the broadest 3-dB axial ratio and -1dB gain bandwidths, as shown in Figure 4.31.

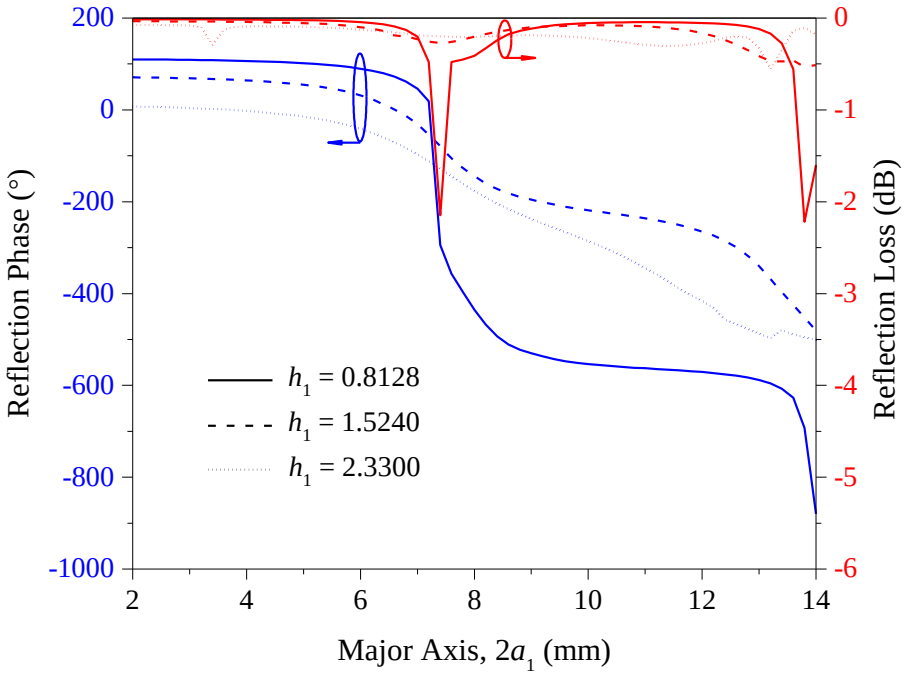

Figure 4.29: Effects of the top substrate (substrate 1) thickness (h_1) on the reflection magnitude and reflection phase of the unit element.

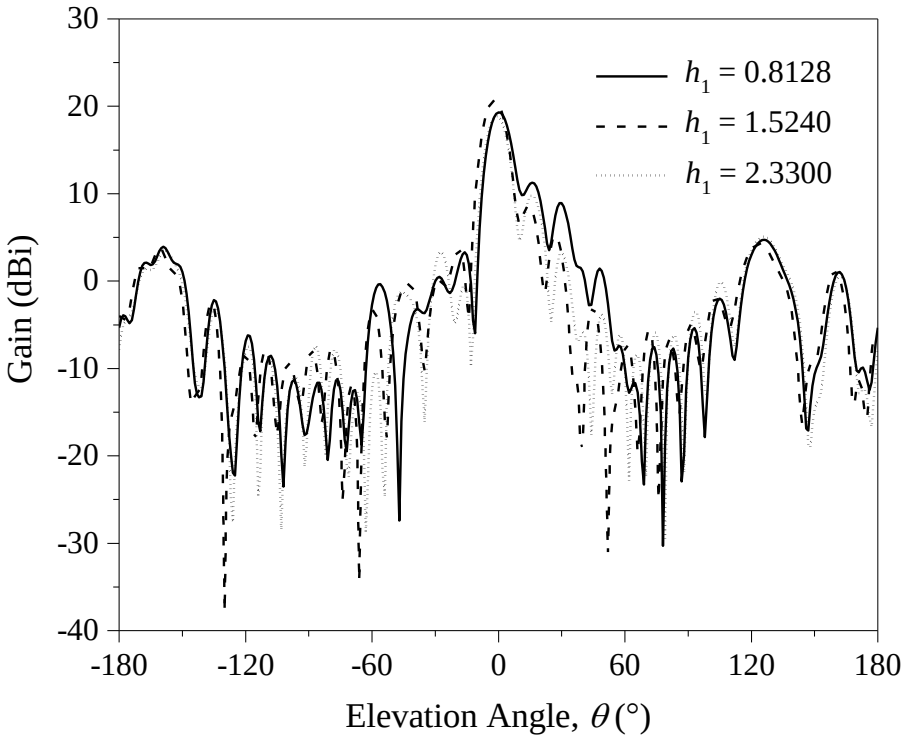

(a)

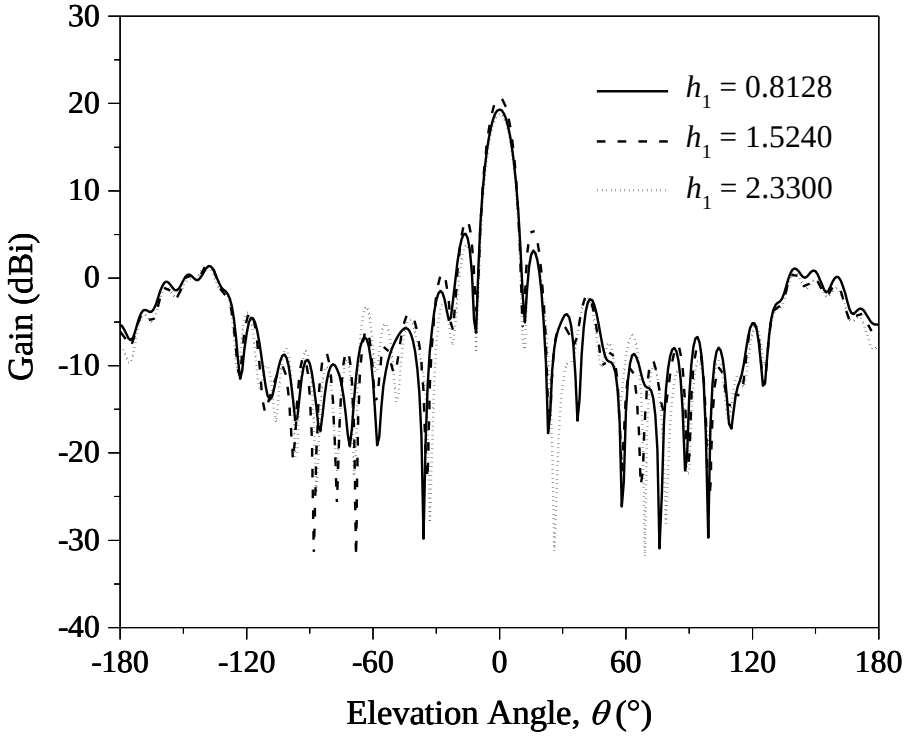

(b)

Figure 4.30: Radiation patterns of the proposed CP elliptical patch reflectarray with different top substrate (substrate 1) thicknesses (h_1). (a) *xz*- and (b) *yz*- planes.

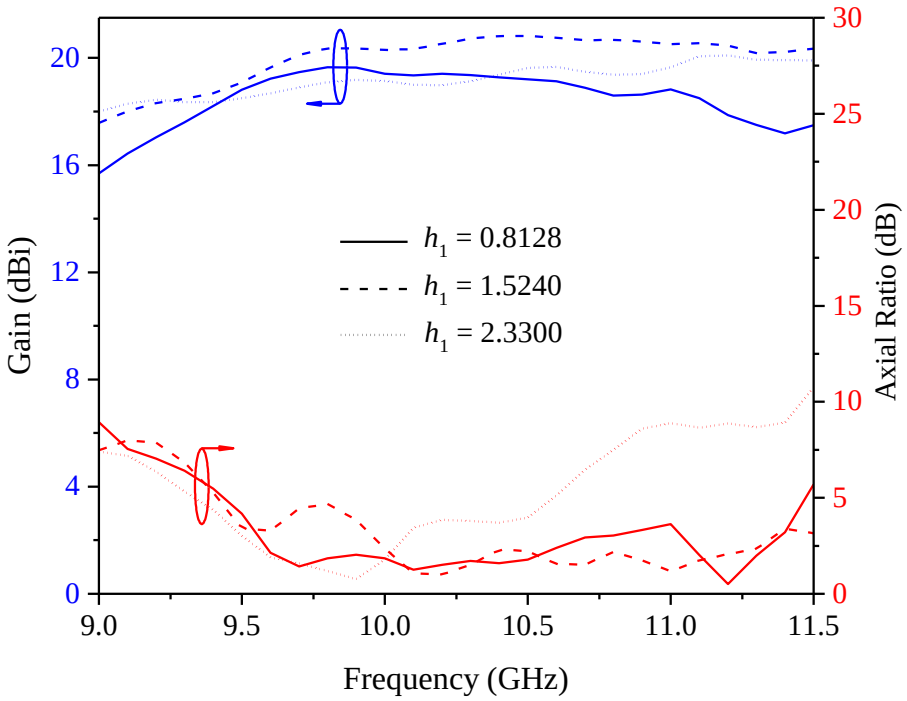

Figure 4.31: Effects of top substrate (substrate 1) thickness (h_1) on the antenna gain and axial ratio of the CP elliptical patch reflectarray.

4.6.6 Feeding Angle

Lastly, the effects of feeding angle (θ_i) on the reflection characteristics are studied and the performances are illustrated in Figure 4.32. With reference to Figure 4.32, larger feeding angle is found to be able to give a broad phase angle, but the gradient of its phase slope is very steep. For θ_i = 15°, an almost linear phase curve is achieved with its total phase range larger than that for θ_i = 20°. However, as can be seen from Figure 4.33, its boresight antenna gain is lower than those for θ_i = 20° and 25°. The highest boresight antenna gain is observed at the feeding angle of θ_i = 20°, which is ~3dB larger than that for θ_i = 25°. Besides that, larger side lobes are observed for the reflectarray with θ_i = 15° and 25°. Axial ratio and antenna gain performances of the proposed reflectarray are depicted in Figure 4.34. It is found that the reflectarray with θ_i = 15° is not able to provide low axial ratio across all frequencies. For θ_i = 25°, low axial ratio is observed across 9 - 10 GHz, but the antenna gains are still lower than those for θ_i = 20°. To have broad 3-dB axial ratio bandwidth and high antenna gain across the desired -1dB gain bandwidth, the reflectarray with θ_i = 20° is chosen for our design.

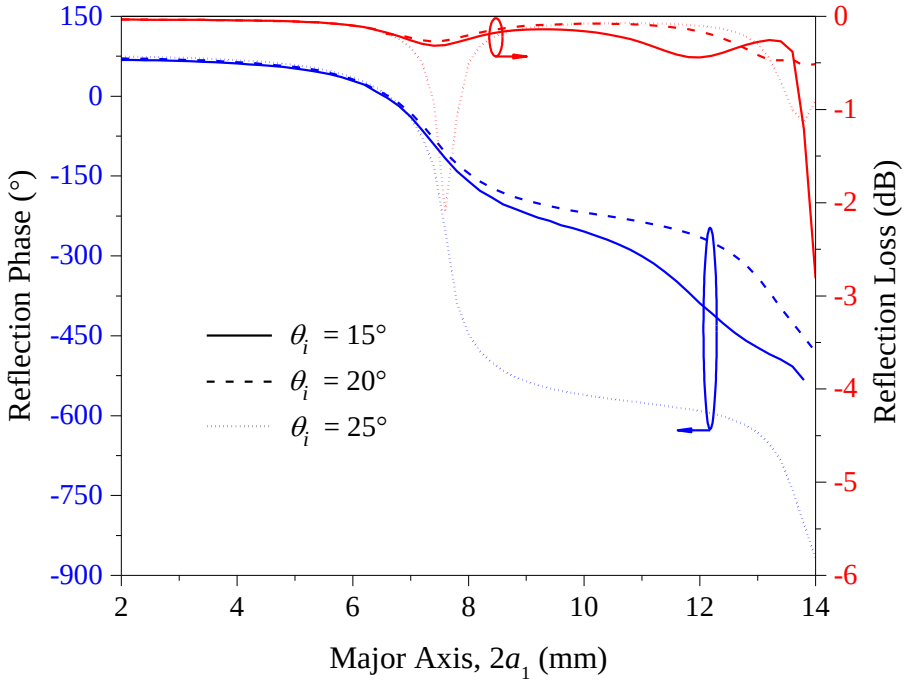

Figure 4.32: Effects of the feeding angle (θ_i) on the reflection magnitude and reflection phase of the unit element.

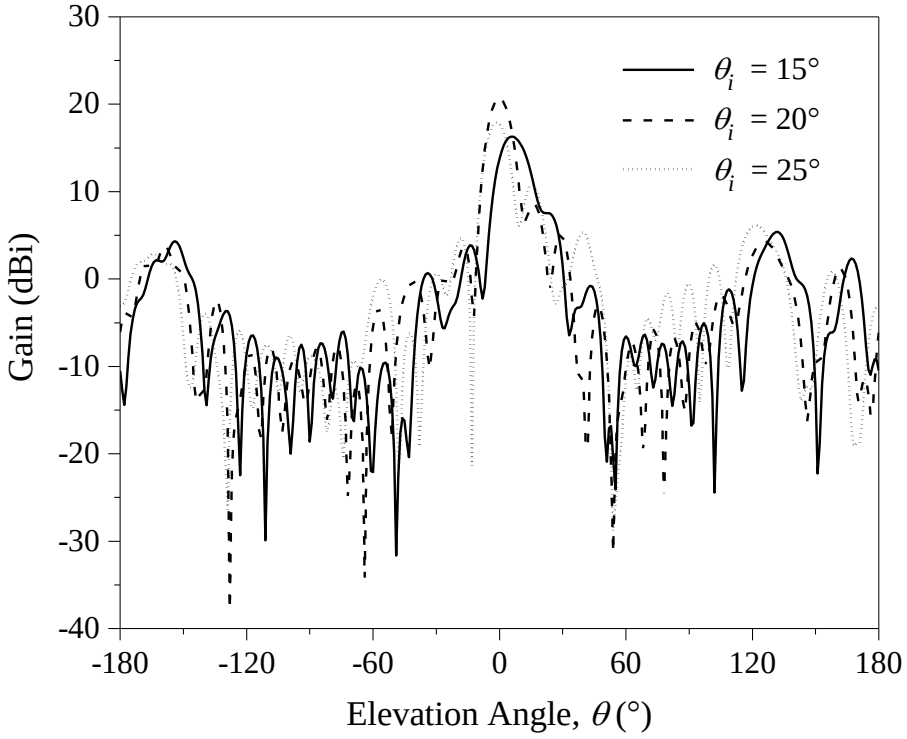

(a)

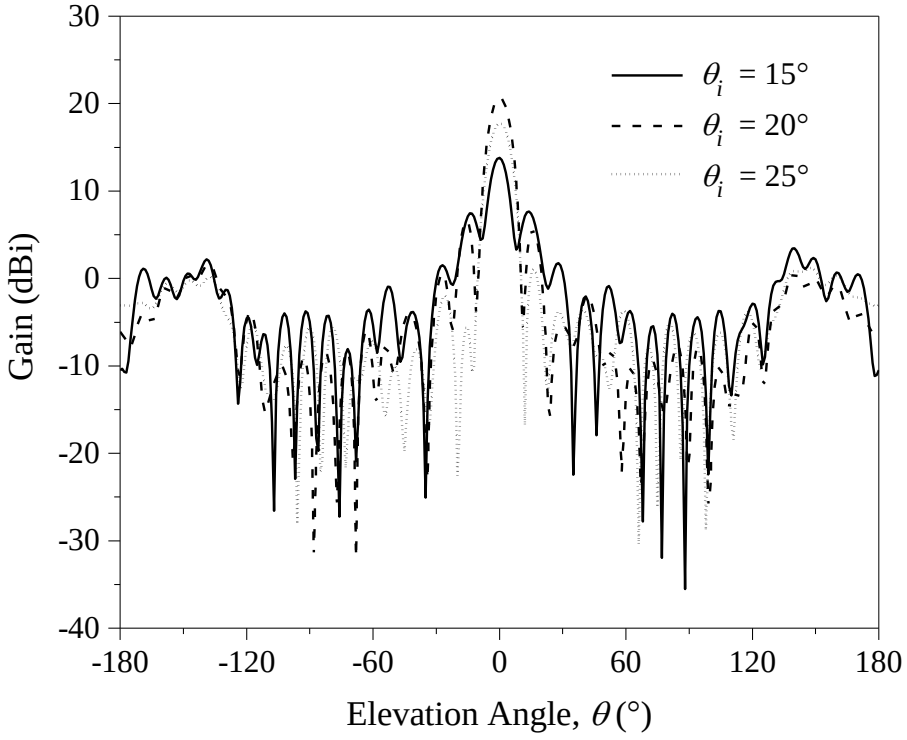

(b)

Figure 4.33: Radiation patterns of the proposed CP elliptical patch reflectarray with different feeding angles (θ_i). (a) *xz*- and (b) *yz*-planes.

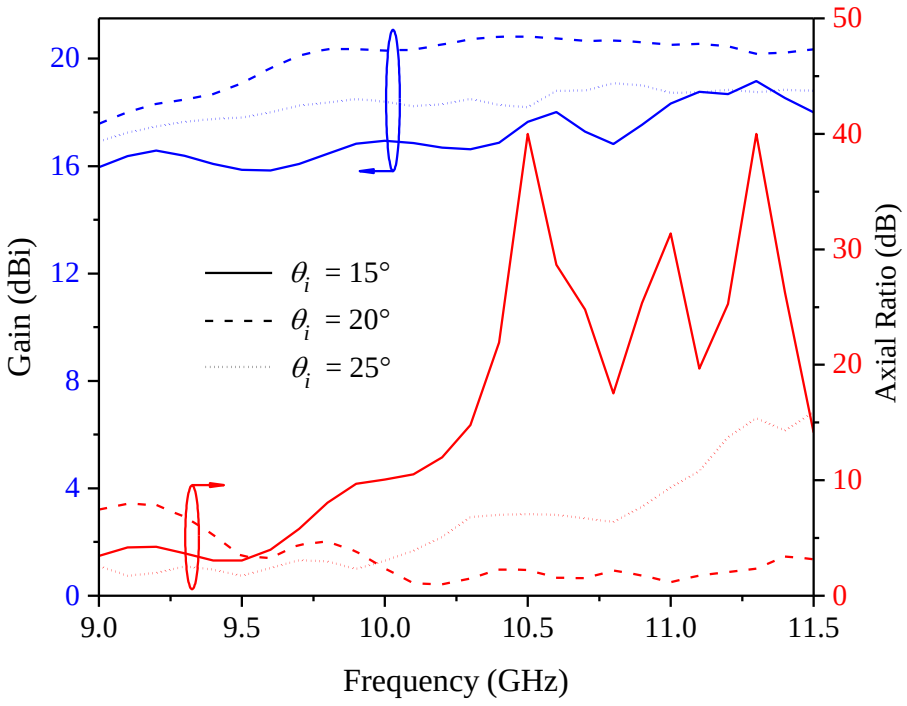

Figure 4.34: Effects of feeding angle (θ_i) on the antenna gain and axial ratio of the CP elliptical patch reflectarray.

4.7 Conclusion

A double-layered circularly polarized elliptical microstrip patch reflectarray has been proposed. Instead of using the conventional angular rotation technique, the proposed unit element has its major axis changed to provide broad phase range. The unit element is proven to be able to generate a broad reflection phase range of 550°, with low reflection magnitude of less than -0.5dB. When translated into a full-fledge reflectarray, an antenna gain of 20.38dBi has been achieved, with a -1dB gain bandwidth of 11.6%. The CP reflectarray is able to provide a 3-dB axial-ratio bandwidth of 12.47%. With the use of a LP feed horn, the proposed CP reflectarray is proven to be able to generate circularly polarized waves in the boresight direction. Parametric analysis has been performed and the effects of some of the important design parameters have been analyzed. It is found that the radiation performance of the proposed reflectarray can be further optimized by manipulating the major-to-minor axis ratio, patch inclination angle, and F/D ratio.

CHAPTER 5

SUMMARY AND FUTURE WORKS

In this dissertation, two different reflectarrays have been proposed and verified experimentally. Also, the research objectives for both of the projects have been met. In the first part, an E-shaped patch resonator has been designed and deployed for designing a linearly polarized reflectarray. A measured antenna gain of ~23.7dBi and a measured -1dB gain bandwidth of 8.1% are achievable, without the use of any dielectric substrate. The measured aperture efficiency is found to be 36%. In the second part, elliptical patch resonators have been used for designing an 11×11 circularly polarized reflectarray. The proposed reflectarray was found to be able to generate circularly polarized waves by inclining the top and middle elliptical patches in the clockwise and anticlockwise directions, respectively. With the use of a linearly polarized feed horn as the feeding source, the proposed reflectarray has a measured antenna gain of 20.38dBi and a measured -1dB gain bandwidth of 11.6%. A broad 3-dB axial ratio bandwidth of 12.47% is also achieved. Reasonable agreement has been observed between the simulated and measured results. In future, the E-shaped patch resonator will be used for designing a dual-band single layer E-patch reflectarray to increase the data transfer rates. On the other hand, the size of the elliptical patch element will be reduced and further increase the number of radiating elements of the CP reflectarray so that its antenna gain and its aperture efficiency can be improved.

BIBLIOGRAPHY

Abd-Elhady, M. and Hong, W., 2010. Ka-band linear polarized air vias reflectarray. *IEEE Middle East Conference on Antennas and Propagation (MECAP 2010)*, pp. 1–3.

Ang, B.-K. and Chung, B.-K., 2007. A wideband E-shaped microstrip patch antenna for 5 - 6 GHz wireless communications. *Progress In Electromagnetics Research*, 75, pp. 397–407.

Arshad, M.K., Tahir, F.A. and Rashid, A., 2014. Design of a single layer reflectarray unit cells based on hexagonal ring for wideband operation. *2014 IEEE Antennas and Propagation Society International Symposium (APSURSI)*, pp. 815–816.

Berry, D., Malech, R. and Kennedy, W., 1963. The reflectarray antenna. *IEEE Transactions on Antennas and Propagation*, 11(6), pp. 645–651.

Bialkowski, M.E., Robinson, A.W. and Song, H.J., 2002. Design, development, and testing of X-band amplifying reflectarrays. *IEEE Transactions on Antennas and Propagation*, 50(8), pp. 1065–1076.

Boccia, L., Venneri, F., Amendola, G. and Di Massa, G., 2002. Application of varactor diodes for reflectarray phase control. *IEEE Antennas and Propagation Society International Symposium (IEEE Cat. No.02CH37313)*, 3, pp. 132–135.

Bozzi, M., Germani, S. and Perregrini, L., 2004. A figure of merit for losses in printed reflectarray elements. *IEEE Antennas and Wireless Propagation Letters*, 3(1), pp. 257–260.

Capozzoli, A., Curcio, C., D'Elia, G., Liseno, A., Bresciani, D. and Legay, H., 2009. Fast phase-only synthesis of faceted reflectarrays. *3rd European Conference on Antennas and Propagation*, pp. 1329–1333.

Capozzoli, A., Curcio, C., D'Elia, G. and Liseno, A., 2010. Fast phase-only synthesis of conformal reflectarrays. *IET Microwaves, Antennas & Propagation*, 4(12), p. 1989.

Carrasco, E., Arrebola, M., Encinar, J. and Barba, M., 2008. Demonstration of a shaped beam reflectarray using aperture-coupled delay lines for LMDS central station antenna. *IEEE Transactions on Antennas and Propagation*, 56(10), pp. 3103–3111.

Carrasco, E., Arrebola, M. and Encinar, J.A., 2007. Shaped beam reflectarray using aperture- coupled delay lines for LMDS central station. *IET Seminar Digests*, p. 216.

Chaharmir, M.R., Shaker, J., Cuhaci, M. and Sebak, A., 2002. Circularly polarised reflectarray with cross-slot of varying arms on ground plane. *Electronics Letters*, 38(24), pp. 1492–1493.

Chakrabarty, A., Wang, F., Minkowski, F., Sun, K. and Wei, Q., 2012. Cavity modes and their excitations in elliptical plasmonic patch nanoantennas. *Optics Express*, 20(11), pp. 11615–11624.

Chang, D.C. and Huang, M.C., 1995. Multiple-polarization microstrip reflectarray antenna with high efficiency and low cross-polarization. *IEEE Transactions on Antennas and Propagation*, 43(8), pp. 829–834.

Chen, H.-W., Lei, X., Zhang, G., Chen, G.-H. and Hou, L., 2015. A slotted hollow ring element for Ku-band high-efficiency circularly polarized reflectarrays. *2015 Asia-Pacific Microwave Conference (APMC)*, 1, pp. 1–3.

Chen, Y., Yang, S. and Nie, Z., 2010. Bandwidth enhancement method for low profile E-shaped microstrip patch antennas. *IEEE Transactions on Antennas and Propagation*, 58(7), pp. 2442–2447.

Colin, J.-M., 1996. Phased array radars in France: present and future. *Proceedings of International Symposium on Phased Array Systems and Technology*, pp. 458–462.

Deng, R., Yang, F., Xu, S. and Li, M., 2015. Design of a dual-frequency broadband reflectarray using triple-resonance elements. *2015 IEEE International Symposium on Antennas and Propagation & USNC/URSI National Radio Science Meeting*, pp. 2169–2170.

Encinar, J.A. and Zornoza, J.A., 2003. Broadband design of three-layer printed reflectarrays. *IEEE Transactions on Antennas and Propagation*, 51(7), pp. 1662–1664.

Encinar, J.A. and Zornoza, J.A., 2004. Three-layer printed reflectarrays for contoured beam space applications. *IEEE Transactions on Antennas and Propagation*, 52(5), pp. 1138–1148.

Encinar, J.A., 2001. Design of two-layer printed reflectarrays using patches of variable size. *IEEE Transactions on Antennas and Propagation*, 49(10), pp. 1403–1410.

Florencio, R., Boix, R.R. and Encinar, J.A., 2013. Design of a reflectarray antenna at 300 GHz based on cells with three coplanar dipoles. *2013 IEEE Antennas and Propagation Society International Symposium (APSURSI)*, pp. 1350–1351.

Georgiadis, A. and Collado, A., 2010. Active reconfigurable reflectarray based on voltage-controlled oscillators. *2010 IEEE International Symposium on Phased Array Systems and Technology*, pp. 700–706.

Ghorbani, H., Tavakoli, A., Rabbani, M. and Dehkhoda, P., 2015. Dual-polarized reflectaray element using open-loop patches. *2015 IEEE International Symposium on Antennas and Propagation & USNC/URSI National Radio Science Meeting*, pp. 2179–2180.

Guo, J., Wu, F. and Wang, J., 2015. Design of broadband circularly polarized reflectarrays with novel ring-stub elements. *2015 Asia-Pacific Microwave Conference (APMC)*, 3, pp. 1–3.

Guo, L., Tan, P.-K. and Chio, T.-H., 2013. Design of an X-band reflectarray using double circular ring elements. *7th European Conference on Antennas and Propagation*, pp. 2947–2950.

Hamzavi-Zarghani, Z. and Atlasbaf, Z., 2015. A new broadband single-layer dual-band reflectarray antenna in X- and Ku-bands. *IEEE Antennas and Wireless Propagation Letters*, 14, pp. 602–605.

Han, C., Huang, J. and Chang, K., 2006. Cassegrain offset subreflector-fed X/Ka dual-band reflectarray with thin membranes. *IEEE Transactions on Antennas and Propagation*, 54(10), pp. 2838–2844.

Han, C., Rodenbeck, C., Huang, J. and Chang, K., 2004. A C/Ka dual - frequency dual layer circularly polarized reflectarray antenna with microstrip ring elements. *IEEE Transactions on Antennas and Propagation*, 52, pp. 2871 – 2876.

Hasani, H., Kamyab, M. and Mirkamali, A., 2010. Broadband reflectarray antenna incorporating disk elements with attached phase-delay lines. *IEEE Antennas and Wireless Propagation Letters*, 9, pp. 156–158.

Huang, J. and Encinar, J.A., 2007. *Reflectarray antennas*. Hoboken, NJ, USA: John Wiley & Sons, Inc.

Huang, J. and Pogorzelski, R.J., 1998. A Ka-band microstrip reflectarray with elements having variable rotation angles. *IEEE Transactions on Antennas and Propagation*, 46(5), pp. 650–656.

Huang, J. and Zawadzki, M., 2003. A dual-band reflectarray for X- and Ka-bands. *Progress in Electromagnetics Research Symposium (PIERS)*.

Huang, J., 1995. Bandwidth study of microstrip reflectarray and a novel phased reflectarray concept. *IEEE Antennas and Propagation Society International Symposium. 1995 Digest*, 1, pp. 582–585.

Huang, J., 1996. Capabilities of printed reflectarray antennas. *Proceedings of International Symposium on Phased Array Systems and Technology*, pp. 131–134.

Hum, S. V. and Okoniewski, M., 2004. An electronically tunable reflectarray using varactor diode-tuned elements. *IEEE Antennas and Propagation Society Symposium, 2004.*, 2, pp. 1827–1830.

Ismail, M.Y. and Sulaiman, N.H., 2011. Enhanced bandwidth reflectarray antenna using variable dual gap. *2011 2nd International Conference on Instrumentation, Communications, Information Technology, and Biomedical Engineering*, pp. 92–96.

Karnati, K., Ebadi, S. and Gong, X., 2011. Effect of dielectric thickness on phase swing of a Ka-band microstrip reflectarray unit cell. *2011 IEEE International Symposium on Antennas and Propagation (APSURSI)*, pp. 948–951.

Kelkar, A., 1991. FLAPS: conformal phased reflecting surfaces. *Proceedings of the 1991 IEEE National Radar Conference*, pp. 58–62.

Kishor, K.K. and Hum, S. V., 2012. An amplifying reconfigurable reflectarray antenna. *IEEE Transactions on Antennas and Propagation*, 60(1), pp. 197–205.

Li, L., Chen, Q., Yuan, Q., Sawaya, K., Maruyama, T., Furuno, T. and Uebayashi, S., 2009. Novel broadband planar reflectarray with parasitic dipoles for wireless communication applications. *IEEE Antennas and Wireless Propagation Letters*, 8, pp. 881–885.

Liu, S., Wu, W. and Fang, D.-G., 2016. Single-feed dual-layer dual-band E-shaped and U-slot patch antenna for wireless communication application. *IEEE Antennas and Wireless Propagation Letters*, 15, pp. 468–471.

Liu, Z.-G. and Guo, Y.-X., 2012. Broadband reflectarray with single layer sub-wavelength patch elements fed by SIW tapered slot antenna. *2012 Asia Pacific Microwave Conference Proceedings*, pp. 352–354.

Luo, J., Yang, F. and Xu, S., 2014. E-shaped element design for linearly polarized transmitarray antennas. *2014 International Symposium on Antennas and Propagation Conference Proceedings*, pp. 269–270.

Mahmoud, A., Zainudeen, S.H., Mitkees, A.A. and Kishk, A.A., 2014. Electronically tunable dielectric resonator reflectarray. *2014 16th International Symposium on Antenna Technology and Applied Electromagnetics (ANTEM)*, pp. 1–2.

Makdissy, T., Gillard, R., Fourn, E., Girard, E. and Legay, H., 2014. Phase-shifting cell for dual linearly polarized reflectarrays with reconfigurable potentialities. *IEEE Antennas and Wireless Propagation Letters*, 13, pp.11–14.

Malagisi, C.S., 1978. Microstrip disc element reflect array. *Electronics and Aerospace Systems Convention*, pp. 186–192.

Malfajani, R.S. and Atlasbaf, Z., 2012a. Design and implementation of a broadband single layer circularly polarized reflectarray antenna. *IEEE Antennas and Wireless Propagation Letters*, 11, pp. 973–976.

Malfajani, R.S. and Atlasbaf, Z., 2012b. Design and implementation of a broadband single-layer reflectarray antenna with large-range linear phase elements. *IEEE Antennas and Wireless Propagation Letters*, 11, pp. 1442–1445.

Mener, S., Gillard, R., Sauleau, R., Cheymol, C. and Potier, P., 2013. Design and characterization of a CPSS-based unit-cell for circularly polarized reflectarray applications. *IEEE Transactions on Antennas and Propagation*, 61(4), pp. 2313–2318.

Niaz, M.W., Ahmed, Z. and Ihsan, M.B., 2010. Performance comparison of different aperture shapes for microstrip reflectarray. *German Microwave Conference*, pp. 250 – 253.

Pan, Y., Zhang, Y. and Karimkashi, S., 2012. Broadband low-cost reflectarray for multi-mission radar applications. *2012 IEEE Radar Conference*, pp. 613–617.

Phelan, H.R., 1977. Spiralphase reflectarray for multitarget radar. *Microwave Journal*, 20, pp. 67–73.

Pozar, D.M. and Metzler, T.A., 1993. Analysis of a reflectarray antenna using microstrip patches of variable size. *Electronics Letters*, 29(8), pp. 657–658.

Pozar, D.M., Targonski, S.D. and Syrigos, H.D., 1997. Design of millimeter wave microstrip reflectarrays. *IEEE Transactions on Antennas and Propagation*, 45(2), pp. 287–296.

Rajagopalan, H. and Rahmat-Samii, Y., 2010. On the reflection characteristics of a reflectarray element with low-loss and high-loss substrates. *IEEE Antennas and Propagation Magazine*, 52(4), pp. 73–89.

Razzaqi, A.A., Mustaqim, M. and Khawaja, B.A., 2013. Wideband E-shaped antenna design for WLAN applications. *2013 IEEE 9th International Conference on Emerging Technologies (ICET)*, pp. 1–6.

Ren, L.S., Jiao, Y.C., Li, F., Zhao, J.J. and Zhao, G., 2011. A dual-layer T-shaped element for broadband circularly polarized reflectarray with linearly polarized feed. *IEEE Antennas and Wireless Propagation Letters*, 10, pp. 407–410.

Strassner, B., Han, C. and Chang, K., 2004. Circularly polarized reflectarray with microstrip ring elements having variable rotation angles. *IEEE Transactions on Antennas and Propagation*, 52(4), pp. 1122–1125.

Toh, B.Y., Cahill, R. and Fusco, V.F., 2003. Understanding and measuring circular polarization. *IEEE Transactions on Education*, 46(3), pp. 313–318.

Ucuncu, G., 2013. X band two layer printed reflectarray with shaped beam. *IEEE International Symposium on Phased Array Systems and Technology*, pp. 106–110.

Vosoogh, A., Keyghobad, K., Khaleghi, A. and Mansouri, S., 2014. A high-efficiency Ku-band reflectarray antenna using single-layer multiresonance elements. *IEEE Antennas and Wireless Propagation Letters*, 13, pp. 891–894.

Wang, B.K., Lam, K.Y., Leong, M.S. and Kooi, P.S., 1994. Elliptical waveguide analysis using improved polynomial approximation. *IEE Proceedings - Microwaves, Antennas and Propagation*, 141(6), pp. 483–488.

Wu, Z.H., Zhang, W.X., Liu, Z.G. and Shen, W., 2005. Circularly polarised reflectarray with linearly polarised feed. *Electronics Letters*, 41(7), pp. 387–388.

Yang, F., Zhang, X., Ye, X. and Rahmat-Samii, Y., 2001. Wide-band E-shaped patch antennas for wireless communications. *IEEE Transactions on Antennas and Propagation*, 49(7), pp. 1094–1100.

Yang, X., Xu, S., Yang, F. and Li, M., 2015. Design of a 2-bit reconfigurable reflectarray element using two MEMS switches. *2015 IEEE International Symposium on Antennas and Propagation & USNC/URSI National Radio Science Meeting*, pp. 2167–2168.

Yoon, J., Yoon, Y., Lee, W. and So, J., 2015. Broadband microstrip reflectarray with five parallel dipole elements. *IEEE Antennas and Wireless Propagation Letters*, 14, pp. 1109–1112.

Yu, A., Yang, F., Elsherbeni, A.Z., Huang, J. and Kim, Y., 2012. An offset-fed X-band reflectarray antenna using a modified element rotation technique. *IEEE Transactions on Antennas and Propagation*, 60(3), pp. 1619–1624.

Yu, A., Yang, F., Elsherbeni, A.Z., Huang, J. and Rahmat-Samii, Y., 2010. Aperture efficiency analysis of reflectarray antennas. *Microwave and Optical Technology Letters*, 52(2), pp. 364–372.

Yu, A., Yang, F., Elsherbeni, A.Z. and Huang, J., 2009. A single layer broadband circularly polarized reflectarray based on the element rotation technique. *2009 IEEE Antennas and Propagation Society International Symposium*, pp. 1–4.

Zainud- Deen, S.H., Gaber, S.M. and Awadalla, K.H., 2012. Beam steering reflectarray using varactor diodes. *2012 Japan-Egypt Conference on Electronics, Communications and Computers*, pp. 178–181.

Zhao, G., Jiao, Y.C., Zhang, F. and Zhang, F.S., 2010. A subwavelength element for broadband circularly polarized reflectarrays. *IEEE Antennas and Wireless Propagation Letters*, 9, pp. 330–333.

Zhao, M.-Y., Zhang, G.-Q., Lei, X., Wu, J.-M. and Shang, J.-Y., 2013. Design of new single-layer multiple-resonance broadband circularly polarized reflectarrays. *IEEE Antennas and Wireless Propagation Letters*, 12, pp. 356–359.

Zhou, M., Sorensen, S.B., Kim, O.S., Jorgensen, E., Meincke, P. and Breinbjerg, O., 2013. Direct optimization of printed reflectarrays for contoured beam satellite antenna applications. *IEEE Transactions on Antennas and Propagation*, 61(4), pp. 1995–2004.

Zhuang, Y., Wu, K.-L., Wu, C. and Litva, J., 1993. Microstrip reflectarrays: full-wave analysis and design scheme. *Proceedings of IEEE Antennas and Propagation Society International Symposium*, pp. 1386–1389.

APPENDIX A

Reflection phase; (Arm length, L_1)	Column 1	Column 2	Column 3	Column 4	Column 5	Column 6	Column 7	Column 8	Column 9	Column 10	Column 11
Row 1	100° (5.0 mm)	69.7° (7.7 mm)	62.7° (8.1 mm)	79° (7.1 mm)	-241.8° (17.9 mm)	-180.8° (14.9 mm)	-99.4° (11.3 mm)	0.4° (9.7 mm)	-243.4° (17.9 mm)	-112.5° (11.5 mm)	31° (9.1 mm)
Row 2	-6.2° (9.8 mm)	-37.8° (10.3 mm)	-45.2° (10.4 mm)	-28.2° (10.1 mm)	12.8° (9.4 mm)	76.5° (7.3 mm)	-198.8° (16.9 mm)	-95.2° (11.2 mm)	25.2° (9.2 mm)	-199.8° (17.0 mm)	-52.1° (10.5 mm)
Row 3	-92.3° (11.1 mm)	-125.1° (11.8 mm)	-132.8° (12.0 mm)	-115.1° (11.6 mm)	-72.5° (10.8 mm)	-6.5° (9.8 mm)	81.1° (6.9 mm)	-171.9° (14.0 mm)	-48.1° (10.4 mm)	90.5° (5.9 mm)	-118.3° (11.7 mm)
Row 4	-155.8° (13.0 mm)	-189.7° (16.0 mm)	-197.6° (16.8 mm)	-179.3° (14.7 mm)	-135.5° (12.1 mm)	-67.6° (10.7 mm)	22.3° (9.3 mm)	-228.3° (17.8 mm)	-101.7° (11.3 mm)	39.6° (8.8 mm)	-166.5° (13.6 mm)
Row 5	-194.8° (16.6 mm)	-229.3° (17.8 mm)	-237.4° (17.9 mm)	-218.8° (17.7 mm)	-174.2° (14.2 mm)	-105.1° (11.4 mm)	-13.8° (9.9 mm)	97.3° (5.0 mm)	-134.4° (12.1 mm)	8.6° (9.5 mm)	-195.9° (16.7 mm)
Row 6	-208° (17.4 mm)	-242.7° (17.9 mm)	-250.8° (18.0 mm)	-232.1° (17.9 mm)	-187.2° (15.7 mm)	-117.7° (11.6 mm)	-25.9° (10.1 mm)	85.7° (6.5 mm)	-145.4° (12.5 mm)	-1.8° (9.7 mm)	-205.7° (17.3 mm)
Row 7	-194.8° (16.6 mm)	-229.3° (17.8 mm)	-237.4° (17.9 mm)	-218.8° (17.7 mm)	-174.2° (14.2 mm)	-105.1° (11.4 mm)	-13.8° (9.9 mm)	97.3° (5.0 mm)	-134.4° (12.1 mm)	8.6° (9.5 mm)	-195.9° (16.7 mm)
Row 8	-155.8° (13.0 mm)	-189.7° (16.0 mm)	-197.6° (16.8 mm)	-179.3° (14.7 mm)	-135.5° (12.1 mm)	-67.6° (10.7 mm)	22.3° (9.3 mm)	-228.3° (17.8 mm)	-101.7° (11.3 mm)	39.6° (8.8 mm)	-166.5° (13.6 mm)
Row 9	-92.3° (11.1 mm)	-125.1° (11.8 mm)	-132.8° (12.0 mm)	-115.1° (11.6 mm)	-72.5° (10.8 mm)	-6.5° (9.8 mm)	81.1° (6.9 mm)	-171.9° (14.0 mm)	-48.1° (10.4 mm)	90.5° (5.9 mm)	-118.3° (11.7 mm)
Row 10	-6.2° (9.8 mm)	-37.8° (10.3 mm)	-45.2° (10.4 mm)	-28.2° (10.1 mm)	12.8° (9.4 mm)	76.5° (7.3 mm)	-198.8° (16.9 mm)	-95.2° (11.2 mm)	25.2° (9.2 mm)	-199.8° (17.0 mm)	-52.1° (10.5 mm)
Row 11	100° (5.0 mm)	69.7° (7.7 mm)	62.7° (8.1 mm)	79° (7.1 mm)	-241.8° (17.9 mm)	-180.8° (14.9 mm)	-99.4° (11.3 mm)	0.4° (9.7 mm)	-243.4° (17.9 mm)	-112.5° (11.5 mm)	31° (9.1 mm)

APPENDIX B

Reflection phase; (Major axis, $2a_1$)	Column 1	Column 2	Column 3	Column 4	Column 5	Column 6	Column 7	Column 8	Column 9	Column 10	Column 11
Row 1	-146.5° (8.0 mm)	-146.3° (8.0 mm)	-133° (7.9 mm)	-106.7° (7.6 mm)	-67.9° (7.3 mm)	-17.3° (6.8 mm)	44.6° (5.6 mm)	-243° (11.3 mm)	-161.1° (8.2 mm)	-70.5° (7.3 mm)	28.1° (6.1 mm)
Row 2	-206.6° (9.4 mm)	-206.4° (9.4 mm)	-192.7° (8.9 mm)	-165.8° (8.3 mm)	-126° (7.8 mm)	-74.1° (7.4 mm)	-10.8° (6.8 mm)	63° (4.2 mm)	-213.4° (9.7 mm)	-121° (7.7 mm)	-20.7° (6.9 mm)
Row 3	-254.4° (11.7 mm)	-254.2° (11.7 mm)	-240.2° (11.2 mm)	-212.8° (9.7 mm)	-172.2° (8.4 mm)	-119.3° (7.7 mm)	-54.9° (7.2 mm)	20.3° (6.3 mm)	-254.8° (11.7 mm)	-161° (8.0 mm)	-59.2° (7.2 mm)
Row 4	70.8° (2.1 mm)	-289.0° (12.4 mm)	-274.8° (12.2 mm)	-246.9° (11.5 mm)	-205.8° (9.4 mm)	-152.1° (8.1 mm)	-86.8° (7.5 mm)	-10.7° (6.8 mm)	-284.7° (12.4 mm)	-189.9° (8.8 mm)	-87.1° (7.5 mm)
Row 5	49.6° (5.3 mm)	49.8° (5.3 mm)	64.2° (4.0 mm)	-267.7° (12.1 mm)	-226.2° (10.4 mm)	-172.0° (8.4 mm)	-106.1° (7.6 mm)	-29.4° (7.0 mm)	57.2° (4.8 mm)	-207.4° (9.4 mm)	-103.9° (7.6 mm)
Row 6	-317.5° (12.8 mm)	42.7° (5.6 mm)	57.1° (4.8 mm)	-274.6° (12.2 mm)	-233° (10.8 mm)	-178.7° (8.5 mm)	-112.6° (7.7 mm)	-35.7° (7.0 mm)	51.1° (5.2 mm)	-213.2° (9.7 mm)	-109.6° (7.6 mm)
Row 7	49.6° (5.3 mm)	49.8° (5.3 mm)	64.2° (4.0 mm)	-267.7° (12.1 mm)	-226.2° (10.4 mm)	-172.0° (8.4 mm)	-106.1° (7.6 mm)	-29.4° (7.0 mm)	57.2° (4.8 mm)	-207.4° (9.4 mm)	-103.9° (7.6 mm)
Row 8	70.8° (2.1 mm)	-289.0° (12.4 mm)	-274.8° (12.2 mm)	-246.9° (11.5 mm)	-205.8° (9.4 mm)	-152.1° (8.1 mm)	-86.8° (7.5 mm)	-10.7° (6.8 mm)	-284.7° (12.4 mm)	-189.9° (8.8 mm)	-87.1° (7.5 mm)
Row 9	-254.4° (11.7 mm)	-254.2° (11.7 mm)	-240.2° (11.2 mm)	-212.8° (9.7 mm)	-172.2° (8.4 mm)	-119.3° (7.7 mm)	-54.9° (7.2 mm)	20.3° (6.3 mm)	-254.8° (11.7 mm)	-161° (8.0 mm)	-59.2° (7.2 mm)
Row 10	-206.6° (9.4 mm)	-206.4° (9.4 mm)	-192.7° (8.9 mm)	-165.8° (8.3 mm)	-126° (7.8 mm)	-74.1° (7.4 mm)	-10.8° (6.8 mm)	63° (4.2 mm)	-213.4° (9.7 mm)	-121° (7.7 mm)	-20.7° (6.9 mm)
Row 11	-146.5° (8.0 mm)	-146.3° (8.0 mm)	-133° (7.9 mm)	-106.7° (7.6 mm)	-67.9° (7.3 mm)	-17.3° (6.8 mm)	44.6° (5.6 mm)	-243° (11.3 mm)	-161.1° (8.2 mm)	-70.5° (7.3 mm)	28.1° (6.1 mm)